UCLouvain

École polytechnique de Louvain

Real time optimization of a network of wastewater treatment plants

Author: **Cassandre Tasiaux**
Supervisors: **Denis Dochain, Julien Hendrickx**
Readers: **François Glineur, Alain Rapaport, Joshua Taylor**
Academic year 2022–2023
Master [120] in Mathematical Engineering

Abstract

This master thesis aims to propose a control strategy through the use of convex optimization to optimize the distribution of wastewater in the SIAAP network of Paris, with the objective of minimizing pollutant concentrations in the Seine River. SIAAP (Syndicat Interdépartemental pour l'Assainissement de l'Agglomération Parisienne) is a public utility responsible for the transportation and treatment of waste, rain, and industrial water for 9 million people in Paris and its suburbs. It treats a daily volume of 2.4 million cubic meters of wastewater, which is discharged into the Seine River. Through its operations, SIAAP plays a crucial role in safeguarding water resources and making a significant environmental impact. The objective of this master thesis is to present a control strategy that minimizes the substrates concentration entering the Seine River by optimizing the distribution of wastewater among the wastewater treatment plants within the SIAAP network. To address this problem, convex optimization has been employed, utilizing second-order cones (SOC) to approximate microbial growth in the treatment plants. The alternating direction method of multipliers (ADMM) algorithm has been implemented to solve the biconvexity in the objective function. To test and validate the control strategy, a simplified model of the western part of the Seine River Basin has been developed. The control strategy was tested under different weather conditions, including dry, rainy, and stormy weather, and was compared against real measurements for two distinct periods. Evaluation using non-optimized data demonstrated the effectiveness of the model in all weather conditions and revealed, for example, a 12% improvement in ammonia nitrogen concentration and an 11% improvement in nitrite concentration during rainy conditions. These results indicate that the existing partitioning of wastewater is suboptimal and that the convex optimization control strategy offers an optimized partitioning approach that can improve water quality.

Acknowledgement

The writing of this thesis would not have been possible without the help of several individuals, whom I would like to acknowledge.

Firstly, I sincerely thank my master thesis supervisor, Prof. Denis Dochain, for his continuous assistance, support, valuable advice, and unwavering availability throughout the academic year.

Next, I express my heartfelt gratitude to Prof. Alain Rapaport, Prof. Joshua Taylor, Prof. Peter Vanrolleghem, and Shuyao Tan for generously sharing their knowledge, offering support, and dedicating their time to me.

Finally, I extend my thanks to my mother for her support, and to my friends for their constant encouragement and companionship during the countless hours spent in the library.

Acronyms

ADMM: alternating direction method of multiplier
ASM1: Activated Sludge Model no. 1
BOD_5: five-day biochemical oxygen demand
BSM1: Benchmark Simulation Model no. 1
COD: chemical oxygen demand
EU: European Union
LP: linear program
MBR: membrane bioreactor
MOCOPEE: modélisation, contrôle et optimisation des procédés d'épuration des eaux
MPC: model predictive control
PSO: particle swarm optimization
S1: scenario S1
S2: scenario S2
SAV: Seine Aval
SDP: semidefinite programming
SEC: Seine Centre
SEG: Seine Grésillons
SIAAP: Syndicat Interdépartemental pour l'Assainissement de l'Agglomération Parisienne
SOC: second order cone
SOCP: second order cone program
SRT: sludge retention time
SS: suspended solid
TSS: total suspended solid
UWWTD: Urban Waste Water Treatment Directive
WFD: Water Framework Directive
WWTP: wastewater treatment plant

Nomenclature

Symbol	Description	Unit
α	decision variable controlling the SEC influent flow rate division	-
α_1	fraction of SEC influent flow rate to be treated	-
α_2	fraction of SEC influent flow rate to be by-passed	-
α_3	fraction of SEC influent flow rate to SAV	-
α_4	fraction of SEC influent flow rate to SEG	-
β	decision variable controlling the SAV influent flow rate division	-
β_1	fraction of SAV influent flow rate to be treated	-
β_2	fraction of SAV influent flow rate to be by-passed	-
γ	decision variable controlling the SEG influent flow rate division	-
γ_1	fraction of SEG influent flow rate to be treated	-
γ_2	fraction of SEG influent flow rate to be by-passed	-
ϵ	error on the substrate concentration	mg/L
η	vector that selects the entries of S_i of WWTP i	-
κ_i	stoichiometric matrix of WWTP i	-
μ	mean value of data without optimization	mg/L
$\bar{\mu}$	mean value of simulated data	mg/L
$\bar{\mu}'$	mean value of simulated data with another objective	mg/L
$\bar{\mu}''$	mean value of simulated data with a different objective and different maximum substrate concentration vectors	mg/L
μ_{CO}	mean value of simulated data with convex optimisation	mg/L
μ_{MPC}	mean value of simulated data with MPC and PSO	mg/L

Symbol	Description	Unit
μ_{rm}	mean value of real measurements	mg/L
$\mu_{i,j}^{\max}$	maximum specific rate of reaction of substrate j from WWTP i	1/d
ξ_j	concentration of component j in the liquid phase	mg/L
ρ	penalty parameter	-
τ	period	d
φ_j	reaction rate of component j	mg/Ld
$\phi_i(S_i)$	vector representing the reaction kinetics in WWTP i	mg/Ld
$\sum_{r\sim j}$	summation over all reactions r in which the component with index j is involved during the reaction	-
B	bed width	m
BOD_5	concentration of biological demand	mgO_2/L
$BOD_{5,in}$	inlet concentration of biological demand	mgO_2/L
C_i	residual containing the dynamics of the WWTP i	-
$C_{j,m}$	the concentration of substrate j at measurement point m	mg/L
D	diffusion rate	-
d_{ih}	the diffusion from tank i to tank h	m^2/d
d_k	hydraulic response time of the path k	min
$dist_k$	distance of the path k	m
F_j	mass feed rate in the reactor of component j	-
f_X	the fraction of heterotrophic biomass	-
$gBest$	best value obtained by any particle in the entire swarm	-
H	prediction horizon	d
h_0	water height	m
i	wastewater treatment plant (WWTP)	-
j	substrate	-
J	cost function	-
k	path	-
K_{ij}	half saturation coefficient for substrate j of WWTP i	mg/L
K	vector containing half saturation coefficients	mg/L
L_f	best learning factor	-
m	measurement point	-
m'	number of inputs to the measurement point m	-
M	number of reactions	-
N	number of components	-

Symbol	**Description**	**Unit**
NH_4^+	concentration of ammonia nitrogen	mgNH_4/L
$NH_{4,in}^+$	inlet concentration of ammonia nitrogen	mgNH_4/L
NO_2^-	concentration of nitrite	mgNO_2/L
$NO_{2,in}^-$	inlet concentration of nitrite	mgNO_2/L
NO_3^-	concentration of nitrate	mgNO_3/L
$NO_{3,in}^-$	inlet concentration of nitrate	mgNO_3/L
P_1	performance criteria based on the deviation from the good state limit	%
P_2	performance criteria measuring the gain achieved compared to measurements without using optimization	%
$p(i)$	particle representing a potential solution of the optimization problem	-
$pBest$	best solution of the problem	
Q	total influent flow rate in Clichy-LaBriche	m^3/d
$Q_{0,k}$	average flow rate over a period on the path k	m^3/d
$Q_{i,T}$	treated flow rate of WWTP i	m^3/d
$Q_{i,P}$	by-passed flow rate of WWTP i	m^3/d
Q_{ih}	flow rate from tank i to tank h	m^3/d
$Q_{in,i}$	influent flow rate of WWTP i	m^3/d
Q_j	rate of mass outflow of the component j from the reactor in gaseous form	m^3/d
Q_m	flow rate at the measurement point m	m^3/d
$Q_{max,i}$	maximum allowable flow rate of WWTP i	m^3/d
$Q_{min,i}$	minimum allowable flow rate of WWTP i	m^3/d
$Q_{out,i}$	effluent flow rate of WWTP i	m^3/d
Q_w	waste flow rate	m^3/d
r_j	kinetics described by Monod equation for the reaction of substrate j	1/d
R_i	vector of the respective good limits values of WWTP i	mg/L
$rand$	random value	-
s_d	sludge retention time	s
S	effluent substrate concentration vector	mg/L
$\bar{S}$	average effluent substrate concentration vector	mg/L
S_i	effluent substrate concentration vector of WWTP i	mg/L
$\dot{S}_i$	dynamic process state of WWTP i	mg/Ld

Symbol	Description	Unit
$\hat{S}_i$	concentration vector containing ammonium and nitrite of each WWTP i	mg/L
$S_{in,i}$	influent substrate concentration vector of WWTP i	mg/L
S_L	good state limit vector	mg/L
$S_{max,i}$	maximum substrate concentration vector of WWTP i	mg/L
$S_{min,i}$	minimum substrate concentration vector of WWTP i	mg/L
$\bar{S}_{\text{w/o opti}}$	average non-optimized effluent substrate concentration vector	mg/L
t	continuous time variable	15min
T	vector representing reaction kinetics	mg/Ld
T_i	vector representing reaction kinetics in WWTP i	mg/Ld
TL_i	lower bound of the reaction kinetics in WWTP i	mg/Ld
TSS	concentration of total suspended solid	mg/L
TSS_{in}	inlet concentration of total suspended solid	mg/L
TU_i	upper bound of the reaction kinetics in WWTP i	mg/Ld
U_i^k	scaled dual variable of WWTP i at iteration k	-
V_i	volume of the reactor of the WWTP i	m^3
$v(i)$	velocity to direct particles fly	-
w	inertia weight	-
W	weighting matrix	-
X	concentration of the biomass of one microbial population	mg X/L
X_i	concentration of the biomass of one microbial population of WWTP i	mg X/L
y_i	total influent flow rate division to the WWTP i	-
y_{rj}	strictly positive constant yield coefficient for reaction r and component j	-
Y_{S_1/S_2}	yield conversion coefficient of the reaction from S_1 into S_2	mgS_1/mgS_2

Contents

List of Tables

List of Figures

Introduction

Context

According to the United Union Office for the Coordination of Humanitarian Affairs, climate change is not a distant future threat that is far away but rather a primary catalyst for the increasing demand for humanitarian assistance, and its effect is being witnessing firsthand [1]. While numerous environmental problems exist, wastewater treatment stands out as a prominent environmental issue in the twenty-first century. Survival without water is an arduous task for living organisms, i.e. both plants and animals. Consequently, water is categorized as the most indispensable resource for human existence. The quality of water is compromised by pollution caused by human activities, agricultural activities, deforestation, mining, energy generation, industries [2]. Despite the fact that approximately 70% of the Earth's surface is covered by water, the majority, roughly 97%, consists of saline water from the sea and oceans, making it unsuitable for drinking, industrial, and agricultural purposes due to its high salt content. Therefore only a small fraction, about 3%, is freshwater. Unfortunately, approximately 69% of this freshwater is inaccessible, trapped in locations such as mountainous regions, Greenland, ice caps, and glaciers. The remaining 30% is found underground, often at great depths, making it challenging to utilize. The only accessible water source available for human and animal consumption is less than 1% of the accessible freshwater, present in water bodies like lakes, rivers, ponds, streams, and reservoirs. Consequently, prioritizing the preservation and cleanliness of these water bodies is of utmost importance for our survival on Earth [3].

However, it has only been recognized in the past forty years that water is not an unlimited public resource but a heritage that requires protection, defense, and preservation [4]. Regulations governing urban wastewater treatment have been established and the preservation of water quality along a river basin has become a task that must meet strict regulations. The initial step was taken through the implementation of the Urban Waste Water Treatment Directive (UWWTD) in 1991 [5]. This directive aims to safeguard human health and the environment, particularly surface waters, from the harmful effects of untreated urban wastewater, which may contain viruses, bacteria, phosphorus, nitrogen, and other pollutants. The approach involves: (1) implementing decentralized treatment systems to reduce pollution from households in remote areas, (2) imposing stricter regulations on municipal wastewater treatment plant effluents, and (3) addressing diffuse pollution from agriculture. In 2000, the Water Framework Directive (WFD)[4] sets rules to cutoff the deterioration of the status of European Union (EU) water bodies and ensure the good status of rivers, lakes and groundwater. The WFD is the primary legislation supported by two directives focusing on groundwater quality and quantity, as well as surface water quality. The EU Directive demands integrated pollution prevention, control of surface freshwater, and good quality in the complete basin of water bodies. Despite significant improvements in the quality of European rivers, lakes, groundwater, and seas since the adoption of the UWWTD, there are still pollution issues that remain unaddressed under the current regulations [6]. To tackle these challenges, the Commission had proposed an update to the Directive [7]. Furthermore, climate change will impact hydrology in the coming years, with a particular concern being the potential degradation of water quality due to reduced low flows in central European rivers. Any decrease in flow is expected to lead to increased water concentrations. With reduced dilution capacity for discharges and population growth contributing to higher concentrations, maintaining good water quality conditions will become increasingly challenging.

The organism in charge of improving the water quality along the Seine River basin in the region of Île-de-France is the "Syndicat interdépartemental pour l'assainissement de l'agglomération parisienne" (SIAAP), which translates to Interdepartmental Syndicate for Sanitation of the Paris conurbation. Established in 1970, SIAAP is a public utility in charge of the transport and the treatment of wastewater, stormwater and industrial water for approximately 9 million people residing in Paris and its suburbs. In 2014, SIAAP initiated the research program "MOdélisation, Contrôle et Optimisation des Procédés d'Epuration des Eaux" (MOCOPEE) translated to Modeling, Control and Optimization of Water Treatment Processes [8]. This program is a permanent space for work and knowledge exchange between scientists and operational actors in wastewater treatment. It revolves around four research areas dedicated to topics such as meteorology applied to water treatment, modelling of the operation of treatment processes, treatment processes control and the emergence of innovative concepts in the field of sanitation.

Proposed Work

In this context, the focus of this master thesis is on developing a model and applying convex optimization to the west part of the SIAAP wastewater treatment network. Building upon a simplified model, this thesis undertake the challenge of implementing convex optimization to control the network. The aim is to optimize the distribution of wastewater within the network in order to minimize the substrates concentration entering the Seine River.

By utilizing convex optimization and implementing a second-order cone (SOC) approximation as well as the alternating direction method of multipliers (ADMM) algorithm to address the biconvexity, this thesis successfully solves the convex optimization problem for minimizing pollution in the river. This approach allows for easier control of the network by making optimal choices at the flow divider and demonstrates the effectiveness of the model in addressing various weather conditions.

Work structure

The master thesis is organised as follows:

Chapter 1 - Model of the wastewater treatment network: Firstly, the chapter provides a description of the wastewater network serving Paris and its suburbs, focusing on the modeling of the west part of the SIAAP network, which will be utilized throughout the rest of the work. Following this, the model of the sewers is presented. Subsequently, it delves into an explanation of the functioning of wastewater treatment plants and presents a simplified model for these plants. Lastly, the model for the Seine River is introduced.

Chapter 2 - Convex Optimization: The second part of this thesis is dedicated to the theory of convex optimization. It is structured as follows: Firstly, a comprehensive overview of convex optimization is provided. This is followed by a general explanation of second-order cone optimization. Next, the formulation of the general optimization problem for the wastewater treatment network with a second-order cone constraint is presented. Finally, the chapter concludes with a description of the alternating direction method of multipliers algorithm.

Chapter 3 - Model Implementation: The third part presents the implementation of the model presented in Chapter 1 solved using convex optimization. It begins by defining the objective and parameters to formulate the convex optimization problem based on the selected model. Next, the alternating direction method of multipliers algorithm is applied to solve the biconvexity. Finally, a description of the code used for the implementation is provided.

Chapter 4 - Results: In the last part, the convex optimization control strategy is evaluated across three representative periods: dry, rain, and storm. The performance of the model will be assessed by comparing it to the good value limit and the non-optimized data for these periods. This evaluation aims to provide insights into the capabilities, limitations, and potential areas for improvement of the program. Additionally, a modified objective program will be presented to highlight all the changes made to the solution. Finally, a comparison between the studied model and model predictive control (MPC) on the same network will be conducted.

Chapter 1

Model of the wastewater treatment network

The effective management of wastewater treatment is crucial for maintaining the health and sustainability of the environment. To address this challenge, the development of accurate and reliable models for wastewater treatment plant networks plays a pivotal role. This chapter is devoted to providing the contextual and theoretical basis for the rest of the work on wastewater treatment plant networks, aiming to provide a comprehensive understanding of their structure and dynamics. As the network is composed of sewers, wastewater treatment plants (WWTPs), and the river, it begins by describing the WWTP network and explaining the composition of wastewater. Subsequently, the model of the network that is to be optimized is presented. Then the model for the sewers is provided, followed by essential information regarding the functioning of WWTPs. Additionally, a description of a general state space model of stirred tank bioreactors is given, which leads to the model used for WWTPs in the remainder of the work. Finally, the model for the river is described. Through this chapter, the aim is to provide a comprehensive overview of the modeling aspects of the wastewater treatment plant network. By understanding the underlying principles, build a model for each component of the network and enhance our overall understanding of its dynamics and behavior.

1.1 Model of the network

1.1.1 Description of the network and wastewater composition

The megacity of Paris is located in the Seine Basin, which is one of the eight major drainage basins in France. The Seine River, along with its two primary tributaries, serves as the main drainage axis within the basin. The Seine River exhibits an oceanic regime characterized by a low-flow period from June to early fall, followed by a flood period in February. Its flow rate can range from 100 to 1000 m^3/s, depending on weather conditions. The climate in the Paris region is temperate with an oceanic influence. Rainfall is relatively evenly distributed throughout the year, and temperatures tend to be mild. The SIAAP is in charge of collecting and treating the wastewater in a significant portion of Paris and its suburbs. It also plays a crucial role in ensuring the ecological and chemical quality of the Seine River and its two main tributaries, the Marne and the Oise, within the Île-de-France region. The SIAAP's coverage area, depicted in green in Figure 1.1, encompasses a total of 284 municipalities and spans an area of 1,800 km^2. By treating 2.4 million cubic meters of wastewater per day, generated by over 9 million citizens, the SIAAP is actively engaged in the daily protection of water resources [9].

The collection and transport network of Paris and its suburbs is predominantly combined, wherein runoff water from sources such as rain and street cleaning is channeled into the same system as water contaminated by domestic and industrial activities. Within this framework, four primary categories of effluent can be distinguished.

- **Domestic wastewater** consists of two main components: black water, which originates from toilets, and grey water, which is derived from kitchen and bathroom sources. This type of wastewater contains biodegradable organic matter as well as mineral matter. On average, the daily flow of domestic wastewater in France is estimated to be 150 liters per person [10].

- **Industrial wastewater** is generated by industrial and commercial activities. The composition of industrial effluent depends on the specific nature of the emitting company. For instance, the wastewater from the processing and food industry is predominantly organic while the electronics industry, dry cleaners, photographic laboratories and printing houses produce effluent with chemical components and metallic effluent are from the steel, metal and foundry industry.

- **Rainwater** refers to water that originates from rainfall and has not infiltrated the soil. It carries various impurities, including organic pollutants, metallic pollutants, chemical pollutants, suspended solids, and mineral matters. The specific characteristics of rainwater depend on the rainfall itself and the meteorological conditions leading up to the rain event. For instance, a period of dry weather followed by a heavy storm can result in concentration peaks of certain pollutants, unlike a fine and regular rainfall. In the Paris region, during intense rainy episodes, the volume of water flowing through the collection network can be double the amount found in the Seine River.

- **Parasite water** is water that originates from seepage, groundwater drainage, or the catchment areas of watercourses.

The water treated by the SIAAP consists of a mixture of various effluents, with wastewater accounting for approximately 60% of the total annual volume received by SIAAP's treatment plants [9]. The exact proportion of industrial water within this wastewater is currently unknown. It should be noted that many municipalities fail to establish discharge agreements in the collection network with industries, despite it being a requirement under Article L 1331-10 of the Public Health Code [11].

Wastewater carries a wide variety of materials, which can be organic or mineral. These materials are considered pollutants when they cause a disturbance in a given environment. The pollutants present in wastewater are diverse and can be classified into four categories of pollution, each generating different types of nuisances and requiring specific treatment. These categories include carbon, nitrogen, phosphorus pollution, and micropollutants. The first three categories account for the majority of the materials in the water, while the last category consists of various elements that are currently not considered in the sizing of treatment plants.

Carbon pollution corresponds to organic matter, and its degradation by aquatic organisms leads to a decrease in the level of dissolved oxygen in the water, which is harmful to the fauna residing in the water bodies. The measurement of carbon pollution is performed using two parameters with specific operating procedures: Five-day Biochemical Oxygen Demand (BOD_5), Chemical Oxygen Demand (COD). BOD_5 is determined by mixing a small amount of wastewater with pure water saturated with oxygen and allowing it to sit in a closed bottle at a temperature of 20°C in the dark for five days. This laboratory test simulates the oxygen consumption that occurs when wastewater is discharged into a well-oxygenated river. BOD_5 quantifies the amount of oxygen taken from the natural environment during a wastewater discharge. COD represents the total organic content of the water, whether it is biodegradable or not.

Nitrogen pollution can be divided into two main families: reduced nitrogen, which is a form of organic nitrogen that quickly converts into ammonium (NH_4^+), and oxidized nitrogen, which includes nitrites (NO_2^-) and nitrates (NO_3^-). Oxidized nitrogen is produced through the chemical transformation of reduced nitrogen in the presence of oxygen.

Phosphorus pollution primarily originates from human metabolism and detergents. Nitrogen and phosphorus are essential nutrients for plant and algae growth, but their excessive presence in the aquatic environment can lead to the proliferation of plant species, a phenomenon known as eutrophication. The consequences of eutrophication include disruptions in drinking water production, economic activities, and water sports.

Within the area covered by SIAAP, the collection, conveyance and treatment of the wastewater are divided among several operators:

1. **Collection:** The municipalities are responsible for the primary collection of urban wastewater, which occurs directly at the discharge points of homes and businesses. They are also responsible for the collection of stormwater through a 15 000 km system.

2. **Conveyance:** The departments and inter-municipal sanitation authorities have the responsibility of intermediate conveyance between the entities in charge of basic collection and the transfer sewers that lead to the WWTPs.

3. **Treatment:** The SIAAP is in charge of the final conveyance of wastewater to its wastewater treatment facilities.

The final conveyance of the wastewater of Paris and its suburbs is done through 444 km of sewers spread across 1800 km^2 of territory (Figure 1.1). These sewers are located at depths ranging from 10 to 100 m, depending on the topography. They have a diameter that varies between 2.5 and 6.8 m and transport approximately 2.5 million m^3 of wastewater during dry periods. The wastewater is directed to the six wastewater treatment plants within the network. The WWTPs include Seine Amont, Seine Morée, and Marne Aval, which discharge the water into the Seine upstream from Paris and Seine Centre (SEC), Seine Aval (SAV), and Seine Grésillons (SEG) which discharge the water downstream.

To mitigate the risk of network saturation and prevent overflow of pollutants during adverse weather conditions, the SIAAP has implemented various measures. These include 8 storage basins with a combined capacity of 685 000 m^3 and 4 reservoir tunnels with a capacity of 270 000 m^3. These storage facilities collect excess

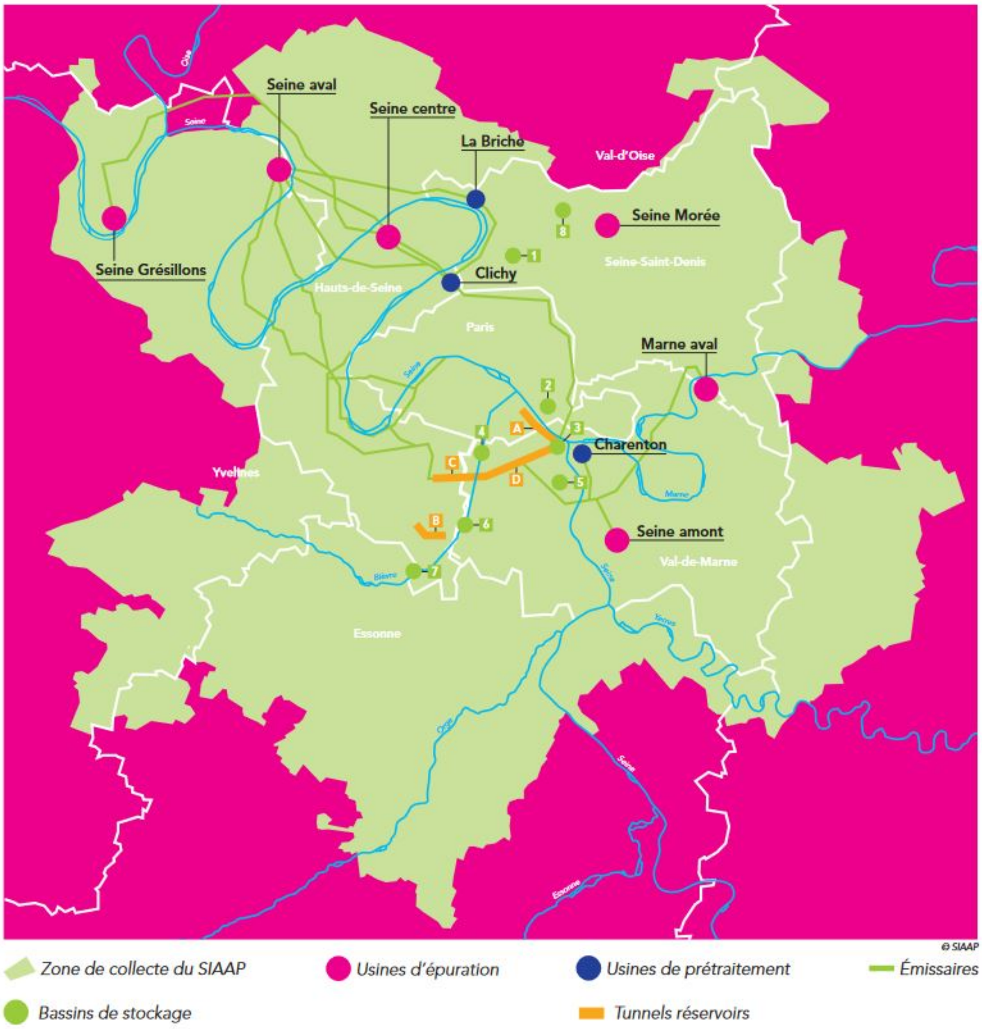

Figure 1.1: Collecting area and wastewater treatment network of the SIAAP [9]

water during periods of inclement weather and subsequently transport it to the treatment plants to be treated once the weather conditions normalize. Additionally, the SIAAP has also pre-treatment facilities that play a role in pre-treating the wastewater and dispatching the flow in the treatment plants network. Certain facilities, such as Clichy-la-Garenne, can function as pumping stations to prevent flooding by evacuating excessive rainwater into the Seine River.

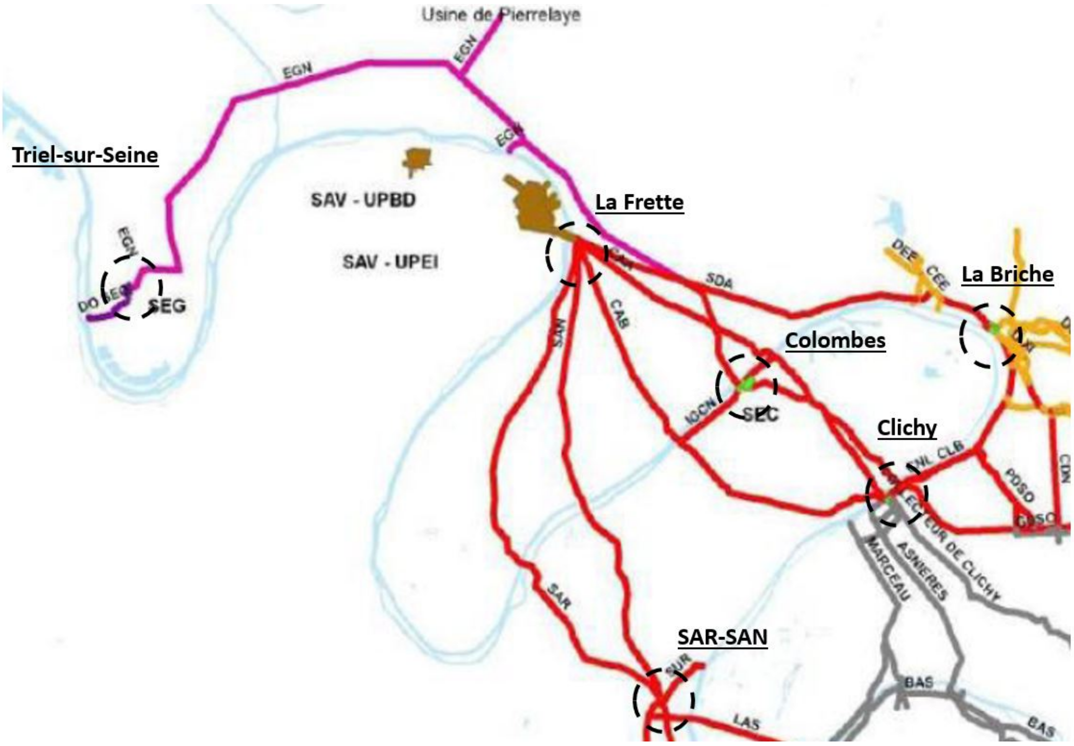

Figure 1.2: West part of the wastewater treatment network operated by the SIAAP

Numerous system interconnections have been created to guide flows according to the available capacity of downstream main sewers, storage and treatment works, and also to allow by-passing. One of the special assets of SIAAP area is its high water transfer capacity between WWTPs through an interconnected sewer network. In this work, the focus is on the west part of the network located downstream from Paris and its suburbs. This area includes three wastewater treatment plants, Seine Centre, Seine Aval and Seine Grésillons, and the main pre-treatment facilities of Clichy and La Briche. Figure 1.2 provides an illustration of the connection between the different facilities in the area. The six encircled points (Colombes, La Frette, Triel-sur-Seine, SAR-SAN, Clichy and La Briche) would allow a unique control system. Indeed, the two latter points serve as pumping stations within the sewer system, allowing the transfer of wastewater from one station to another. From there, with the help of a flow divider, the wastewater is distributed to the different treatment plants. The SEC treatment plant is located in Colombes, the SAV plant is situated near La Frette, and the SEG plant is established in Triel-sur-Seine. Before each WWTP, there is a flow divider that prevents flooding by by-passing excess wastewater into the Seine River and before SEC the wastewater can also be redirected to SAV and SEG.

1.1.2 Model description and assumptions

The integrated urban wastewater system can be viewed as a set of interconnected sub-systems comprising sewers, wastewater treatment plants, and the river. Each WWTP is individually controlled and discharges the water into the river. The model, schematized in Figure 1.3, consists of a single input node that combines the Clichy and La Briche pre-treatment facilities, which can also function as a pumping station to prevent flooding by draining rainwater. This combined facility, known as Clichy-LaBriche, receives wastewater from the sewers and distributes it to three wastewater treatment plants: SEC, SAV, and SEG. It is assumed that no pre-treatment occurs at the Clichy-LaBriche facility. Its flow rate is divided into three portions, which are directed to SEC, SAV, and SEG respectively. Before reaching each wastewater treatment plant, there is an additional flow divider that splits the incoming wastewater into two streams: the portion treated by the respective WWTP and the by-passed portion. The flow divider before SEC also has the capability to divert a portion of the flow to SAV and to SEG.

Within the study area, there are multiple measurement points, of which five will be considered in this work as shown in Figure 1.3. These points correspond to Suresnes (1) located before the WWTPs, this point represents the state of the Seine River upstream from the WWTPs, Sartrouville (2) positioned after SEC, this point indicates the condition of the Seine River following its treatment process, Conflans (3) situated downstream from SAV, this measurement point reflects the state of the Seine River after the treatment at SAV, Poissy (4) found after the convergence of the Oise with the Seine, and Triel (5) positioned after SEG, this measurement point signifies the condition of the Seine River following the three WWTP. These five measurement points allow for the assessment of water quality and changes in the river as it receives contributions from various sources.

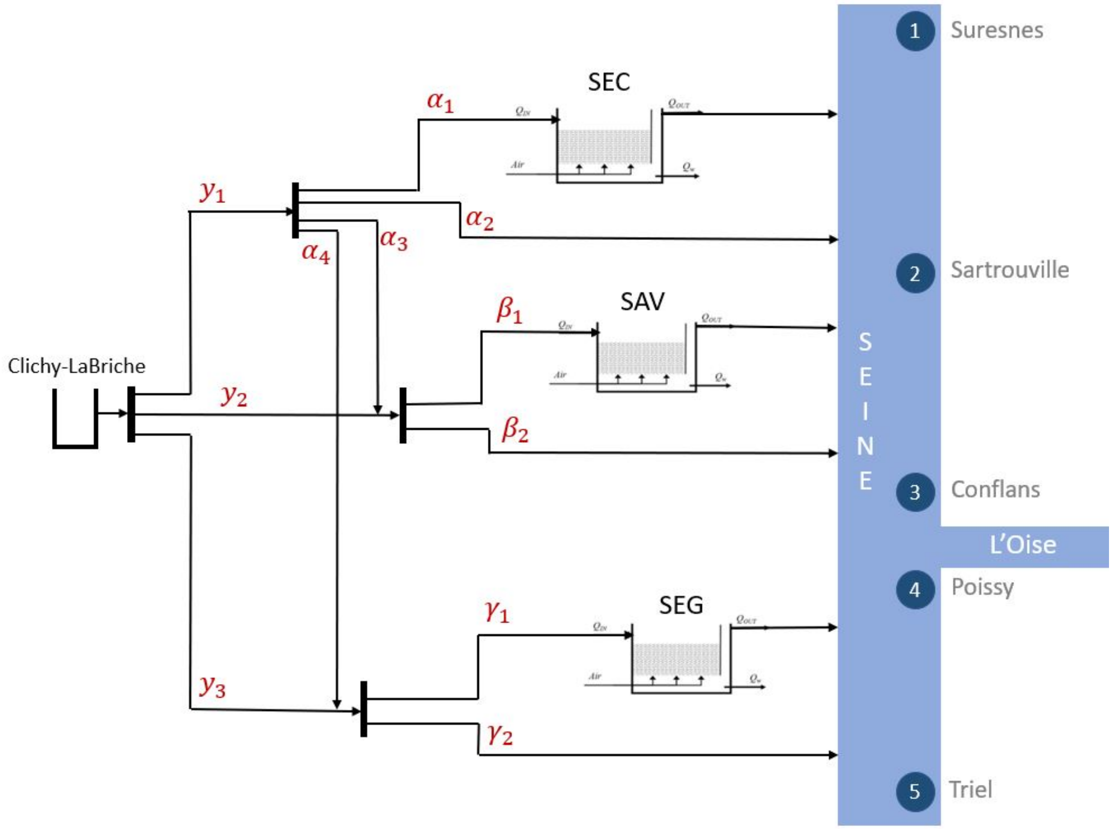

Figure 1.3: Model of the wastewater treatment network

In this study, the degradation of water quality in both the Seine River and the sewers is neglected. It is assumed that there is instantaneous mixing between the treated water from the WWTPs and the water in the Seine River at their respective discharge points. The mixing time is considered to be negligible compared to the hydraulic response time and the biochemical time constants within the WWTPs. This assumption allows for simplified modeling and analysis, focusing primarily on the hydraulic behavior and the overall impact of the WWTP discharges on the Seine River.

1.2 Model of the sewers

The modeling of sewer systems plays a crucial role in understanding and managing the transport of wastewater within the network. The sewers are modeled using the concept of virtual tanks, where the output of the sewers is a delayed representation of the input. This delay, denoted as d, accounts for the time it takes for the wastewater to flow through the sewer system. Mathematically, this can be expressed as follows:

$$Q_{\text{out}}(t) = Q_{\text{in}}(t-d)$$
$$S_{\text{out}}(t) = S_{\text{in}}(t-d)$$

where $Q_{\text{in}}(t)$ and $Q_{\text{out}}(t)$ represent the input and output flow rates of the sewer at time t, respectively. Similarly, $S_{\text{in}}(t)$ and $S_{\text{out}}(t)$ represent the input and output substrate concentrations, respectively. By incorporating this delay, the model captures the dynamics of the sewer system and allows for accurate representation of the time lag between the input and output variables.

Therefore, the parameter required is the hydraulic response time, i.e. the time it takes a flow variation to propagate through the sewers from upstream to downstream. One approach to estimating the hydraulic response time is by calculating the flow velocity for a uniform stationary profile.

For a uniform stationary profile, the flow rate is constant throughout the sewer, denoted as Q_0. The water height h_0, on the other hand, is a solution of a non-linear ordinary differential equation. But for the particular case where the friction forces compensate exactly the slope term, a uniform water height is obtained along the entire length of the sewer. Therefore, if the shape of the sewer is known, the velocity of this uniform stationary profile can be determined. For a rectangular channel, $Q_0 = Bh_0v_0$ holds, where B is the bed width, v_0 is the flow velocity and h_0 is the water height. In this work all the sewers are assumed to be a square with dimensions 2×2 meters, resulting in $B = 2$ and $h_0 = 2$ as the sewers are assumed to be full. Q_0 is estimated by the average flow rate on a period.

To compute the hydraulic response time and so the corresponding delay d, the flow velocity needs to be divided by the length of the sewers. An approximation of the distance $dist$ between the cities located at the two ends of the sewer can be obtained using Google Maps measurement tool. The flow and the concentration delay are given by the following relation:

$$d_k = \frac{dist_k \cdot B_k h_{0,k}}{Q_{0,k}} \tag{1.1}$$

where k is the number of the path. And the delay of their respective path is computed in Table 3.2.

By accurately modeling the sewers, it becomes possible to assess the performance of the system and optimize the design and operation of the network. This information is crucial for effective wastewater management.

1.3 Model of the wastewater treatment plants

1.3.1 Description of the wastewater treatment plants

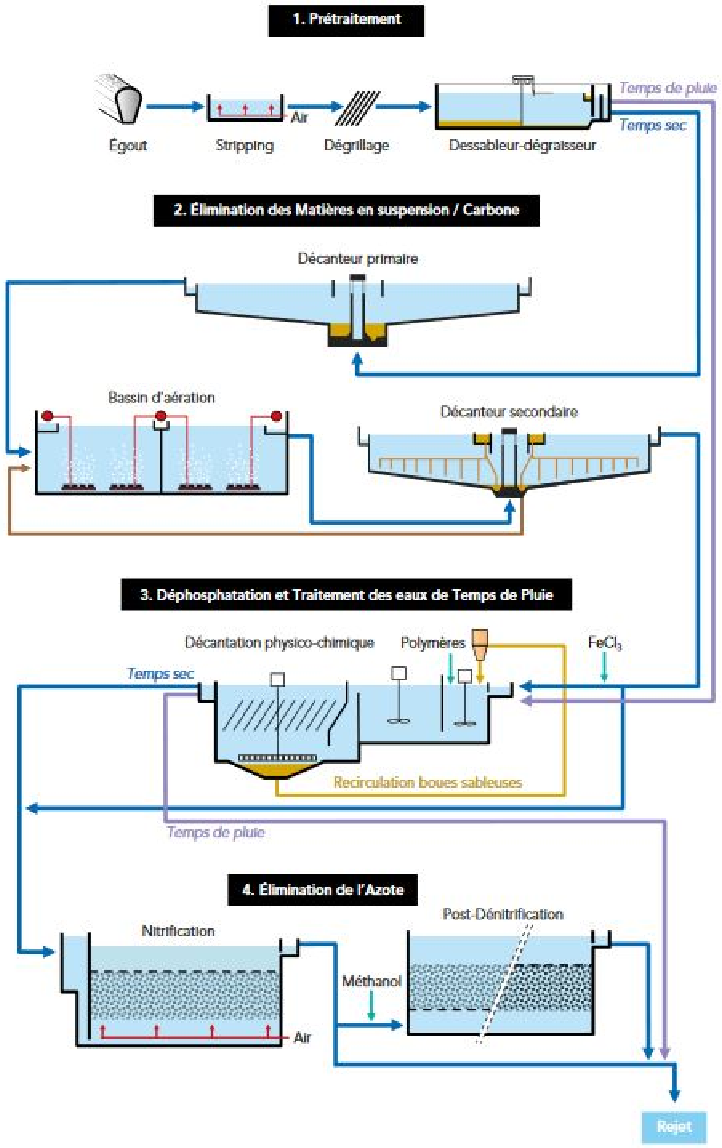

Figure 1.4: Schema of the treatment steps of SAV [13]

Wastewater treatment plants play a vital role in removing pollutants and contaminants from wastewater before it is discharged back into the environment. These facilities are designed to treat large volumes of wastewater, ensuring that it meets the required quality standards and does not pose a risk to human health or the ecosystem. At WWTPs, a combination of physical, chemical, and biological processes are employed to treat the incoming wastewater. The treatment processes typically include several successive stages, each targeting specific pollutants and contaminants. It can be divided into four steps (see Figure 1.4).

First a pre-treatment which aims to remove undesirable elements (coarse solids, sand oil, etc.) from entering the plant. It consists of retaining separable materials by simple processes. Bulky materials that might interfere with further treatment are removed by means of screens and grid removal. Gravel, sand and mineral particles that could cause abrasion of pipes and pumps, as well as clogging and silting of the structures are retained thanks to grit chambers. Products that are less dense than water and coarser floating materials are collected by a grease trap mechanically. This last operation is important in order to avoid foam in the aeration tanks and biological treatment performance reduction due to oil and grease.

Next, the second step is the removal of the suspended solids (SS). This is carried out by means of a primary and a secondary decanter. The primary treatment removes the smallest particles in suspension, mainly of organic matter, by settling. It is essentially a physical process that allows, by the force of gravity alone, the separation of the easily settable SS from the liquid fraction. The wastewater is left to settle in basins (decanters) so that the heavier SS falls at the bottom. Their accumulation forms a layer called "primary sludge". This sludge is then sent to its own treatment plant. The secondary treatment removes organic compounds and nutrients that are dissolved in the water. The water undergoes physico-chemical decantation to reduce the total suspended solids (TSS). The process used is a treatment by activated sludge where bacteria are in suspension in the wastewater. The process is broken down into two successive phases and requires two basins. The aeration basin is fed continuously in which the water to be purified is put in the presence of heterotrophic bacterial colonies and oxygen. The oxygenation is necessary for the growth of bacteria so that the bacteria grow in the form of flocs in suspension. Then the wastewater and the sludge mixture passes into a secondary decanter where the SS is separated from the wastewater. Nevertheless, membrane bioreactors (MBRs) have been widely developed in recent years for the treatment of urban wastewater. MBR is composed of an activated sludge biological reactor coupled with ultrafiltration or microfiltration membranes to separate the treated water from the bacterial flocs instead of conventional clarification with decanters. MBR is installed in the three downstream WWTPs.

The tertiary step aims to remove the phosphorus. Bacteria that are able to assimilate large quantities of orthophosphates, a dissolved mineral form of phosphates are utilized. After a period of deprivation, the bacteria are reintroduced to an oxygen-rich environment, leading to an over-assimilation of phosphorus. This results in an overall decrease of phosphates in the water.

The fourth and last treatment stage targets the removal of remaining pollutants such as nitrogen. Nitrogen removal is achieved through two steps: nitrification and denitrification. Nitrification involves the conversion of ammonia nitrogen (NH_4^+) first into nitrites (NO_2^-) and then into nitrates (NO_3^-) through two successive oxidation reactions, nitritation and nitratation. This process is controlled by the action of aerobic autotrophic bacteria that utilize the oxidation of their substrate as their only energy source and carbon dioxide as their exclusive source of carbon. As it involves nitrifying bacteria, the presence of a primary oxygen source for the microorganisms to turn into nitrates is required. Following nitrification, denitrification occurs, during which nitrate is reduced to nitrous oxide (N_2O) before turning into nitrogen gas (N_2). This process involves numerous types of heterotrophic bacteria that use nitrates as a source of oxygen to oxidize organic matter.

It is important to note that in rainy condition some treatments steps may be by-passed to handle larger input flow, changing therefore the dynamic of the WWTP.

The allowable nominal, the treatment capacities and the reactor volume of the WWTPS in the study area are as follows:

- Seine Centre [12]:
  - Allowable nominal flow: 240 000 m^3/d
  - Treatment capacity during rainy periods: 404 800 m^3/d
  - Volume of the reactor: 20 600 m^3
- Seine Aval [13]:
  - Allowable nominal flow: 1 500 000 m^3/d
  - Treatment capacity during rainy periods: 2 900 000 m^3/d
  - Volume of the reactor: 163 300 m^3
- Seine Grésillons [14]:
  - Allowable nominal flow: 300 000 m^3/d
  - Treatment capacity during rainy periods: 315 000 m^3/d
  - Volume of the reactor: 29 680 m^3

These values indicate the maximum flow rates that the WWTPs can handle under normal and rainy conditions, as well as the respective volumes of the reactors.

1.3.2 General dynamical model of bioreactor

G.Bastin et al.[15] developed a general state space model, described by Equation (1.2), to characterized biotechnological processes in stirred tank bioreactors. The model considers N components (ξ_j, where $j = 1, \cdots, N$) and M reactions ($r = 1, \cdots, M$) involved in the process. The equation describes the dynamics of the concentration of each component ξ_j as follows:

$$\frac{d\xi_j}{dt} = \sum_{r \sim j} (\pm) y_{rj} \varphi_j - D\xi_j - Q_j + F_j \tag{1.2}$$

The notation ξ_j is used to denote a component or its concentration in the liquid phase of the reactor. y_{rj} denotes the strictly positive constant yield coefficient without dimension, φ_j the reaction rates of component j, D the diffusion rate and Q_j the rate of mass outflow of the component ξ_j from the reactor in gaseous form. F_j represents the mass feed rate in the reactor of the component ξ_j. The notation $r \sim j$ means that the summation is taken on the reactions with index r which involve the component with index j.

The following matrix notations can be introduced:

$$\begin{aligned}
\xi^\top &= [\xi_1, \xi_2, \ldots, \xi_N] \\
\varphi^\top &= [\varphi_1, \varphi_2, \ldots, \varphi_M] \\
Q^\top &= [Q_1, \ldots, Q_N] \\
F^\top &= [F_1, \ldots, F_N] \\
Y = [Y_{rj}] &: N \times M \text{ matrix with } \begin{cases} Y_{rj} = (\pm) y_{rj} & \text{if } r \sim j \\ Y_{rj} = 0 & \text{otherwise} \end{cases}
\end{aligned}$$

Then the dynamics of a bioprocess can thus be represented by the following general nonlinear state space model, written in matrix form:

$$\frac{d\xi}{dt} = Y\varphi(\xi, t) - D\xi - Q(\xi) + F$$

1.3.3 Model description

Robles et al. [16] presents a simplified model for wastewater treatment plants based on Activated Sludge Model no. 1 (ASM1) with only one microbial population. The model focuses on three WWTPs located in Paris (Seine Centre, Seine Aval, Seine Grésillons). The model aims to predict the concentration of various key parameters, including ammonia, nitrites, nitrates, biological demands, and total suspended solids.

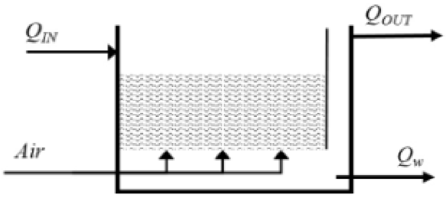

Figure 1.5: System representation of the reduced WWTP

The proposed model reduces the WWTP into an aerobic membrane bioreactor (MBR) based on ASM1, as shown in Figure 1.5. In the model, Q_{in} represents the influent rate, Q_{out} denotes the flow rate of the effluent going into the Seine River, and Q_w corresponds to the waste flow rate. It is assumed that there is an adequate air supply to support microbial growth, and alkalinity is neglected as the pH in the wastewater treatment plant is maintained at a neutral level.

The model considers the conversion of carbon by heterotrophic bacteria and the autotrophic conversion of ammonia nitrogen (NH_4^+) first into nitrites (NO_2^-) and then into nitrates (NO_3^-). This process, known as nitrification, involves nitrifying bacteria. Subsequently, denitrification occurs, where nitrate is reduced to nitrous oxide (N_2O) before being converted into gas (N_2). Denitrification involves heterotrophic and requires the presence of a carbon source, such as methanol (CH_3OH), under anoxic conditions. It has been observed that maintaining a sufficient carbon supply is necessary to prevent the accumulation of N_2O.

$$\begin{aligned}
NH_4^+ + 3O_2 &\rightarrow 2NO_2^- + 4H_2O + 4H^+ \\
4NO_2^- + O_2 &\rightarrow 2NO_3^- \\
6NO_3^- + 5CH_3OH &\rightarrow 2\ N_2 + 5CO_2 + 7H_2O + 6OH^-
\end{aligned}$$

The model takes into account a single microbial population (X) that merges heterotrophic and autotrophic microorganisms. Consequently, the dynamic is reduced to four reactions, which include: (i) Growth of microorganisms; (ii) Decay of microorganisms; (iii) Hydrolysis of entrapped organics, and (iv) Hydrolysis of entrapped organic nitrogen.

The simple model assumes a constant value (s_d) to account for the high sludge retention time (SRT) required for the degradation of total suspended solids (TSS). Additionally, it assumes that a fraction of TSS present in the influent was accounted as an active biomass, while no biomass is considered for the effluent due to the membrane utilization. The model does not include phosphorus treatment, and it does not differentiate between different weather conditions, such as rain and dry periods.

The reduced system that represents the dynamics of the biological demand (BOD_5), the ammonia nitrogen (NH_4^+), nitrite (NO_2^-), nitrate (NO_3^-) and the total suspended solids (TSS) can be described by the following mass balance equations:

$$\frac{dBOD_5}{dt} = BOD_{5,\text{ in}}\frac{Q_{in}}{V} - BOD_5\frac{Q_{\text{out}}}{V} - BOD_5\frac{Q_w}{V} - r_1X \tag{1.3}$$

$$\frac{dNH_4^+}{dt} = NH_{4,in}^+\frac{Q_{in}}{V} - NH_4^+\frac{Q_{\text{out}}}{V} - NH_4^+\frac{Q_w}{V} - r_2X \tag{1.4}$$

$$\frac{d\mathrm{NO}_2^-}{dt} = \mathrm{NO}_{2,\text{ in}}^-\frac{Q_{\text{in}}}{V} - \mathrm{NO}_2^-\frac{Q_{\text{out}}}{V} - \mathrm{NO}_2^-\frac{Q_w}{V} - r_3X + \frac{1}{Y_{\mathrm{NH_4/NO_2}}}r_2\mathrm{X} \tag{1.5}$$

$$\frac{d\mathrm{NO}_3^-}{dt} = \mathrm{NO}_{3,\text{ in}}^-\frac{Q_{\text{in}}}{V} - \mathrm{NO}_3^-\frac{Q_{\text{out}}}{V} - \mathrm{NO}_3^-\frac{Q_w}{V} - r_4X + \frac{1}{Y_{\mathrm{NO_2/NO_3}}}r_3X \tag{1.6}$$

$$\frac{dX}{dt} = f_X\,\mathrm{TSS}_{in}\frac{Q_{in}}{V} - X\frac{Q_w}{V} + Y_{X/BOD}r_1X + Y_{X/NH}r_2X - bX \tag{1.7}$$

$$\frac{dTSS}{dt} = (1-f_X)\,\mathrm{TSS}_{in}\frac{Q_{in}}{V} - TSS\frac{Q_{\text{out}}}{V}s_d - TSS\frac{Q_w}{V} \tag{1.8}$$

In those equations, X represents the biomass (mgX/L) of a single microbial population, while V (m^3) denotes the volume of the reactor. Q_{in} holds for the influent flow rate, while the output of the plant is divided into the effluent flow rate Q_{out} and the waste flow rate Q_w. For simplicity, Q_w is assumed to be negligible, resulting in $Q_{out} = Q_{in}$. $BOD_{5,\text{ in}}$, $NH_{4,in}^+, \mathrm{NO}_{2,\text{ in}}^-$, $\mathrm{NO}_{3,\text{ in}}^-$ represents the influent concentration of the biological demand, the ammonia nitrogen, the nitrite and the nitrate, respectively. Similarly, $BOD_5, NH_4^+, \mathrm{NO}_2^-$ and NO_3^- are used to denote the component or its concentration. $Y_{X/BOD}$ and $Y_{X/NH}$ are the yield coefficient for biomass production, whilst $Y_{\mathrm{NO_2/NO_3}}$ and $Y_{\mathrm{NH_4/NO_2}}$ are the yield conversion coefficient for ammonium into nitrites and nitrites into nitrates, respectively. f_X represents the fraction of heterotrophic biomass. The kinetics are described by Monod equations for the consumption of carbon (r_1), the nitrification of ammonia into nitrites (r_2), the nitrification of nitrites into nitrates (r_3), and the denitrification of nitrates into N_2 gas (r_4).

$$r_1 = \mu_{\mathrm{BOD}}^{\max} \frac{\mathrm{BOD}_5}{K_{\mathrm{BOD}} + \mathrm{BOD}_5} \tag{1.9}$$

$$r_2 = \mu_{\mathrm{NH}_4}^{\max} \frac{\mathrm{NH}_4^+}{K_{\mathrm{NH}} + \mathrm{NH}_4^+} \tag{1.10}$$

$$r_3 = \mu_{\mathrm{NO}_2}^{\max} \frac{\mathrm{NO}_2^-}{\mathrm{K}_{\mathrm{NO}_2} + \mathrm{NO}_2^-} \tag{1.11}$$

$$r_4 = \mu_{\mathrm{NO}_3}^{\max} \frac{\mathrm{NO}_3^-}{\mathrm{K}_{\mathrm{NO}_3} + \mathrm{NO}_3^-} \tag{1.12}$$

Here, $\mu_j^{\max}$ where $j = \mathrm{BOD}, \mathrm{NH}_4^+, \mathrm{NO}_2^-, \mathrm{NO}_3^-$ represent the maximum specific rates of the reaction to get j. The parameters K_{BOD}, K_{NH}, K_{NO2} and K_{NO3} are the half saturation coefficients for their respective components. The model is based on daily data over a period of four years (2009-2012) and was calibrated on three data sets of 150 days each. The model was then validated using the remaining data to determine the calibrated parameters presented in Table 1.1.

It is assumed that the biomass concentrations of SEC, SAV and SEG are exogenous parameters. This assumption is justified by the fact that the dynamics of the biomass concentration is typically much slower compared to the dynamic process of the other components and have a larger amplitude. Therefore, treating them as constant values is reasonable. The TSS concentrations are neglected in the model, as it was found in [17] that high values were primarily caused by the high concentrations in the Seine River from Suresnes. These values cannot be significantly improved due to the high flow rate of the Seine River, regardless of the optimization results. Therefore including TSS would only increase the complexity of the model without providing substantial improvements. The model employed in this work is not intended to be descriptive but rather aims to capture the dynamics of substrate concentration in the river during heavy rain and storm events. Thus the following model is used for the rest of this work, with the calibrated values presented in Table 1.1,

$$\frac{dBOD_5}{dt} = BOD_{5,\text{ in}} \frac{Q_{in}}{V} - BOD_5 \frac{Q_{\text{out}}}{V} - r_1 X \tag{1.13}$$

$$\frac{dNH_4^+}{dt} = NH_{4,in}^+ \frac{Q_{in}}{V} - NH_4^+ \frac{Q_{\text{out}}}{V} - r_2 X \tag{1.14}$$

$$\frac{d\mathrm{NO}_2^-}{dt} = \mathrm{NO}_{2,\text{ in}}^- \frac{Q_{\text{in}}}{V} - \mathrm{NO}_2^- \frac{Q_{\text{out}}}{V} - r_3 X + \frac{1}{Y_{\mathrm{NH_4/NO_2}}} r_2 \mathrm{X} \tag{1.15}$$

$$\frac{d\mathrm{NO}_3^-}{dt} = \mathrm{NO}_{3,\text{ in}}^- \frac{Q_{\text{in}}}{V} - \mathrm{NO}_3^- \frac{Q_{\text{out}}}{V} - r_4 X + \frac{1}{Y_{\mathrm{NO_2/NO_3}}} r_3 X \tag{1.16}$$

Parameter	**Unit**	**SEC**	**SAV**	**SEG**
$\mu_{BOD,\text{max}}$	1/d	3.99	2.56	1.93
$\mu_{NH_4,\text{max}}$	1/d	0.84	0.83	0.89
$\mu_{NO_2,\text{max}}$	1/d	1.68	1.27	0.92
$\mu_{NO_3,\text{max}}$	1/d	1.21	1.38	0.85
K_{BOD}	mgO_2/L	13.67	11.65	14.26
K_{NH_4}	$mgNH_4/L$	6.59	14.98	8.53
K_{NO_2}	$mgNO_2/L$	2.46	1.15	2.55
K_{NO_3}	$mgNO_3/L$	1.4	2.69	4.20
$Y_{\mathrm{NH_4/NO_2}}$	$mgNH_4/mgNO_2$	0.28	0.25	0.27
$Y_{\mathrm{NO_2/NO_3}}$	$mgNO_2/mgNO_3$	0.68	0.64	0.67

Table 1.1: Calibrated parameters for the model

WWTP modeling provides a valuable tool to study and optimize the performance of wastewater treatment plants, leading to more efficient and sustainable wastewater treatment processes.

1.4 Model of the river

By simulating the behavior of river, it can gain insights into the transport and dispersion of pollutants, assess water quality, and make informed decisions to protect and preserve these valuable natural resources. The river is considered to be perfectly mixed and it is assumed that the flows are additive. Specifically, the flow rate only increases in relation to the inputs from the WWTPs and the intakes in the Seine. Therefore, the flow rate of the Seine River in Suresnes considered to be the same as the flow rate of the Seine River in Austerlitz, as there is no water input in the Seine between these two measurement points. In this context, there are two aspects to consider: (i) the flow rate and (ii) the concentrations.

Regarding the flow rate, the flow rate at Conflans, point (3) in Figure 1.3, is considered to be equal to the combined flow rate from Sartrouville (2), from the by-passed flow rate and from the treated flow rate at SAV. This relationship can be expressed by the following equation:

$$Q_m = \sum_{f=1}^{m'} Q_f \tag{1.17}$$

where m is the point where the flow rate is calculated, f represents all the elements that contribute water to that point, and m' denotes the number of input to point m.

Concerning the concentrations, the concentration $C_{j,m}$ where $j \in [\mathrm{BOD}_5, \mathrm{NH}_4, \mathrm{NO}_2, \mathrm{NO}_3]$ at Conflans (m=3) can be calculated using the following equation:

$$C_{j,m} = \frac{C_{j,\text{Sartrouville}} \cdot Q_{\text{Sartrouville}} + C_{j,\text{by-passed}} \cdot Q_{\text{by-passed}} + C_{j,\text{treated at SAV}} \cdot Q_{\text{treated at SAV}}}{Q_{\text{Sartrouville}} + Q_{\text{by-passed}} + Q_{\text{treated at SAV}}}$$

Hence the concentration $C_{j,m}$ at each measurement point m can be calculated as follows:

$$C_{j,m} = \frac{\sum_{f=1}^{m'} (C_{j,f} \cdot Q_f)}{\sum_{f=1}^{m'} (Q_f)} \tag{1.18}$$

where m' represents the number of inputs to the point m.

Overall, river modeling provides a powerful tool for understanding the complex dynamics of rivers, predicting water quality, and making informed decisions to protect and manage these important natural resources in a sustainable manner.

Chapter 2

Convex Optimization

This chapter delves into the theoretical basis of convex optimization and its application to WWTPs network. Convex optimization provides a systematic framework for solving optimization problems with guaranteed global optimality. It starts by a general introduction to convex optimization, covering key concepts and properties. Building upon this foundation, it introduces second-order cones, which extend the concept of convexity to a broader class of optimization problems. Second-order cone programming provides a powerful framework for handling complex constraints and is particularly relevant in the context of wastewater treatment plants. The formulation of a general problem for a WWTP network is presented, incorporating a second-order cone constraint. Finally, the chapter proceeds with a detailed explanation of the alternating direction method of multipliers (ADMM) algorithm, a widely used optimization technique for convex problems. This algorithm is well-suited for solving large-scale problems with complex structures and constraints. It is demonstrated how ADMM can be applied to the general problem formulation for WWTPs network, showcasing its effectiveness in optimizing the operation and performance of these systems. Throughout this chapter, mathematical formulations and practical examples are provided to illustrate the concepts and applications of convex optimization on a general dynamical bioprocess model.

2.1 Overview

The goal is to optimize a model of dynamical bioprocesses, which becomes nonconvex due to the microbial growth occurring in the biochemical reactors. Nonconvex optimization poses challenges in finding optimal solutions. To address this, Taylor et al. [18] formulated a relaxation and proved its exactitude to the nonconvex constraint describing the microbial growth. The relaxation has second-order cone representations for Monod [19] and Contois [20] growth rates, enabling efficient optimization. Additionally, by replacing derivatives with numerical approximations, a second-order cone program is derived, which can be effectively solved at large scales using industrial software such as Gurobi [21] and Mosek [22].

The general problem for the control strategy for a WWTP network involves exhibits biconvexity in the objective function. This biconvexity arises from the presence of flow dividers and the concentration of substrates at the outlets. To handle this bilinearity and solve the optimization problem, the ADMM algorithm is employed. The ADMM algorithm provides an effective approach to handle the biconvexity and optimize the control actions in the WWTP network.

2.2 Convex optimization problem

Convex optimization is a branch of optimization that aims to find the optimal solution for optimization problems by minimizing a convex function over a convex set. The feasible set is defined by a set of inequalities involving convex functions and a set of linear equality constraints [23]. One fundamental property of convex optimization problems is that any locally optimal point is also globally optimal. As a result, several efficient algorithms exist to solve convex optimization problems with a high level of accuracy. A convex optimization problem takes the form:

$$\begin{array}{ll} \text{minimize} & f_0(x) \\ \text{subject to} & f_i(x) \leq 0, \quad i=1,\ldots,m \\ & a_i^T x = b_i, \quad i=1,\ldots,p \end{array} \tag{2.1}$$

where $f_0, \cdots, f_m$ are convex functions. Any vector x that satisfies all the constraints in the problem is said to be feasible and, if a solution to the problem exists, any vector x^* satisfying

$$f_0(x) \geq f_0\left(x^*\right) \tag{2.2}$$

is said to be an optimal solution to the problem. The value $f\left(x^*\right)$ represents the optimal value of the optimization problem. For a convex optimization problem, there are three requirements:

- the objective function f_0 must be convex,

- the functions that determine the inequality constraints $f_1, \cdots, f_m$ must be convex,

- the functions that determine the equality constraints $h_i(x) = a_i^T x - b_i$ must be affine.

Note that an important property is that the feasible set of such a problem is convex, which is a significant property.

2.3 Second-order cone

Conic optimization is a subfield of convex optimization that focuses on solving problems involving the minimization of a convex function over the intersection of an affine subspace and a convex cone, which contains the set of admissible points. A cone is a three-dimensional geometric shape formed by a collection of line segments, half-lines, or lines connecting a common point to all the points on a base. The basic ingredient of a conic optimization is a convex cone. A convex cone is defined as follows [24]:

Definition 2.3.1 *A cone $\mathcal{C}$ is convex if and only if it is closed under addition,*

$$x \in \mathcal{C} \Rightarrow \lambda x \in \mathcal{C} \textit{ for all } \lambda \in \mathbb{R}_+$$

There are various types of convex cones, but this work specifically focuses on the second-order cone (SOC), also known as the Lorentz cone or ice-cream cone, which leads to second-order cone optimization. The second-order cone, denoted as $\mathbb{L}^n$, is defined as follows:

Definition 2.3.2 *The second order cone L^n is the subset of R^{n+1} defined by*

$$\mathbb{L}^n = \left\{(x_0, x_1, \ldots, x_n) \in \mathbb{R}^{n+1} \textit{ such that } x_0 \geq \|(x_1, x_2, \ldots, x_n)\|\right\}$$

where $\|\cdot\|$ denotes the usual Euclidean norm on $\mathbb{R}^n$, and n is the dimension of $\mathbb{L}^n$.

The convex optimization problem (2.3), known as a second-order cone program (SOCP), can be formulated as follows:

$$\begin{array}{ll} \text{minimize} & f^T x \\ \text{subject to} & \|A_i x + b_i\|_2 \leq c_i^T x + d_i, \quad i = 1, \ldots, m \end{array} \tag{2.3}$$

where $x \in \mathbb{R}^n$ is the optimization variable, $A \in \mathbb{R}^{m \times n}$, $b \in \mathbb{R}^m$, $c \in \mathbb{R}^n$ and $d \in \mathbb{R}$ are problem parameters. SOCP problems can be solved in polynomial time using interior point methods. For example, Mosek uses a parallel interior-point algorithm.

The computational effort per iteration required by these methods to solve SOCP problems is greater than that required to solve linear program (LP) but less than that required to solve semidefinite programming (SDP) or similar-sized and structured non-convex problem [25]. A constraint of the form

$$\|Ax + b\| \leq c^T x + d \tag{2.4}$$

is referred to be a standard form SOC constraint where the left-hand side is the two-norm. This constraint is equivalent to requiring the affine function $(Ax+b, c^T x+d)$ where $A \in \mathbb{R}^{k\times n}$ to lie in the second-order cone in $\mathbb{R}^{k+1}$. Note that the constraint reduces to a linear constraint if $A = 0$.

SOCP is a generalization of LP because any linear constraint can be written as a SOC constraint. The SOC is self dual, which means that its dual cone is the SOC itself, i.e. $\mathbb{L}^n = (\mathbb{L}^n)^*$. Therefore, the dual of a SOCP is also a SOCP. The dual problem of the SOCP (2.3) can be expressed as follows:

$$\begin{aligned} \min_{u_i, v_i, i=1,\ldots,m} \quad & \sum_{i=1}^{m} b_i^\top u_i + d_i v_i + g_i w_i \\ \text{subject to} \quad & \sum_{i=1}^{p} A_i^\top u_i + c_i v_i = f \\ & \|u_i\|_2 \leq v_i, \quad i = 1, \ldots, m \end{aligned} \tag{2.5}$$

Strong duality is achieved if the problem is convex and if the constraints qualification holds. It implies that the primal and the dual optimizations have the same objective value.

The constraint $x_1^2 + x_2^2 \leq x_0^2$ is a widely used constraint with SOC form. It can be written as:

$$\left\| \begin{bmatrix} x_1 \\ x_2 \end{bmatrix} \right\| \leq x_0. \tag{2.6}$$

It must also be required that $x_0 \geq 0$.

2.4 Formulation of the general problem

The formulation of the general problem of a WWTP network involves defining the mathematical model and optimization framework to address the operational challenges and objectives of the network. This problem aims to ensure the good chemical quality of the river, as stated in the European WFD (2000/60/EC) [4]. This requires that the concentrations of certain substances, such as biological oxygen demand (BOD_5), ammonium (NH_4^+), nitrites (NO_2^-), and nitrates (NO_3^-), remain below their respective regulation limits.

A dynamical bioprocess model consisting of a set of interconnected biochemical reactors is optimized. Each reactor contains several microbial reactions that convert substrates into biomass and/or products, as described in Section 1.3.

The system consists of n perfectly mixed interconnected tanks. Each tank i has inlet water flow rate $Q_{\text{in},i} \in \mathbb{R}_+$ and an outlet flow rate $Q_{\text{out},i} \in \mathbb{R}_+$. Let $Q_{ih} \in \mathbb{R}_+$ and $d_{ih} \in \mathbb{R}_+$ denote the flow and the diffusion from tank i to tank h, respectively. To model the microbial growth, there are p substrates in each WWTP. $S_i \in \mathbb{R}_+^p$ denotes the substrate concentration vector. Similarly, $S_{in,i} \in \mathbb{R}_+^p$ represents the corresponding influent concentration vector and $\dot{S}_i \in \mathbb{R}^q$ represents the dynamic process states. There are r different types of reactions that convert substrates to other substrates, and $\phi_i(S_i) \in \mathbb{R}_+^r$ is a vector representing the reaction kinetics in tank i. The basic optimization problem is:

$$
\begin{aligned}
&\min_{S,Q_{in}T} \mathcal{F}(S,T) \\
&\text{s.t. } T_i^i = \phi_i\left(S_i\right) && (2.7) \\
&\quad V_i\dot{S}_i = V_i\kappa_i T_i - Q_{out,i}S_i - \sum_h \left(Q_{ih} + d_{ih}\right) S_i \\
&\qquad\quad + Q_{in,i}S_{in,i} + \sum_h \left(Q_{hi} + d_{hi}\right) S_h && (2.8) \\
&\quad i, h = 1, 2, \ldots n && (2.9) \\
&\qquad (S, Q, d) \in \Omega && (2.10)
\end{aligned}
$$

where $V_i \in \mathbb{R}_+$ stands for volume of the tank i, and κ_i is the stoichiometric matrix.

The flows and the diffusion between tanks are not considered as decision variables, hence (2.8) is linear. The set Ω in (2.10) consists of linear constraints, such as the initial condition, total input matter and the maximum substrate concentration. The only non-convex function is therefore (2.7), which represents the growth constraint. To obtain a convex relaxation, a SOC relaxation of this constraint can be constructed, as described in [18]. If all the elements of the vector $\phi(\cdot)$ are concave functions, a convex relaxation is obtained by replacing (2.7) with the inequality:

$$T(t) \leq \phi(S_i(t)) \qquad (2.11)$$

The focus lies on situations where (2.11) is concave and can be expressed as SOC constraints. This is the case for some growth rates, therefore the growth rate that will be used in the rest of the work is Monod growth rate [19]. With Monod growth rate, the constraint (2.11) takes the form:

$$T(t) \leq \frac{\mu^{max} S(t) X(t)}{K + S(t)} \tag{2.12}$$

where $X(t)$ represents the concentration of the biomass, assumed to be constant as discussed in Section 1.3. Under this assumption (2.12) is a convex constraint because the right-hand side, the Monod function, is concave. Therefore (2.12) is equivalent to the hyperbolic constraint:

$$\hat{S}(t)^2 + \hat{T}(t)^2 \leq \left(\hat{S}(t) - \hat{T}(t)\right)\left(2\mu^{\max} K X(t) + \hat{S}(t) - \hat{T}(t)\right) \tag{2.13}$$

$$0 \leq \hat{S}(t) - \hat{T}(t) \tag{2.14}$$

where $\hat{S}(t) = \mu^{\max} S(t) X(t)$ and $\hat{T}(t) = KT(t), t \in \mathcal{T}$. Note that (2.14) ensures the non-negativity of both multiplicative terms on the right-hand side of (2.13) and it is implied by (2.12). This can be shown by straightforward calculations.

To demonstrate the equivalence between (2.12) and (2.13), follow the given steps:

Multiply both sides of (2.12) by $K + S(t)$ and move everything to the right-hand side

$$0 \leq \mu^{max} S(t) X(t) - KT(t) - S(t)T(t)$$

Multiply both sides by $2\mu K X(t)$

$$0 \leq 2(\mu^{max})^2 S(t) K X(t)^2 - 2\mu^{max} K^2 T(t) X(t) - 2\mu K X(t) S(t) T(t)$$

Add $(\mu^{\max} S(t) X(t))^2 + (KT(t))^2$ to both sides

$$\begin{aligned}(\mu^{\max} S(t) X(t))^2 + (KT(t))^2 \leq{}& (\mu^{\max} S(t) X(t))^2 + (KT(t))^2 + 2(\mu^{max})^2 S(t) K X(t)^2 \\ & - 2\mu^{max} K^2 T(t) X(t) - 2\mu K X(t) S(t) T(t)\end{aligned}$$

Factorize the right-hand side

$$
\begin{aligned}
(\mu^{\max} S(t)X(t))^2 + (KT(t))^2 \leq {} & (\mu^{\max} S(t)X(t) - KT(t)) \\
& (2\mu^{\max} KX(t) + \mu^{\max} S(t)X(t) - KT(t))
\end{aligned}
$$

Denote $\hat{S}(t) = \mu^{\max} S(t)X(t)$ and $\hat{T}(t) = KT(t)$, which leads to the following result

$$
\hat{S}(t)^2 + \hat{T}(t)^2 \leq \left(\hat{S}(t) - \hat{T}(t)\right)\left(2\mu^{\max} KX(t) + \hat{S}(t) - \hat{T}(t)\right)
$$

This demonstrates the equivalence between (2.12) and (2.13).

Now to demonstrate that (2.13) can be written in standard SOC form as in Section 2.3, follow the given steps:

Distribute first the right-hand side of the inequality

$$
\begin{aligned}
\hat{S}(t)^2 + \hat{T}(t)^2 &\leq \left(\hat{S}(t) - \hat{T}(t)\right)\left(2\mu^{\max} KX(t) + \hat{S}(t) - \hat{T}(t)\right) \\
\hat{S}(t)^2 + \hat{T}(t)^2 &\leq 2\hat{S}(t)\mu^{\max} KX(t) + \hat{S}(t)^2 - \hat{T}(t)\hat{S}(t) \\
&\quad - 2\hat{T}(t)\mu^{\max} KX(t) - \hat{T}(t)\hat{S}(t) + \hat{T}(t)^2
\end{aligned}
$$

Reorder and add $(\mu^{\max} KX(t))^2$ on both sides

$$
\begin{aligned}
\hat{S}(t)^2 + \hat{T}(t)^2 + (\mu^{\max} KX(t))^2 \leq {} & \hat{S}(t)^2 + \hat{T}(t)^2 + (\mu^{\max} KX(t))^2 \\
& + 2(\hat{S}(t)\mu^{\max} KX(t) - \hat{T}(t)\hat{S}(t) - 2\hat{T}(t)\mu^{\max} KX(t))
\end{aligned}
$$

Identify the formula $(a + b - c)^2 = a^2 + b^2 + c^2 + 2(ab - bc - ca)$ and simplify

$$
\hat{S}(t)^2 + \hat{T}(t)^2 + (\mu^{\max} KX(t))^2 \leq (\hat{S}(t) + \hat{T}(t) - (\mu^{\max} KX(t)))^2
$$

This form is similar to the standard SOC form, as seen in Section 2.3

$$
\left\| \begin{bmatrix} \mu^{\max} S(t)X(t) \\ KT(t) \\ \mu_{\max} KX(t) \end{bmatrix} \right\| \leq \mu_{\max} KX(t)^{\mathrm{c}} + \mu^{\max} S(t)X(t) - KT(t). \tag{2.15}
$$

Therefore, it is shown that (2.13) can be written in the standard SOC form.

Knowing that the wastewater treatment plants are not interconnected, assuming Monod growth rate with constant biomass and assuming that the inlet and outlet flow rates of the wastewater treatment plant are equal, i.e. $Q_{in,i} = Q_{out,i} = Q$. The general optimization problem of a WWTP network, taking into account the assumptions mentioned, is as follows:

$$\min_{T,S,y} \sum_i y_i Q S_i \tag{2.16}$$

$$\text{s.t.} \quad \left\| \begin{bmatrix} \mu^{\max} S_i(t) X_i(t) \\ K T_i(t) \\ \mu^{\max} K X_i(t) \end{bmatrix} \right\|_2 \leq \mu^{\max} K X_i(t) + \mu^{\max} S_i(t) X_i(t) - K T_i(t) \tag{2.17}$$

$$V_i \dot{S}_i = V_i \kappa_i T_i(t) - y_i Q(t) S_i(t) + y_i Q(t) S_{i,\text{ in}}(t) \tag{2.18}$$

$$\sum_i y_i = 1 \tag{2.19}$$

$$Q_{\min,i} \leq y_i Q(t) \leq Q_{\max,i} \tag{2.20}$$

where y is the decision variable controlling how the total inflow is divided among each WWTP i. $Q_{\min,i}$ and $Q_{\max,i}$ represent the minimum and the maximum allowable flow rate of WWTP i, respectively.

2.5 Alternating direction method of multipliers algorithm

The bilinear term $y_i S_i$ in the constraint of the general problem introduces non-convexity into the problem. In this work, the bilinearity is handled by employing nonlinear programming to find a local minimum. Specifically, the biconvex structure of the problem is exploited using the Alternating Direction Method of Multipliers (ADMM). Using ADMM, it is possible to update y_i first while keeping S_i constant, then S_i can be updated while keeping y_i constant.

This section presents the theoretical framework associated with the ADMM algorithm. It refers to the book Distributed Optimization and Statistical Learning via the Alternating Direction Method of Multiplier of Boyd et al. [26].

2.5.1 Overview

The ADMM method, although originally proposed in the mid-1970s by Glowinski & Marrocco and Gabay & Mercier, has its roots in similar ideas that emerged in the 1950s. ADMM is closely related or equivalent to many other algorithms, such as dual decomposition [27], the method of multipliers [28], Dykstra's alternating projections [29], and others. Two optimization algorithms that are precursors to ADMM are the dual ascent and the method of multipliers. ADMM aims to combine the decomposability of dual ascent with the superior convergence properties of the method of multipliers. The key idea behind ADMM is to break down a complex optimization problem into smaller, more manageable subproblems. It is a simple but powerful algorithm. ADMM has found applications in various fields, including machine learning, signal processing, image reconstruction, and distributed optimization. The algorithm follows a decomposition-coordination procedure in which the solutions to smaller subproblems are coordinated to obtain a solution to a larger global problem. This decomposition-coordination approach allows for parallel and distributed computation, making ADMM particularly suitable for large-scale distributed convex optimization.

2.5.2 Theory

The algorithm follows an iterative process, where at each iteration, it updates the variables of the subproblems in a coordinated manner. These updates involve minimizing augmented Lagrangian functions, which combine the original objective function with penalty terms related to the constraints. The ADMM iterations continue until convergence, typically measured by the satisfaction of certain stopping criteria.

The algorithm aims to solve problems in the form

$$\begin{array}{ll} \text{minimize} & f(x) + g(z) \\ \text{s.t.} & Ax + Bz = c \end{array} \tag{2.21}$$

where the variables are $x \in \mathbb{R}^n$ and $z \in \mathbb{R}^m$. Where $A \in \mathbb{R}^{p \times n}$, $B \in \mathbb{R}^{p \times m}$, and $c \in \mathbb{R}^p$. The objective function is separable with respect to x and z. The augmented Lagrangian function is defined as:

$$L_\rho(x, z, y) = f(x) + g(z) + y^T(Ax + Bz - c) + (\rho/2)\|Ax + Bz - c\|_2^2$$

The ADMM algorithm for problem (2.21) consists of the iterations:

$$x^{k+1} := \underset{x}{\operatorname{argmin}} \quad L_\rho \left(x, z^k, y^k\right) \tag{2.22}$$

$$z^{k+1} := \underset{z}{\operatorname{argmin}} \quad L_\rho \left(x^{k+1}, z, y^k\right) \tag{2.23}$$

$$y^{k+1} := y^k + \rho \left(Ax^{k+1} + Bz^{k+1} - c\right) \tag{2.24}$$

where the penalty parameter $\rho > 0$. The algorithm involves an x-minimization step (2.22), a z-minimization step (2.23), and a dual variable update (2.24). The variables x and z are updated alternately. The state of the algorithm consists of z^k and y^k, while the variable x^k is not part of the state as it is computed from the previous state (z^{k-1}, y^{k-1}). It is worth noting that this form is the unscaled form.

The scaled form of ADMM is more convenient and can be written in a slightly different manner:

$$x^{k+1} := \underset{x}{\operatorname{argmin}} \left(f(x) + (\rho/2)\|Ax + Bz^k - c + u^k\|_2^2\right) \tag{2.25}$$

$$z^{k+1} := \underset{z}{\operatorname{argmin}} \left(g(z) + (\rho/2)\|Ax^{k+1} + Bz - c + u^k\|_2^2\right) \tag{2.26}$$

$$u^{k+1} := u^k + Ax^{k+1} + Bz^{k+1} - c \tag{2.27}$$

where u represents the scaled dual variable. Both forms of ADMM, the scaled and unscaled, are equivalent, but the formulas in the scaled form are often shorter and more concise. The algorithm is given in Algorithm 1.

Algorithm 1 Alternating Direction Method of Multipliers

1: **Input:** functions f and g, matrices A and B, vector c, parameter ρ
2: Initialize x^0, z^0, u^0
3: **repeat**
4: $\quad x^{k+1} = \underset{x}{\operatorname{argmin}} f(x) + \frac{\rho}{2}\|Ax + Bz^k - c + u^k\|_2^2$
5: $\quad z^{k+1} = \underset{z}{\operatorname{argmin}} g(z) + \frac{\rho}{2}\|Ax^{k+1} + Bz - c + u^k\|_2^2$
6: $\quad u^{k+1} = u^k + Ax^{k+1} + Bz^{k+1} - c$
7: **until** meet stopping criterion

As proven by Boyd et al., the ADMM iterations exhibit residual convergence, objective convergence, and dual variable convergence. This implies that the ADMM algorithm does converge, although it can be relatively slow to achieve high accuracy, as it can be shown by simple examples. ADMM typically converges within a few dozen iterations, making it practically useful, especially in scenarios where modest accuracy is sufficient. This is particularly relevant for large-scale problems where achieving high precision may not be necessary.

2.5.3 Formulation of the general problem with ADMM

ADMM is applied to the general problem (2.16) - (2.20) using forward Euler method to approximate the derivatives. The first step is to update y, which is the decision variable controlling how the total inflow is divided among each tank. This step solves y that minimize the objective function $\sum_i y_i Q S_i^k$ along with a penalty term related to the constraint. The constraint equation C_i is the residual that represents the dynamics of each tank. The second step is to update the states variables S, X and T. This optimization problem ensures that the state variables satisfy the system dynamics and other constraints. The constraint equation C_i is the same as in the previous step. In the last step, the dual variable U is updated by adding the residual term C_i. The residual C_i accounts for the mismatch between the predicted and actual values of the dynamics equation in each tank. The algorithm proceeds iteratively, repeating steps 1-3 until convergence. Convergence is typically determined by satisfying a certain stopping criterion.

1. Solve

$$y_i^{k+1} = \underset{y}{\operatorname{argmin}} \sum_i y_i Q S_i^k + \frac{\rho}{2} \left\| C + U_i^k \right\|_2^2 \tag{2.28}$$

$$\begin{aligned} \text{s.t. } C_i &= V_i \left(-S_i^k(t+1) + S_i^k(t) \right) + V_i \kappa_i T_i^k(t) \\ &\quad - y_i Q(t) S_i^k(t) + y_i Q(t) S_{\text{ in },i}(t) \end{aligned} \tag{2.29}$$

$$\sum_i y_i = 1 \tag{2.30}$$

$$Q_{\min,i} \leq y_i Q(t) \leq Q_{\max,i} \tag{2.31}$$

2. Solve

$$\left(S_i^{k+1}, X_i^{k+1}, T_i^{k+1}\right) = \underset{S,X,T}{\operatorname{argmin}} \sum_i y_i^{k+1} Q S_i + \frac{\rho}{2} \left\| C + U_i^k \right\|_2^2 \tag{2.32}$$

$$\text{s.t. } C_i = V_i \left(-S_i(t+1) + S_i(t)\right) + V_i \kappa_i T_i(t)$$
$$- y_i^{k+1} Q(t) S_i(t) + y_i^{k+1} Q(t) S_{in,i}(t) \tag{2.33}$$

$$\left\| \begin{bmatrix} \mu^{\max} S_i X_i \\ K T_i \\ \mu^{\max} K X_i \end{bmatrix} \right\|_2 \leq \mu^{\max} K X_i + \mu^{\max} S_i X_i - K T_i \tag{2.34}$$

$$S(0) = S_{\text{initial}} \tag{2.35}$$

$$S, T \geq 0 \tag{2.36}$$

3. Set

$$U_i^{k+1} = U_i^k + C_i \tag{2.37}$$

where

$$C_i(t) = V_i \left(-S_i^{k+1}(t+1) + S_i^{k+1}(t)\right) + V_{\kappa i} T_i^{k+1} \tag{2.38}$$

$$- y_i^{k+1} Q(t) S_i^{k+1}(t) + y_i^{k+1} Q(t) S_{in,i}(t) \tag{2.39}$$

where C_i is residual containing the dynamics of the WWTP i and U_i^k is the running sum of the residual at iteration k.

Chapter 3

Model Implementation

This chapter provides a comprehensive overview of implementing the convex optimization problem for the wastewater treatment network. It covers essential aspects of model implementation, highlighting the steps and methodologies required to bring the model to life. The chapter begins by establishing the objective and parameters of the convex optimization problem and presenting a time discretization approach. It leads to the formulation of the convex optimization problem, which solves the model of the wastewater treatment plants network introduced in Section 1. Next, the chapter delves into the detailed formulation of the ADMM algorithm applied to the convex optimization problem. The ADMM algorithm is explained and it presents the initial conditions and the stopping criteria. Finally, the chapter provides insights into the structure of the code used for implementing the model. The implementation is carried out using Matlab [30], leveraging its advantages such as excellent data visualization capabilities and a user-friendly graphical interface. By providing practical insights and guidelines, this chapter aims to enhance the understanding of the convex optimization problem and the nuances involved in implementing the model.

3.1 Formulation of the problem

3.1.1 Objective

In 2000, the Water Framework Directive (WFD) (2000/60/EC) [4] was introduced, imposing the requirement for European member states to achieve a good chemical and ecological state of their surface and groundwater by 2015. This means that one of the main challenges in the field of water management is to maintain water quality at the good status, as defined by the WFD. Therefore the WFD and its incorporation into the French law [31] (the methods and criteria for assessing the ecological status, chemical status and ecological potential of surface waters) established the ecological classes states for water bodies and specify the limits that need to be achieved in France. The assigned class states range from 'High' to 'Bad' and are determined based on the biological, physico-chemical quality, and the hydromorphology. The class states limits of the Seine River quality are calculated from the 90 percentile of the concentrations present in the river on two consecutive years and are presented in Table 3.1.

Substrates	Classes state limits				
	High	Good	Moderate	Poor	Bad
BOD_5 [mgO_2/L]	3	6	10	25	
NH_4^+ [mgNH_4/L]	0.1	0.5	2	5	
NO_2^- [mgNO_2/L]	0.1	0.3	0.5	1	
NO_3^- [mgNO_3/L]	10	50	-	-	

Table 3.1: Classification of the Seine quality according to the concentrations of the different substrate in an observation point

The main objective of the control strategy is to guarantee that the chemical quality of the river is at least in class state 'Good'. This requires keeping the concentrations of biological oxygen demand (BOD_5), ammonium (NH_4^+), nitrites (NO_2^-), and nitrates (NO_3^-) below their respective 'Good' limits references. The goal of the model is thus to minimize the substrates concentration entering the Seine River. To achieve this, there are four flow dividers in the network located in Clichy-LaBriche and before each of the three WWTPs. The first flow divider, denoted as y_i, minimizes the total pollutant outflow by determining the allocation of flow rate to each treatment unit i. The flow divider before SEC, denoted as α, decides the portion of the flow rate to be treated by SEC (α_1), by-passed (α_2), sent to SAV (α_3), and sent to SEG (α_4). Similarly, the flow divider before SAV , denoted as β, divides the flow rate between treated by SAV (β_1) and by-passed (β_2). Lastly, the flow divider γ determines the amount of flow rate to be treated by SEG (γ_1) and to be by-passed (γ_2). The decision variables $y, \alpha, \beta, \gamma \in [0, 1]$ represents a fraction of the flow rate and control the division of wastewater to minimize the total pollutant outflow.

The objective is therefore:

$$\begin{aligned}\min_{T,S,y,\alpha,\beta,\gamma} \; & \alpha_1 Q_{in,SEC} S_{SEC}\eta + \alpha_2 Q_{in,SEC} S_{in,SEC}\eta \\ & + \beta_1 Q_{in,SAV} S_{SAV}\eta + \beta_2 Q_{in,SAV} S_{in,SAV}\eta \\ & + \gamma_1 Q_{in,SEG} S_{SEG}\eta + \gamma_2 Q_{in,SEG} S_{in,SEG}\eta\end{aligned} \tag{3.1}$$

where $S_i = \left[BOD_5, \mathrm{NH}_4^+, \mathrm{NO}_2^-, \mathrm{NO}_3^-\right]$ represents the substrate concentration vector and $Q_{in,i}$ denotes the influent flow rate of each WWTP i, respectively. For this work, $i \in [SEC, SAV, SEG]$ corresponds to the WWTPs: SEC refers to the Seine Centre treatment plant, SAV represents the Seine Aval treatment plant, and SEG denotes the Seine Grésillons treatment plant. The vector $\eta = [0.1, 2, 0.3, 0.1]$ is used to select the entries of S_i. The choice of η is explained in Section 3.1.3 where the parameters are discussed.

3.1.2 Discretization in time

To ensure that the system dynamical equations (2.18) are compatible with finite-dimensional optimization, the derivative can be approximated by the forward Euler method. By introducing a time step Δ, the numerical approximation of the derivative is given by:

$$\dot{S} = \frac{S(t+1) - S(t)}{\Delta} \tag{3.2}$$

where $S = [S_{SEC}, S_{SAV}, S_{SEG}]$.

All input parameters are scaled to 15 minutes, so Δ is set to 1. The time periods are indexed as $t \in \mathcal{T} = \{1, \cdots, \tau\}$. Thus, the dynamical equation vector format for each WWTP i derived from (2.18) can be expressed as:

$$\begin{aligned} V_i \left(S_i(t+1) - S_i(t)\right) = V_i \kappa_i T_i(t) - y_i Q_i(t) S_i(t) \\ + y_i Q_i(t) S_{in,i}(t)\end{aligned} \tag{3.3}$$

3.1.3 Parameters

In the context of a WWTP network, various parameters are considered to describe and model the system. These parameters capture the physical, chemical, and operational aspects of the WWTP network and are essential for understanding, optimizing, and ensuring the model's accuracy in reflecting the real-world behavior of the system.

Three scenarios are defined to evaluate the model, each spanning a period of two weeks:

- (1) Dry weather, consisting of two consecutive weeks of dry conditions (Figure 3.1a)
- (2) Rain weather, characterized by one week of dry weather followed by a long rain event during the second week (Figure 3.1b)
- (3) Storm weather, featuring one week of dry weather and two storm events superimposed on the dry weather data within the second week (Figure 3.1c)

The selection of wet periods (2) and (3) was motivated by the desire to assess the model's performance and behaviour under extreme events. The influent data shown in Figures 3.1 and 3.2 are obtained from the Benchmark Simulation Model no. 1 (BSM1) [32] adapted for the three WWTPs using the measurements from MOCOPEE covering the period from January the 1st, 2009 to December the 31st, 2012. The measurements are taken daily.

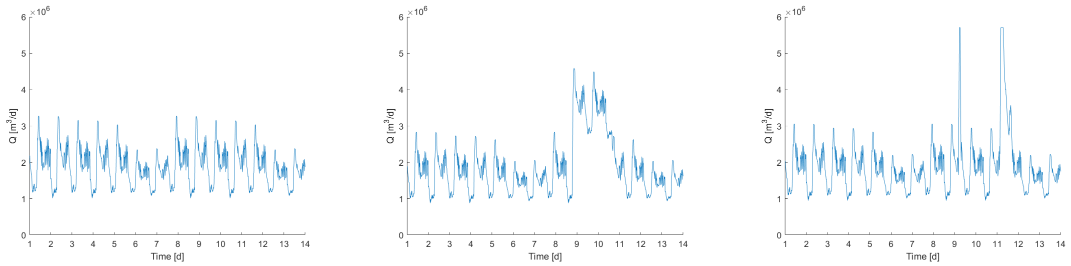

(a) Dry weather (b) Rain weather (c) Storm weather

Figure 3.1: Total inlet flow rate at Clichy for the three scenarios

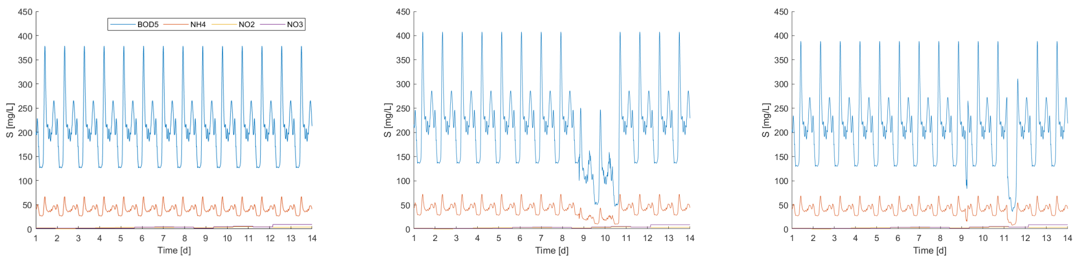

(a) Dry weather (b) Rain weather (c) Storm weather

Figure 3.2: Inlet substrate at Clichy for the three scenarios

It can be observed on Figure 3.2 that during a rainy or a stormy event, the pollutant concentrations decrease as the wastewater mixes with the rainwater, which is less concentrated in substrates compared to wastewater. The influent data exhibits a periodic pattern with a one-day cycle. Figure 3.1 illustrates that the wastewater volume is lower on weekends, specifically on days 6 and 7, and on days 13 and 14.

The substrate concentrations at the measurement point in the Seine River before the WWTPs are also derived from the MOCOPEE data. These concentrations are measured every 7 days and assumed to remain constant within the measured time interval. The corresponding data is depicted in Figure 3.3. The flow rate at the observation points is computed using the Equation (1.17), while the flow rates of the Seine River at Austerlitz and the Oise River when it flows into the Seine are provided on a daily basis. The flow rate at Suresnes, the measurement point before the WWTPs, is assumed to be identical to the flow rate at Austerlitz since there are no water inputs in the Seine between these two points.

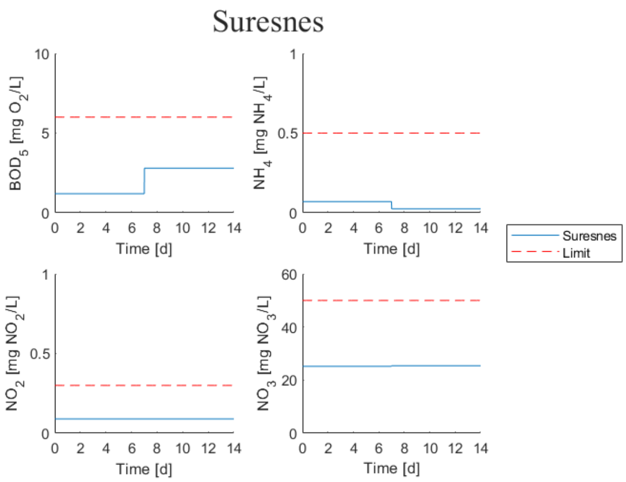

Figure 3.3: State of the Seine River at Suresnes, before the WWTPs.

The biomass concentration is assumed to be constant at 1400 mg/L for all WWTPs. For SAV, since the nitrite and nitrate concentrations are not provided, they are assumed to remain constant over the two-week period and are both set to 0 mg/L. This is because the presence of nitrite and nitrate in SAV is only due to nitrification and denitrification processes that occur within the wastewater treatment plant. For SEC and SEG, the nitrite and nitrate concentrations are obtained from the data file and are assumed to be constant within a single day (Figure 3.2).

The minimum required flow rate into the reactors is set at 1% of the maximum allowable flow rate, which is specified in their respective technical file [12] [13] [14]. The maximum allowable flow rates for SEC, SAV and SEG are 400000 m^3/d, 2900000 m^3/d and 315000 m^3/d, respectively. The volume of their reactor is 20600 m^3, 163300 m^3 and 29680 m^3, respectively.

The stoichiometric matrix κ_i relating the reaction vector to the evolution of the process state in WWTP i is given by:

$$\kappa_i = \begin{bmatrix} -1 & 0 & 0 & 0 \\ 0 & -1 & 0 & 0 \\ 0 & \frac{1}{Y_{\mathrm{NH}_4/\mathrm{NO}_2,i}} & -1 & 0 \\ 0 & 0 & \frac{1}{Y_{\mathrm{NO}_2/\mathrm{NO}_3,i}} & -1 \end{bmatrix}$$

where the yield conversion coefficients, $Y\mathrm{NH}_4/\mathrm{NO2}, i$ and $Y\mathrm{NO}_2/\mathrm{NO}_3, i$, are specific to each WWTP i and are provided in Table 1.1. Additionally, this table provides the half-saturation coefficients, $K_{i,j}$, and the maximum specific rates of the reaction, $\mu_{i,j}^{\max}$, for each substrate j and WWTP i. These values are essential for characterizing the substrate utilization and reaction kinetics in the wastewater treatment process. Throughout the work, the index j represents the substrate, taking values from 1 to 4, corresponding to BOD_5, NH_4^+, NO_2^-, and NO_3^-, respectively.

The vector η is set as [0.1, 2, 0.3, 0.1], which serves as a selection vector for the entries of S_i. It determines the relative importance or weighting of the different substrates in the system. The specific choice of the values in η for BOD_5 and NO_3^- is based on experimental data [17], which indicated that BOD_5 and NO_3^- concentrations were below their corresponding good limits. Therefore, the focus was placed on NH_4^+ and NO_2^-. The values in η were selected such that the convex approximation of microbial growth follows the Monod growth rate. This choice helps ensure that the optimization model accurately represents the dynamics of the microbial processes.

3.1.4 Formulation of the problem

The convex optimization control strategy aims to optimize the distribution of wastewater among the WWTPs with the objective of minimizing the concentration of substrates entering the Seine River. The problem is formulated by considering the parameters and implementing time discretization to effectively capture the dynamics of the system. Furthermore, a convex approximation is utilized to model microbial growth, employing a SOC constraint. The problem can be described as follows:

$$
\begin{aligned}
\min_{T,S,\alpha,\beta,\gamma} \ & \alpha_1(t)Q_{in,SEC}(t)S_{SEC}(t)\eta + \alpha_2(t)Q_{in,SEC}(t)S_{in,SEC}(t)\eta \\
& + \beta_1(t)Q_{in,SAV}(t)S_{SAV}(t)\eta + \beta_2(t)Q_{in,SAV}(t)S_{in,SAV}(t)\eta \\
& + \gamma_1(t)Q_{in,SEG}(t)S_{SEG}(t)\eta + \gamma_2(t)Q_{in,SEG}(t)S_{in,SEG}(t)\eta \\
\text{s.t.} \ & \left\| \begin{bmatrix} \mu_i^{\max} S_i(t)X_i(t) \\ KT_i(t) \\ \mu_i^{\max} KX_i(t) \end{bmatrix} \right\|_2 \leq \mu_i^{\max} KX_i(t) + \mu_i^{\max} S_i(t)X_i(t) - KT_i(t) && (3.4) \\
& T_i(t) \geq TL_i(t) + (TU_i(t) - TL_i(t)) \frac{S_i(t) - S_{min,i}(t)}{S_{max,i}(t) - S_{min,i}(t)} && (3.5) \\
& V_{SEC}\left(S_{SEC}(t+1) - S_{SEC}(t)\right) = V_{SEC}\kappa_{SEC}T_{SEC}(t) \\
& \qquad - \alpha_1(t)Q_{in,SEC}S_{SEC}(t) + \alpha_1(t)Q_{in,SEC}S_{in,SEC}(t) && (3.6) \\
& V_{SAV}\left(S_{SAV}(t+1) - S_{SAV}(t)\right) = V_{SAV}\kappa_{SAV}T_{SAV}(t) \\
& \qquad - \beta_1(t)Q_{in,SAV}S_{SAV}(t) + \beta_1(t)Q_{in,SAV}S_{in,SAV}(t) && (3.7) \\
& V_{SEG}\left(S_{SEG}(t+1) - S_{SEG}(t)\right) = V_{SEG}\kappa_{SEG}T_{SEG}(t) \\
& \qquad - \gamma_1(t)Q_{in,SEG}S_{SEG}(t) + \gamma_1(t)Q_{in,SEG}S_{in,SEG}(t) && (3.8) \\
& Q_{in,SEC}(t) = y_1(t-d_1)Q(t-d_1) && (3.9) \\
& Q_{in,SAV}(t) = y_2(t-d_2)Q(t-d_2) + \alpha_3(t-d_3)Q_{in,SEC}(t-d_3) && (3.10) \\
& Q_{in,SEG}(t) = y_3(t-d_4)Q(t-d_4) + \alpha_4(t-d_5)Q_{in,SEC}(t-d_5) && (3.11) \\
& \sum_{l=1}^{3} y_l(t) = 1 && (3.12) \\
& \sum_{l=1}^{4} \alpha_l(t) = 1 && (3.13) \\
& \sum_{l=1}^{2} \beta_l(t) = 1 && (3.14) \\
& \sum_{l=1}^{2} \gamma_l(t) = 1 && (3.15) \\
& Q_{\min,SEC} \leq \alpha_1(t)Q_{in,SEC}(t) \leq Q_{\max,SEC} && (3.16) \\
& Q_{\min,SAV} \leq \beta_1(t)Q_{in,SAV}(t) \leq Q_{\max,SAV} && (3.17) \\
& Q_{\min,SEG} \leq \gamma_1(t)Q_{in,SEG}(t) \leq Q_{\max,SEG} && (3.18) \\
& S(t), T(t) \geq 0 && (3.19) \\
& y(t), \alpha(t), \beta(t), \gamma(t) \geq 0 && (3.20) \\
& i \in [SEC, SAV, SEG], t \in \mathcal{T} && (3.21)
\end{aligned}
$$

Note that (3.4) - (3.8) represent the plant dynamical equations, where X_i is the constant biomass concentration, V_i is the volume of each treatment plant i, and κ_i is the stoichiometric matrix relating the reaction vector to the evolution of the process state in WWTP i. Inequality (3.4) is the convex relaxation on the growth constraint written as a SOC constraint as described in Section 2.3. Since the reaction rates with the Monod model and constant biomass are concave, the convex relaxation is given by:

$$T_i(t) \leq \begin{bmatrix} \mu_{i,BOD_5}^{max}\left(\frac{BOD_5(t)}{K_{BOD_5}+BOD_5(t)}\right)X_i(t) \\ \mu_{i,\mathrm{NH_4}}^{max}\left(\frac{\mathrm{NH_4}^+(t)}{K_{\mathrm{NH_4}}+\mathrm{NH_4}^+(t)}\right)X_i(t) \\ \mu_{i,\mathrm{NO_2}}^{max}\left(\frac{\mathrm{NO_2}^-(t)}{K_{\mathrm{NO_2}}+\mathrm{NO_2}^-(t)}\right)X_i(t) \\ \mu_{i,\mathrm{NO_3}}^{max}\left(\frac{\mathrm{NO_3}^-(t)}{K_{\mathrm{NO_3}}+\mathrm{NO_3}^-(t)}\right)X_i(t) \end{bmatrix}$$

This convex relaxation ensures that the model captures the dynamics of microbial growth within the constraints of the Monod model, allowing for efficient optimization of the wastewater treatment process.

The inequality (3.5) ensures that the approximation is close to the Monod growth rate, where $TL_i(t)$ and $TU_i(t)$ are defined as:

$$TL_i(t) = \frac{\mu_i^{max} S_{min,i} X_i(t)}{K_i + S_{min,i}}$$
$$TU_i(t) = \frac{\mu_i^{max} S_{max,i} X_i(t)}{K_i + S_{max,i}}$$

where $S_{min,i} = [0, 0, 0, 0]$ and $S_{max,i} = [200, 50, 100, 150]$ $\forall i \in [SEC, SAV, SEG]$. These values define the lower and upper limits for the substrate concentrations.

The constraints (3.9) - (3.11) ensure the conservation of flow rates accounting for the delays d_1 from Clichy to SEC, d_2 from Clichy to SAV, d_3 from SEC to SAV, d_4 from Clichy to SEG, and d_5 from SEC to SEG (as computed in Table 3.2). The total inlet flow rate at Clichy is denoted as Q. The inclusion of delays accounts for the hydraulic response time in the system.

To simplify the optimization process, normalized flow variables are introduced as shown in Figure 1.3. These variables are defined as:

$$
\begin{aligned}
y_1(t) &= Q_{in,SEC}(t)/Q(t)\\
y_2(t) &= Q_{in,SAV}(t)/Q(t)\\
y_3(t) &= Q_{in,SEG}(t)/Q(t)\\
\alpha_1(t) &= Q_{\text{treated,SEC}}(t)/Q_{\text{in,SEC}}(t)\\
\alpha_2(t) &= Q_{\text{by-passed,SEC}}(t)/Q_{\text{in,SEC}}(t)\\
\alpha_3(t) &= Q_{\text{to SAV,SEC}}(t)/Q_{\text{in,SEC}}(t)\\
\alpha_4(t) &= Q_{\text{to SEG,SEC}}(t)/Q_{\text{in,SEC}}(t)\\
\beta_1(t) &= Q_{\text{treated,SAV}}(t)/Q_{\text{in,SAV}}(t)\\
\beta_2(t) &= Q_{\text{by-passed,SAV}}(t)/Q_{\text{in,SAV}}(t)\\
\gamma_1(t) &= Q_{\text{treated,SEG}}(t)/Q_{\text{in,SEG}}(t)\\
\gamma_2(t) &= Q_{\text{by-passed,SEG}}(t)/Q_{\text{in,SEG}}(t)
\end{aligned}
$$

where Q represents the total inlet flow rate at Clichy. The decision variables must satisfy the constraints (3.12) - (3.15).

The allowable nominal flows for each WWTP, denoted as $Q_{\max,i}$ and $Q_{\min,i}$, must be respected. Therefore, the inlet flow rate of each WWTP should fall within the range of these maximum and minimum flow rates. This requirement is represented by constraints (3.16) - (3.18).

Furthermore, constraints (3.19)-(3.20) are physical constraints that ensure all variables remain nonnegative.

The objective of solving this problem is to implement a control strategy, which can be achieved through the decision flow variables. The control strategy aims to minimize the concentration of pollutants entering the river, thereby improving the overall water quality of the Seine River.

3.2 ADMM

The problem exhibits a biconvex objective function, as the decision variables (α, β, γ) are multiplied by the state variables (S_i). To address this biconvexity, the problem is solved using the Alternating Direction Method of Multipliers algorithm, which is described in detail in Section 2.5. The ADMM algorithm proves to be an effective approach in handling such biconvex optimization problems. To solve the problem, the ADMM algorithm is executed until it meets the stopping criterion. During each iteration k, the algorithm updates the decision variables based on a series of subproblems. These subproblems involve minimizing the objective function subject to certain constraints, and they are solved using the Mosek solver. By applying the ADMM algorithm with the Mosek solver, the optimization problem is iteratively solved, and the decision variables as well as the states variables are updated to find the optimal solution that minimizes the concentration of pollutants in the Seine River.

3.2.1 Formulation

The ADMM algorithm solves the optimization problem iteratively by updating the decision variables and the state variables. It updates the decision variables α, β, and γ in separate steps, each with its own subproblem. Additionally, the fourth step is to update the variables S and T, where both sets of variables are updated together by solving a subproblem. These subproblems involve optimizing the objective function with respect to a specific set of variables while satisfying the constraints and considering the current values of the other variables. Finally, the Lagrange multipliers are updated based on the updated decision and state variables. The algorithm iteratively updates these variables until it meets the stopping criterion.

1. To update α, solve

$$\begin{aligned}
\alpha^{k+1}(t) = \underset{\alpha}{\operatorname{argmin}} \quad & \alpha_1(t)Q_{in,SEC}(t)S^k_{SEC}(t)\eta + \alpha_2(t)Q_{in,SEC}(t)S_{in,SEC}(t)\eta \\
& + \beta^k_1(t)Q_{in,SAV}(t)S^k_{SAV}(t)\eta + \beta^k_2(t)Q_{in,SAV}(t)S_{in,SAV}(t)\eta \\
& + \gamma^k_1(t)Q_{in,SEG}(t)S^k_{SEG}(t)\eta + \gamma^k_2(t)Q_{in,SEG}(t)S_{in,SEG}(t)\eta + \frac{\rho}{2}\left\|C + U^k\right\|_2^2 \\
\text{s.t. } C_{SEC}(t) &= V_{SEC}\left(-S^k_{SEC}(t+1) + S^k_{SEC}(t)\right) + V_{SEC}\kappa_{SEC}T^k_{SEC}(t) \\
& - \alpha_1(t)Q_{in,SEC}S^k_{SEC}(t) + \alpha_1(t)Q_{in,SEC}S_{in,SEC}(t) \\
C_{SAV}(t) &= V_{SAV}\left(-S^k_{SAV}(t+1) + S^k_{SAV}(t)\right) + V_{SAV}\kappa_{SAV}T^k_{SAV}(t) \\
& - \beta^k_1(t)Q_{in,SAV}S^k_{SAV}(t) + \beta^k_1(t)Q_{in,SAV}S_{in,SAV}(t) \\
C_{SEG}(t) &= V_{SEG}\left(-S^k_{SEG}(t+1) + S^k_{SEG}(t)\right) + V_{SEG}\kappa_{SEG}T^k_{SEG}(t) \\
& - \gamma^k_1(t)Q_{in,SEG}S^k_{SEG}(t) + \gamma^k_1(t)Q_{in,SEG}S_{in,SEG}(t)
\end{aligned}$$

$$
\begin{aligned}
& Q_{in,SAV}(t) = y_2(t-d_2)Q(t-d_2) + \alpha_3(t-d_3)Q_{in,SEC}(t-d_3) \\
& Q_{in,SEG}(t) = y_3(t-d_4)Q(t-d_4) + \alpha_4(t-d_5)Q_{in,SEC}(t-d_5) \\
& \sum_{l=1}^{4} \alpha_l(t) = 1 \\
& Q_{\min,SEC} \le \alpha_1(t)Q_{in,SEC}(t) \le Q_{\max,SEC} \\
& \alpha(t) \ge 0 \\
& t \in \mathcal{T}
\end{aligned}
$$

Then with the updated α, update

$$
S_{in,SAV}(t) = \frac{S_{in,Clichy}(t-d_2)Q_{in,SAV}(t) + S_{in,SEC}(t-d_3)\alpha_3(t-d_3)Q_{in,SEC}(t-d_3)}{Q_{in,SAV}(t) + \alpha_3(t-d_3)Q_{in,SEC}(t-d_3)}
$$

and

$$
S_{in,SEG}(t) = \frac{S_{in,Clichy}(t-d_4)Q_{in,SEG}(t) + S_{in,SEC}(t-d_5)\alpha_4(t-d_5)Q_{in,SEC}(t-d_5)}{Q_{in,SEG}(t) + \alpha_4(t-d_5)Q_{in,SEC}(t-d_5)}
$$

2. To update β, solve

$$
\begin{aligned}
\beta^{k+1} = \underset{\beta}{\operatorname{argmin}} \quad & \alpha_1^{k+1}(t)Q_{in,SEC}(t)S_{SEC}^{k}(t)\eta + \alpha_2^{k+1}(t)Q_{in,SEC}(t)S_{in,SEC}(t)\eta \\
& + \beta_1(t)Q_{in,SAV}(t)S_{SAV}^{k}(t)\eta + \beta_2(t)Q_{in,SAV}(t)S_{in,SAV}(t)\eta \\
& + \gamma_1^{k}(t)Q_{in,SEG}(t)S_{SEG}^{k}(t)\eta + \gamma_2^{k}(t)Q_{in,SEG}(t)S_{in,SEG}(t)\eta + \frac{\rho}{2}\left\| C + U^k \right\|_2^2 \\
\text{s.t. } \; & C_{SAV}(t) = V_{SAV}\left(-S_{SAV}^{k}(t+1) + S_{SAV}^{k}(t)\right) + V_{SAV}\kappa_{SAV}T_{SAV}^{k}(t) \\
& \qquad - \beta_1(t)Q_{in,SAV}S_{SAV}^{k}(t) + \beta_1(t)Q_{in,SAV}S_{in,SAV}(t) \\
& \sum_{l=1}^{2} \beta_l(t) = 1 \\
& Q_{\min,SAV} \le \beta_1(t)Q_{in,SAV}(t) \le Q_{\max,SAV} \\
& \beta(t) \ge 0 \\
& t \in \mathcal{T}
\end{aligned}
$$

3. To update γ, solve

$$\gamma^{k+1} = \underset{\gamma}{\operatorname{argmin}} \quad \alpha_1^{k+1}(t)Q_{in,SEC}(t)S_{SEC}^k(t)\eta + \alpha_2^{k+1}(t)Q_{in,SEC}(t)S_{in,SEC}(t)\eta$$
$$+ \beta_1^{k+1}(t)Q_{in,SAV}(t)S_{SAV}^k(t)\eta + \beta_2^{k+1}(t)Q_{in,SAV}(t)S_{in,SAV}(t)\eta$$
$$+ \gamma_1(t)Q_{in,SEG}(t)S_{SEG}^k(t)\eta + \gamma_2(t)Q_{in,SEG}(t)S_{in,SEG}(t)\eta + \frac{\rho}{2}\left\|C + U^k\right\|_2^2$$
$$\text{s.t. } C_{SEG}(t) = V_{SEG}\left(-S_{SEG}^k(t+1) + S_{SEG}^k(t)\right) + V_{SEG}\kappa_{SEG}T_{SEG}^k(t)$$
$$- \gamma_1(t)Q_{in,SEG}S_{SEG}^k(t) + \gamma_1(t)Q_{in,SEG}S_{in,SEG}(t)$$
$$\sum_{l=1}^{3}\gamma_l(t) = 1$$
$$Q_{\min,SEG} \leq \gamma 1(t)Q_{in,SEG}(t) \leq Q_{\max,SEG}$$
$$\gamma(t) \geq 0$$
$$t \in \mathcal{T}$$

4. To update S and T, solve

$$\left(S^{k+1}, T^{k+1}\right) = \underset{S,T}{\operatorname{argmin}} \quad \alpha_1^{k+1}(t)Q_{in,SEC}(t)S_{SEC}(t)\eta + \alpha_2^{k+1}Q_{in,SEC}(t)S_{in,SEC}(t)\eta$$
$$+ \beta_1^{k+1}Q_{in,SAV}(t)S_{SAV}(t)\eta + \beta_2^{k+1}Q_{in,SAV}(t)S_{in,SAV}(t)\eta$$
$$+ \gamma_1^{k+1}(t)Q_{in,SEG}(t)S_{SEG}(t)\eta + \gamma_2^{k+1}(t)Q_{in,SEG}(t)S_{in,SEG}(t)\eta$$
$$+ \frac{\rho}{2}\left\|C + U^k\right\|_2^2$$
$$\text{s.t. } C_{SEC}(t) = V_{SEC}\left(-S_{SEC}(t+1) + S_{SEC}(t)\right) + V_{SEC}\kappa_{SEC}T_{SEC}(t)$$
$$- \alpha_1^{k+1}Q_{in,SEC}S_{SEC}(t) + \alpha_1^{k+1}Q_{in,SEC}S_{in,SEC}(t)$$
$$C_{SAV}(t) = V_{SAV}\left(-S_{SAV}(t+1) + S_{SAV}(t)\right) + V_{SAV}\kappa_{SAV}T_{SAV}(t)$$
$$- \beta_1^{k+1}Q_{in,SAV}S_{SAV}(t) + \beta_1^{k+1}Q_{in,SAV}S_{in,SAV}(t)$$
$$C_{SEG}(t) = V_{SEG}\left(-S_{SEG}(t+1) + S_{SEG}(t)\right) + V_{SEG}\kappa_{SEG}T_{SEG}(t)$$
$$- \gamma_1^{k+1}Q_{in,SEG}S_{SEG}(t) + \gamma_1^{k+1}Q_{in,SEG}S_{in,SEG}(t)$$
$$\left\|\begin{bmatrix} \mu^{\max}S_i(t)X_i(t) \\ KT_i(t) \\ \mu^{\max}KX_i(t) \end{bmatrix}\right\|_2 \leq \mu^{\max}KX_i(t) + \mu^{\max}S_i(t)X_i(t) - KT_i(t)$$
$$T_i(t) \geq TL_i(t) + (TU_i(t) - TL_i(t))\frac{S_i(t) - S_{min,i}(t)}{S_{max,i}(t) - S_{min,i}(t)}$$
$$S(0) = S_{\text{initial}}$$
$$S(t), T(t) \geq 0$$
$$t \in \mathcal{T}$$

5. Set

$$U^{k+1} = U^k + C$$

where

$$C = [C_{SEC}, C_{SAV}, C_{SEG}]$$

3.2.2 Initial Conditions

In order to compute the first step ($k = 1$), an initial condition is required for each variable.

The variable y^0 is set to be $[0.12, 0.8, 0.08]$ for dry weather and $[0.17, 0.75, 0.08]$ for rain and storm weather. It is assumed to be constant for every time step to decrease the complexity of the problem. The values of y^0 have been determined through trial and error, aiming to optimize the objective of minimizing pollutant levels in the river. Next, the hydraulic response time d is computed thanks to Equation (1.1) based on the average flow rate during the period for each path k. Using the computed response time, the flow rate $Q_{in,SEC}(t)$ and the influent substrate concentrations $S_{in,SEC}(t)$ are computed according to their respective delays.

$$\begin{aligned} Q_{in,SEC}(t) &= y_1(t - d_1)Q(t - d_1) \\ S_{in,SEC}(t) &= S_{in,Clichy}(t - d_1) \end{aligned}$$

To compute α^0, it is checked whether the flow rate $Q_{in,SEC}(t)$ at time t exceeds the maximum flow rate of SEC. Based on this, α^0 is determined as follows:

$$\alpha^0(t) = \begin{cases} [\frac{Q_{\max,SEC}}{Q_{in,SEC}(t)}, 0, \frac{1}{2}\left(1 - \frac{Q_{\max,SEC}}{Q_{in,SEC}(t)}\right), \frac{1}{2}\left(1 - \frac{Q_{\max,SEC}}{Q_{in,SEC}(t)}\right)] & \text{if } Q_{in,SEC}(t) \geq Q_{\max,SEC} \\ [1, 0, 0, 0] & \text{otherwise} \end{cases}$$

Then the hydraulic response time is computed for the path between SEC and SAV as well as between SEC and SEG using the average flow rate, and it is scaled to a unit of 15 minutes. The delays for each path k for each weather conditions are computed in Table 3.2.

			Dry		Rain		Storm	
k	**Path**	**Dist[km]**	$\mathbf{Q}_0[m^3/d]$	**d[min]**	$\mathbf{Q}_0[m^3/d]$	**d[min]**	$\mathbf{Q}_0[m^3/d]$	**d[min]**
1	Clichy to SEC	4.82	$216{\cdot}10^3$	128	$306{\cdot}10^3$	90	$306{\cdot}10^3$	90
2	Clichy to SAV	13.26	$1442{\cdot}10^3$	52	$1351{\cdot}10^3$	56	$1351{\cdot}10^3$	56
3	SEC to SAV	8.45	-	-	$49{\cdot}10^3$	993	$53{\cdot}10^3$	906
4	Clichy to SEG	27.85	$144{\cdot}10^3$	1125	$144{\cdot}10^3$	1125	$144{\cdot}10^3$	1125
5	SEC to SEG	23.27	-	-	$98{\cdot}10^3$	1367	$26{\cdot}10^3$	4993

Table 3.2: Delay of the substrates concentration depending on the path

The influent substrate concentrations and the influent flow rate of SAV and SEG are computed based on the respective delays.

$$
\begin{aligned}
Q_{in,SAV}(t) &= y_2(t-d_2)Q(t-d_2) + \alpha_3(t-d_3)Q_{in,SEC}(t-d_3) \\
S_{in,SAV}(t) &= \frac{S_{in,Clichy}(t-d_2)Q_{in,SAV}(t) + S_{in,SEC}(t-d_3)\alpha_3(t-d_3)Q_{in,SEC}(t-d_3)}{Q_{in,SAV}(t) + \alpha_3(t-d_3)Q_{in,SEC}(t-d_3)} \\
Q_{in,SEG}(t) &= y_3(t-d_4)Q(t-d_4) + \alpha_4(t-d_5)Q_{in,SEC}(t-d_5) \\
S_{in,SEG}(t) &= \frac{S_{in,Clichy}(t-d_4)Q_{in,SEG}(t) + S_{in,SEC}(t-d_5)\alpha_4(t-d_5)Q_{in,SEC}(t-d_5)}{Q_{in,SEG}(t) + \alpha_4(t-d_5)Q_{in,SEC}(t-d_5)}
\end{aligned}
$$

Similarly to compute β^0 it is checked whether the flow rate $Q_{in,SAV}(t)$ at time t exceeds the maximum flow rate of SAV.

$$
\beta^0(t) = \begin{cases} [\frac{Q_{\max,SAV}}{Q_{in,SAV}(t)}, 1 - \frac{Q_{\max,SAV}}{Q_{in,SAV}(t)}] & \text{if } Q_{in,SAV}(t) \geq Q_{\max,SAV} \\ [1,0] & \text{otherwise} \end{cases}
$$

γ^0 is set based on the allowable flow rate and the influent flow rate in SEG at time t.

$$
\gamma^0(t) = \begin{cases} [\frac{Q_{\max,SEG}}{Q_{in,SEG}(t)}, 1 - \frac{Q_{\max,SEG}}{Q_{in,SEG}(t)}] & \text{if } Q_{in,SEG}(t) \geq Q_{\max,SEG} \\ [1,0] & \text{otherwise} \end{cases}
$$

These calculations ensure that the variables α^0, β^0, and γ^0 satisfy the respective conditions based on the flow rates of SEC, SAV, and SEG.

To compute S^0, the process involves two steps. Firstly, the steady-state model is solved by setting the derivatives of the system's dynamics equation to zero, resulting in $S^0(t)$ at time t=0. Secondly, the dynamics formula is applied to update S^0 from time t to t+1 using the following equation:

$$S^0(t+1) = S^0(t) + \frac{Q_{in}S_{in}(t)}{V} - \frac{Q_{in}S^0(t)}{V} + \kappa T^0(t)$$

where

$$T^0(t) = \frac{\mu_{\max} S^0(t) X}{K + S^0(t)}$$

By applying these formulas iteratively, S^0 can be updated at each time step based on the inflow, outflow, and constant biomass contributions, allowing for the simulation of substrate dynamics in the system.

3.2.3 Stopping criterion

The stopping criterion plays a crucial role in determining when to terminate the execution of ADMM algorithm. It provides a condition to assess the convergence of the algorithm and ensure that the solution obtained is sufficiently accurate. The objective of the stopping criterion is to strike a balance between computational efficiency and solution accuracy. If the criterion is too lenient, the algorithm may terminate prematurely, leading to an inaccurate solution. On the other hand, if the criterion is too strict, the algorithm may continue iterations unnecessarily, consuming additional computational resources.

The choice of the stopping criterion therefore depends on the problem and the desired level of accuracy. Consequently, the ADMM algorithm iterates until the difference between the objective value at iteration k+1 and k is smaller than 1% of the objective value at iteration k+1. The penalty parameter ρ in the objective of each subproblem is set to be 0.0002.

This stopping criterion ensures that the algorithm continues to iterate until the objective value converges to a stable solution, where further iterations result in negligible improvements. By monitoring the difference between consecutive objective values, the algorithm can determine when to terminate and consider the solution sufficiently close to the optimal value.

3.3 Code description

Code description provides a detailed explanation and documentation of the implementation of the problem. It aims to provide readers with a clear understanding of how the code functions, its structure, and the logic behind it. The code is divided into three parts:

- **The parameters part:** This section loads all the required data from the benchmark and the data file from MOCOPEE for the WWTPs and for the measurement points in the Seine River. It also sets all the parameters to the specified values in Section 3.1.3.

- **The initialisation part:** Here, all the initial conditions are computed, and the delays, inlet flow rate, and inlet concentration of each WWTP are adjusted based on the initial condition of each variable.

- **The solving part:** This section solves the model by computing the ADMM algorithm until the stopping criterion is met. Following the steps outlined in Section 3.2.1, it updates the variable α, which represents the flow rate distribution at the flow divider before SEC. Then, it updates the variable β, representing the flow distribution at the flow divider before SAV. Next, it updates the variable γ for the distribution of the flow rate before SEG. Finally, it updates the variables S and T, representing the substrate concentrations and growth dynamics, respectively. The code for this part can be found in the programming appendix (Appendix B).

Chapter 4

Results

This chapter is dedicated to presenting the results and evaluating the performance of the convex optimization problem that solves the model with the objective of minimizing the amount of pollutants entering the Seine River. By examining the obtained results and performance metrics, the chapter aims to shed light on the program's capabilities, limitations, and potential areas for improvement. The chapter begins by outlining the methodology employed for evaluating the convex optimization program by establishing two performance criteria. Subsequently, it presents the results obtained from applying the convex optimization program to the network for dry, rainy and storm weather. It includes a detailed analysis of the solutions obtained, highlighting their quality, optimality, and feasibility. The obtained results are compared against the data obtained without convex optimization to provide a meaningful context for evaluation. Furthermore, it is drawn in parallel to a modified objective program in order to meet the requirement of the WFD. Finally, the convex optimization is compared to the control strategy developed by Rodriguez et al. [17] on the same network.

4.1 Performance criteria

In order to evaluate the performance of the control strategy implemented in this work, two new criteria are addressed. The first criterion is computed based on the deviation from the good state limit of each substrate concentration:

$$P_1 = \frac{S_L - \bar{S}}{S_L}$$

where $\bar{S}$ represents the average effluent concentration of the model output at the measurement points and S_L is the corresponding good state limit, both are expressed in [mg/L].

The second criterion measures the gain achieved compared to measurements without using convex optimization, where no control strategy has been applied:

$$P_2 = \frac{\bar{S}_{\text{w/o opti}} - \bar{S}}{\bar{S}_{\text{w/o opti}}}$$

where $\bar{S}$ is the average effluent concentration at the measurement points where the convex optimization has been applied on the wastewater treatment plant network and $\bar{S}_{\text{w/o opti}}$ is the corresponding average concentration at the same measurement point where no optimization has been applied. Both values are expressed in [mg/L]. The measurements without using convex optimization are obtained from the BSM1 data adapted with the data from MOCOPEE for the input, and from the computation of Equations (3.6 - 3.8) for the output of each WWTP.

It is important to note that both criteria can be negative, indicating lower performance. This means that the substrate concentration exceeds the corresponding good state limit or the measurement without optimization. Additionally, for rain and storm weather periods, the performance criteria will be computed only on days with rainfall or storm conditions.

Another approach used to evaluate the performance of the convex optimization is by comparing the mean values of the data computed without convex optimization μ and the simulated data $\bar{\mu}$.

4.2 Results and performance of convex optimization

This section focuses on the presentation and analysis of the results obtained from applying the convex optimization program to the network under different weather conditions: dry, rainy, and stormy. The selection of wet periods allows for studying the behavior of the convex optimization during extreme events. Figure 3.1 illustrates that rain or storm events lead to an increase in the inlet flow rate, while the concentration of substrates decreases (Figure 3.2). To evaluate and compare the performance of the proposed convex optimization, non-optimized data is utilized. This approach aims to highlight the potential outcomes if the convex optimization of the network was implemented during that specific time frame. The convex optimization control strategy calculates the flow rate distribution for each sample time t (15 min).

4.2.1 Dry weather

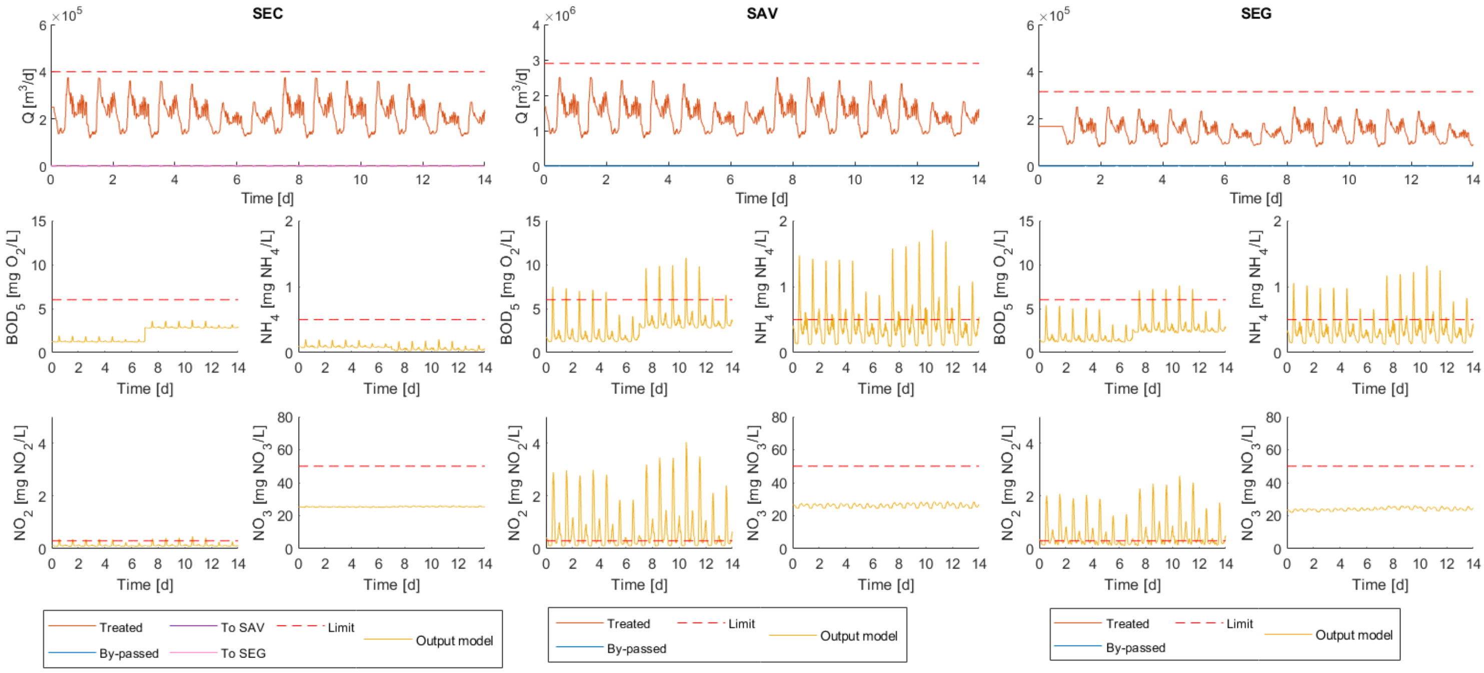

Figure 4.1: Results of the convex optimization during dry weather. The output of the model is obtained at the measurement points after each WWTP: Sartrouville for SEC, Conflans for SAV, and Triel for SEG.

Simulated results for dry weather are depicted in Figure 4.1. It is observed that SEC balances its operation with treating all the incoming wastewater to maintain the concentrations of BOD_5, NH_4^+ and NO_3^- in Satrouville below their respective good limit quality. However, occasional small peaks above the limit are observed for NO_2^- concentration. Regarding SAV, all the incoming water is treated. Data for nitrate are below the limit but the biological demand, ammonium, and nitrite concentrations in Conflans occasionally exceed the limit. Notably, the BOD_5, NH_4^+, NO_2^- concentration show lower averages in Conflans and in Triel between days 5 and 7, as well as between days 12 and 14. This decrease can be attributed to reduced wastewater generation over the weekends when industries operate at a decreased capacity or are closed. This trend is also apparent in Figure 3.2 presenting the influent concentration at Clichy. The substrate concentration in the river significantly increases after SAV, as SAV treats approximately 80% of the wastewater in Clichy due to its large capacity. Triel, the measurement point downstream of SEG, also exhibits peaks above the limit, although they are relatively lower compared to Conflans. This can be attributed to the higher flow rate of the Seine in Triel, as it is located downstream of the confluence of the Oise and Seine Rivers. The occurrence of daily peaks in substrate concentration at the measurement points is closely tied to the corresponding peaks in influent concentration at Clichy, as illustrated in Figure 3.2. These peaks in influent concentration coincide with specific periods of the day when a larger volume of wastewater is generated. The elevated inlet flow rate and higher inlet concentrations during these periods contribute to the significant peaks observed in the river substrate concentrations. It is important to note that higher flow rates can adversely affect the performance of the WWTPs, potentially leading to reduced treatment efficiency and higher substrate concentrations in the effluent. Additionally, an abrupt increase in BOD_5 concentration is observed on day 7 at every measurement point. This increase can be attributed to the conditions of the river in Suresnes (Figure 3.3), which is upstream of the WWTPs. The measured data is provided every 7 days and is assumed to remain constant during that period. However, this weekly measurement frequency does not capture the daily or hourly fluctuations in the river's water quality.

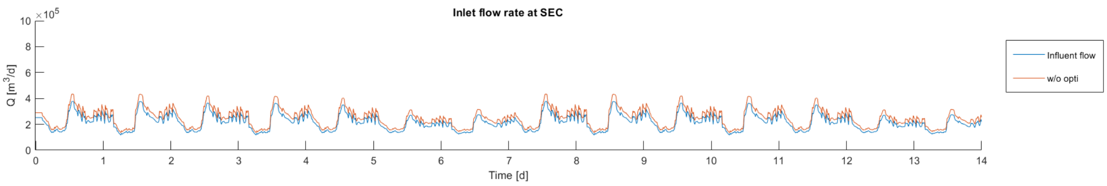

(a) SEC

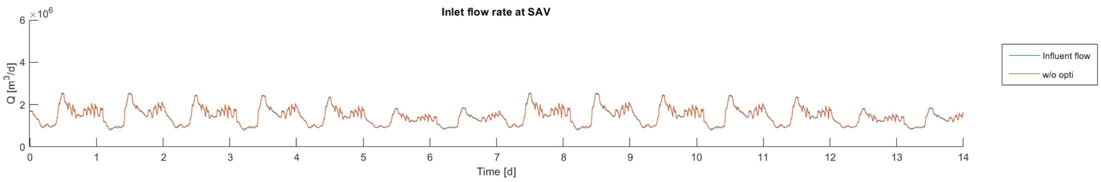

(b) SAV

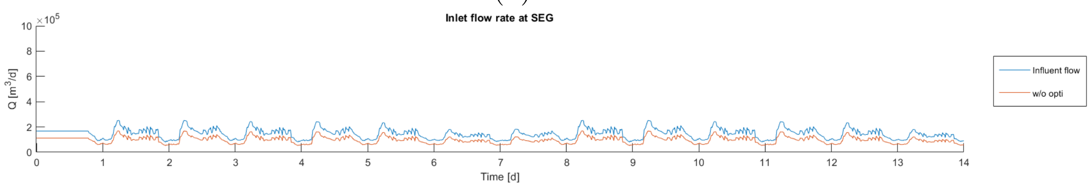

(c) SEG

Figure 4.2: Comparison of influent flow rate between the results with and without convex optimization for dry weather.

Figure 4.2 illustrates the comparison of influent flow rates into the sewers for the three WWTPs. The graph shows the influent flow rate with and without optimization. It is observed that the influent flow rate without optimization is smaller for SEC and SEG, while it is greater for SAV compared to the optimized flow rate.

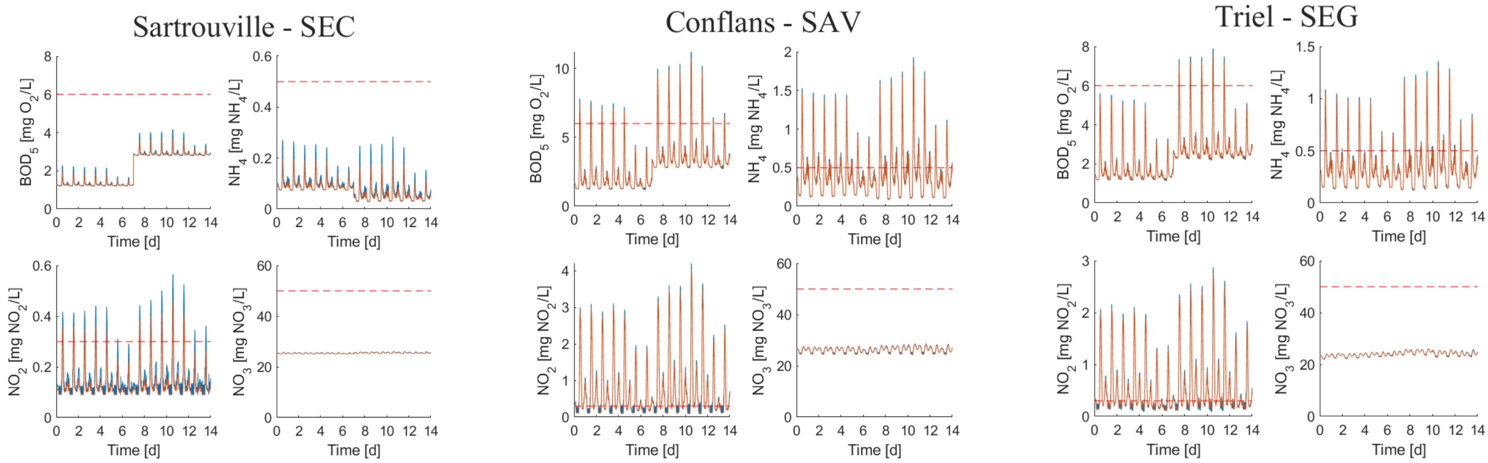

Figure 4.3: Comparison of the model output during dry weather. (—) Model output without optimization, (—) Model output with optimization, (—) Limit

Substrates	P_1 [%]	P_2 [%]
BOD_5	59.36	2.15
NH_4^+	45.25	4.69
NO_2^-	-46.49	7.78
NO_3^-	49.59	0.467

Table 4.1: Performance criteria for each substrate during dry weather

To evaluate the performance of the convex optimization during dry weather, the performance criteria presented in Table 4.1 are utilized. Based on P_1, it is observed that, on average, the substrate concentrations are between 45% and 60% below their corresponding good state limits, except for the NO_2^- concentration, which is 46.5% above the limit. Nevertheless, considering P_2, it can be seen that the highest improvement compared to the non-optimized effluent data is achieved for NO_2^-, with a 7.78% improvement. P_2 indicates that for dry weather, there is always an improvement when using convex optimization as a control strategy compared to non-optimized data, and the improvement is greater for substrate concentrations that are closer to or above the limit. This trend is also apparent in Figure 4.3. It is worth noting that P_1 and P_2 are computed based on the average values over a two-week period. Additionally, the comparison of mean values presented in Table 4.2, which includes both data with convex optimization ($\bar{\mu}$) and data without optimization (μ), demonstrates that, on average, the substrate concentrations with convex optimization are lower than those computed without optimization. Furthermore, it is observed that the only substrate concentration exceeding the limit is nitrite.

Dry weather			
Variable	Limit[mg/L]	μ[mg/L]	$\bar{\mu}$[mg/L]
BOD_5	6	2.49	2.43
NH_4^+	0.5	0.29	0.27
NO_2^-	0.3	0.47	0.43
NO_3^-	50	25.3	25.2

Table 4.2: Mean value comparison for each substrate during dry weather

The analysis of the flow rate distribution and results reveals that in dry weather, there are no significant issues or concerns regarding the flow rate distribution. All the wastewater sent from Clichy is effectively and completely treated by the WWTPs. Therefore, there is no specific need for optimization in this scenario.

4.2.2 Rainy weather

During rainy weather, as shown in Figure 4.4, it can be observed that SEC receives and treats a larger volume of water compared to dry weather conditions. Any excess wastewater that cannot be treated by SEC is directed to SAV and to SEG, except for a period between day 9 and the beginning of day 10 when a portion of the excess wastewater is by-passed. It is noteworthy that more water is directed to SEG compared to SAV, which can be explained by the fact that the flow rate in Triel is greater. Therefore, if more water is by-passed in Triel, it has a lower impact on the overall river quality. In terms of substrate concentrations during rainy weather, Sartrouville consistently maintains concentrations below the good state limit, except for occasional peaks in nitrite concentration that exceed the limit. SAV effectively treats all the water it receives, except during the rainy event between days 8 and 10 when excess wastewater is by-passed. During this period, there is an increase in substrate concentration in Conflans due to the higher inflow rate in SAV. A higher flow rate in WWTP decrease its performance. However,

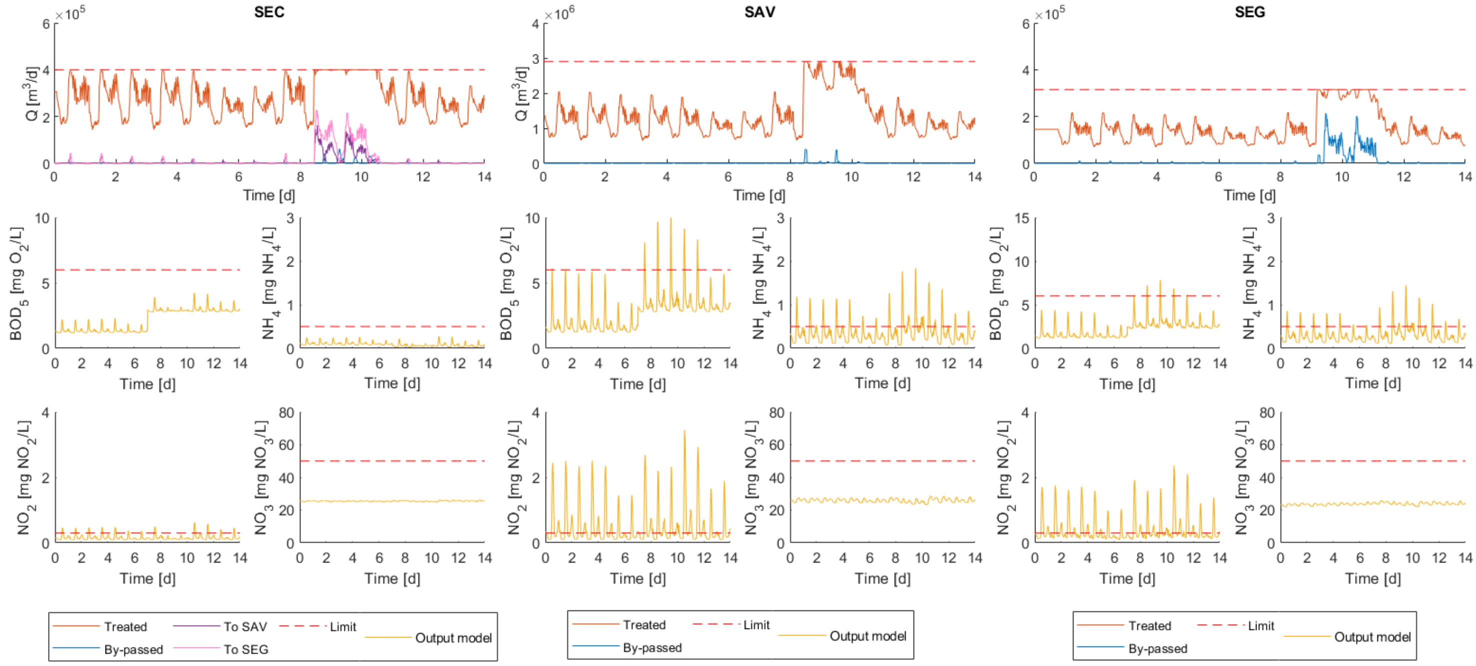

Figure 4.4: Results of the convex optimization during rain weather. The output of the model is obtained at the measurement points after each WWTP: Sartrouville for SEC, Conflans for SAV, and Triel for SEG.

in SEG, the high flow rate resulting from the rain event arrives between days 9 and 11 due to hydraulic response time, resulting in the by-pass of excess water on those days. Apart from that period, all wastewater is treated in SEG. There is an increase in substrate concentrations in Triel between days 9 and 11. In Conflans and Triel, the nitrate concentration consistently remains below the good state limit, while the other substrate concentrations have peaks above the limit. Similar observations can be made in rain weather as in dry weather regarding the jump in BOD_5 concentration, the high values and occurrence of daily peaks, the lower average during weekends, and the higher concentrations in Conflans.

Figure 4.5 provides a comparison of the influent flow rates entering the treatment plants during rain weather. The figure displays the influent flow rate with and without optimization for the three WWTPs. Without optimization, it can be observed that the influent flow rate is lower for SEC and SEG, while it is higher for SAV. Notably, the optimized flow rate for SEG does not simply mirror the non-optimized flow rate. This is due to the distribution of excess wastewater during the rainy event. As mentioned earlier, any excess wastewater that cannot be treated by SEC is directed to SAV and SEG. Consequently, during the rainy event, the

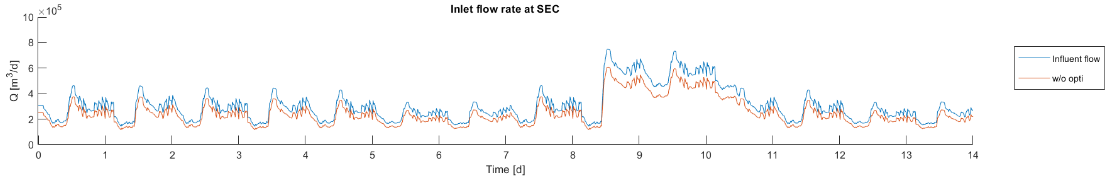

(a) SEC

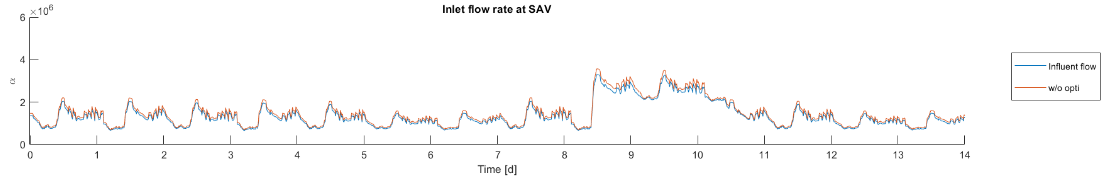

(b) SAV

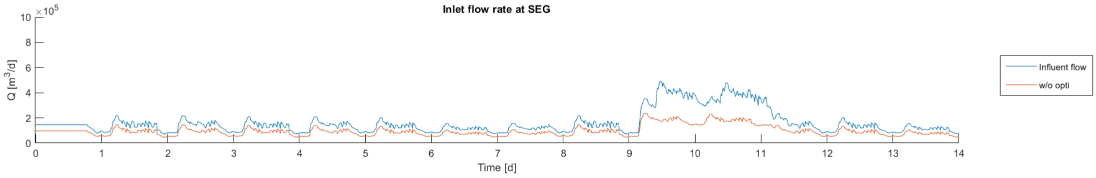

(c) SEG

Figure 4.5: Comparison of influent flow rate between the results with and without convex optimization for rain weather.

volume of wastewater at SEG is significantly higher compared to the non-optimized flow rate. Although it may not be easily discernible in Figure 4.5b because even if more excess water is sent to SEG than in SAV, it is mainly due to the proportion of the water received from SEC compared to the water from Clichy is smaller in SAV than in SEG. This is because SAV has a larger capacity and, on average, treats around 75% of the total flow rate. Overall, the comparison of influent flow rates with and without optimization demonstrates the impact of the convex optimization control strategy on the distribution of wastewater during rainy weather conditions.

Substrates	P_1 [%]	P_2 [%]
BOD_5	45.88	4.8
NH_4^+	37.97	12.32
NO_2^-	-34.55	10.97
NO_3^-	49.87	0.31

Table 4.3: Performance criteria for each substrate during rain weather

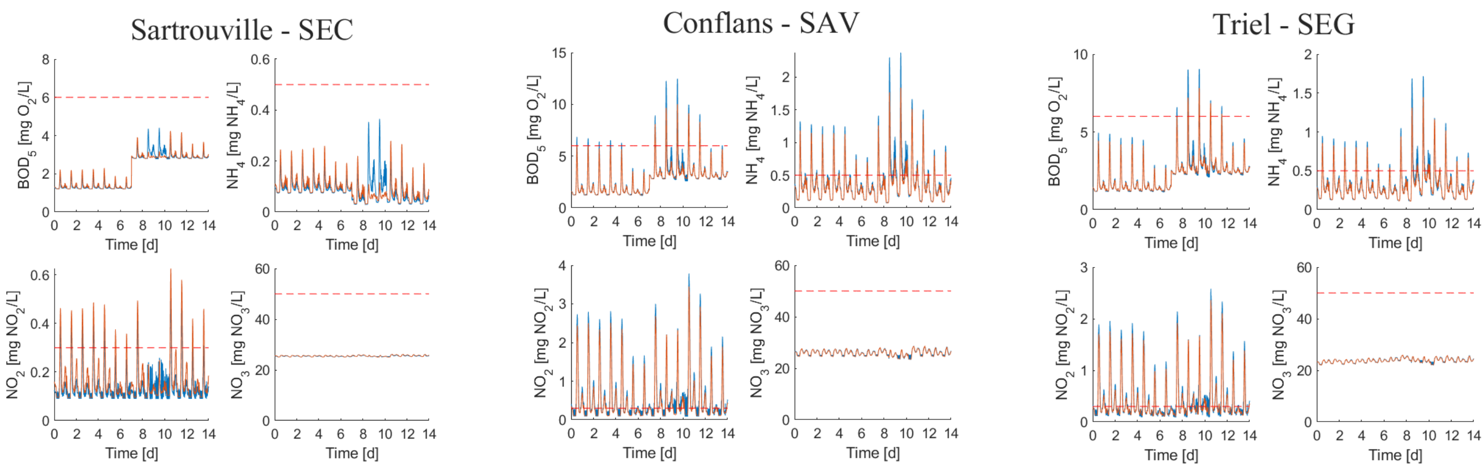

Figure 4.6: Comparison of the model output during rain weather. (—) Model output without optimization, (—) Model output with optimization, (—) Limit

Rainy weather			
Variable	Limit[mg/L]	μ[mg/L]	$\bar{\mu}$[mg/L]
BOD_5	6	2.41	2.35
NH_4^+	0.5	0.27	0.25
NO_2^-	0.3	0.39	0.35
NO_3^-	50	25.11	25.06

Table 4.4: Mean value comparison for each substrate during rain weather

To evaluate the performance of the convex optimization during rainy weather, mean comparisons over the two-week period are used, and performance criteria are computed from day 8 to day 12 to assess the impact of the rainy days on the convex optimization and to allow all the wastewater from the rainy days to be in the Seine River. Table 4.3 reveals that, on average, the concentrations of substrates are between 37% and 50% below their respective acceptable limits, which is lower compared to the performance during dry weather. However, it should be noted that the concentration of NO_2^- is 34% below the limit, indicating a closer proximity to the limit compared to dry weather. It was expected due to the higher inlet flow rate. Moreover, there is an improvement of almost 11% for NO_2^- compared to the non-optimized effluent data between day 8 and day 12. The most significant enhancement is observed for NH_4^+, with an improvement of 12.32%. The use of convex optimization as a control strategy demonstrates improvements compared to no optimization during rainy days, particularly for ammonium and nitrite, as depicted in Figure 4.6. Table 4.4 illustrates that the mean values over the two-week period of the simulated data $\bar{\mu}$ are lower than the limit, except for nitrate. However, these mean values are consistently lower than the mean values of data without the use of convex optimization. The improvement during rainy weather for ammonium and nitrite, compared to data without optimization, is higher than during dry weather. This is beneficial because these two substrates are the ones that frequently exceed the limits in terms of peaks.

4.2.3 Storm weather

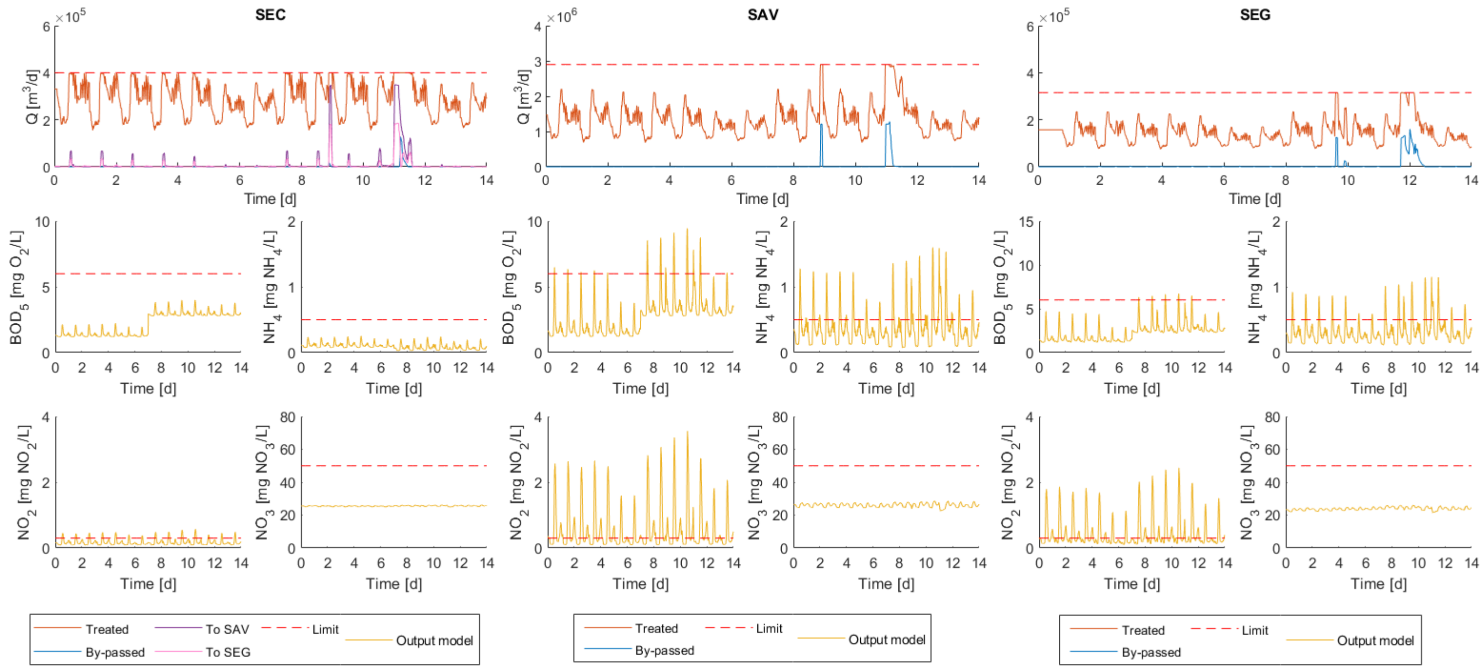

Figure 4.7: Results of the convex optimization during storm weather. The output of the model is obtained at the measurement points after each WWTP: Sartrouville for SEC, Conflans for SAV, and Triel for SEG.

Simulated results for storm weather are displayed on Figure 4.7. It is observed that SEC balances its operation by directing the excess wastewater to SAV and SEG, except on day 11 when some of it is also bypassed. Unlike rainy weather, more excess wastewater from SEC is directed to SAV than to SEG. The concentrations of BOD_5, NH_4^+, and NO_3^- respect their respective good limit quality, while for NO_2^-, there are occasional small peaks that exceed the limit. Regarding SAV, most of the wastewater is treated, and any excess water is by-passed. Data for nitrate remains below the limit, but for the biological demand, ammonium and nitrite, there are peaks that exceed their respective good state limits. During the storm event on day 11, an increase in substrate concentrations is observed in Conflans due to the higher inflow rate. It is worth noting that an increase in the flow rate leads to a decrease in the performance of the WWTP. This effect can also be observed, albeit to a lesser extent, in Triel. SEG by-passed its excess of wastewater at the end of day 9 and at the beginning of day 12 due to the storm event that occurred at the beginning of day 9 and 11, and the hydraulic response time. Similar observations can be made in storm weather as in dry weather regarding the jump in BOD_5 concentration, the occurrence of daily peaks, the lower average during weekends, and the higher concentrations in Conflans.

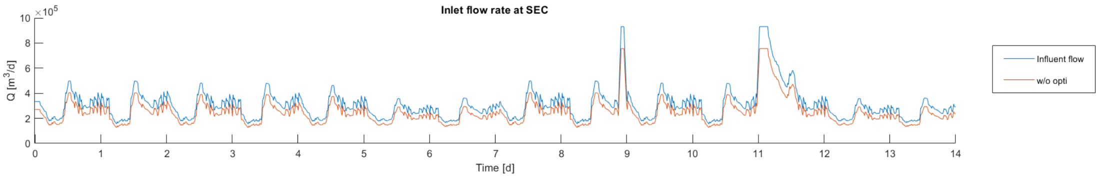

(a) SEC

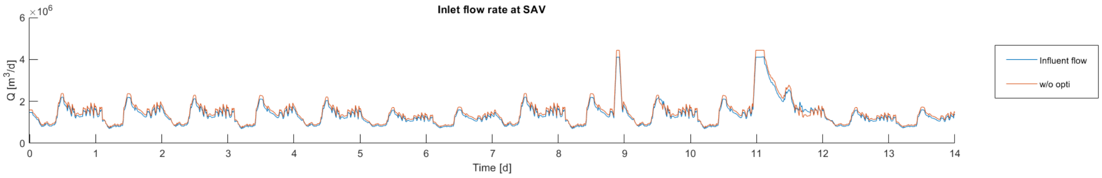

(b) SAV

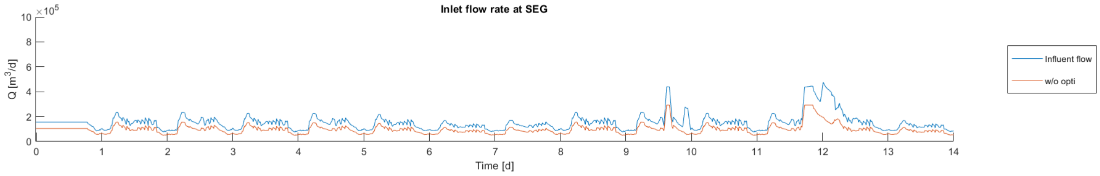

(c) SEG

Figure 4.8: Comparison of influent flow rate between the results with and without convex optimization for storm weather.

The flow rates entering the WWTPs, with and without optimization, are shown in Figure 4.8. Without optimization, the influent flow rate is lower for SEC and SEG compared to the optimized flow rate, while it is higher for SAV. Notably, for SEG, the optimized flow rate is not a translation of the non-optimized one due to the redirection of excess wastewater from SEC to SEG, as depicted in Figure 4.7. Consequently, during the storm event, the volume of wastewater at SEG is significantly higher compared to the non-optimized flow rate. Some wastewater is also sent from SEC to SAV, but its impact on SAV is not easily visible since it represents a small proportion of SAV's total influent flow rate.

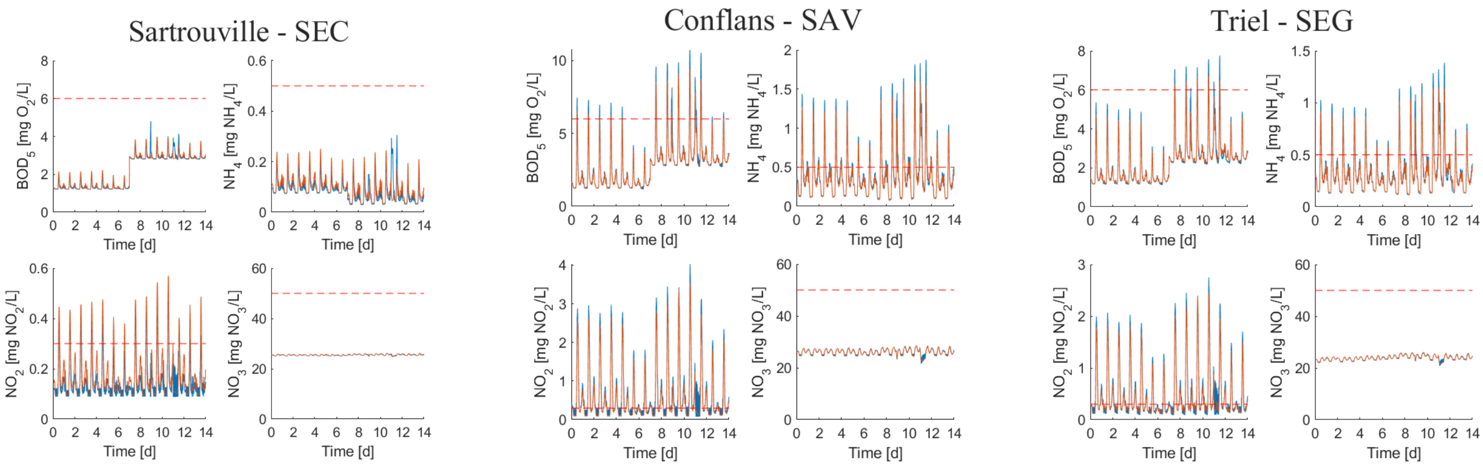

Figure 4.9: Comparison of the model output during storm weather. (_) Model output without optimization, (_) Model output with optimization, (_) Limit

Table 4.5 evaluates the performance of convex optimization during storm weather using performance criteria computed from day 8 to day 13, encompassing both storm events. The results show that, on average, the concentrations are significantly below their respective good state limits, with improvements ranging from 41% to 50%, except for the concentration of NO_2^-. The performance during storm weather is lower than during dry weather but slightly better than during rainy weather. The concentration of NO_2^- is observed to be 43% above the limit, which is worse than the performance during rainy weather but slightly better than during dry weather. However, despite the average concentrations being closer to the limits during dry weather, there are two notable improvements for ammonium and nitrite concentrations during stormy weather, showing an 8% and 11% improvement, respectively, compared to the non-optimized effluent data during stormy days. The use of convex optimization as a control strategy results in improvements, particularly for ammonium and nitrite concentrations, compared to the non-optimized scenario, as shown in Figure 4.9. Table 4.4 demonstrates that the mean values of the simulated data ($\bar{\mu}$) over the two weeks are consistently lower than the limits, except for nitrate. However, these mean values are always below the mean values of data without the use of convex optimization.

Substrates	P_1 [%]	P_2 [%]
BOD_5	45.9	2.93
NH_4^+	41.44	8.1
NO_2^-	-43.58	11.2
NO_3^-	49.4	2.23

Table 4.5: Performance criteria for each substrate during storm weather

Storm weather			
Variable	Limit[mg/L]	μ[mg/L]	$\bar{\mu}$[mg/L]
BOD_5	6	2.46	2.41
NH_4^+	0.5	0.28	0.26
NO_2^-	0.3	0.43	0.38
NO_3^-	50	25.19	25.14

Table 4.6: Mean value comparison for each substrate during storm weather

4.2.4 Program limitation

One limitation of the program is its long computation time, especially when dealing with a large number of variables. For a two-week period, it takes approximately 1 hour to compute, with 90% of this time attributed to the computation of the Euclidean norm. In Matlab, computing the 2-norm of a matrix requires a singular value decomposition, which is computationally expensive [33]. In this case, the Euclidean norm for the SOC constraint needs to be computed 16128 times (as there are 1344 time steps, 3 WWTPs, and 4 reactions). The use of **'vecnorm()'** function is not possible as the SOC constraint includes cvx variables. An alternative solution could have been to code the program in Julia, as the norm computation is faster in Julia and it computes the p-norm (defaulting to p=2). The p-norm is defined as:

$$\|A\|_p = \left(\sum_{i=1}^{n} |a_i|^p \right)^{1/p}$$

Another limitation of the program is that the flow division decision can only be made before each WWTP. If the flow division in Clichy-LaBriche y were to be another decision variable, there would be three variables multiplying each other in the objective function, which cannot be efficiently solved using ADMM. However, if this additional decision variable (y) were included, it could potentially improve the substrate concentration in the river.

Furthermore, the program's performance is impacted by the nitrite concentration. The global solution provided by the convex optimization control strategy for nitrite concentrations always has a mean value above the limit, regardless of the weather conditions. This excessive nitrite concentration is primarily attributed to high concentrations of nitrite at the input of SEC and SEG, as well as elevated ammonium concentrations at the input of Clichy, as shown in Figure 3.2. Nitrite is formed through the nitrification process, where ammonium is converted into nitrite. Additionally, suboptimal control actions could also contribute to this issue, potentially influenced by the weighting assigned to each substrate concentration in the objective function. To mitigate this issue, one potential solution is to allow for by-passing during dry weather conditions, particularly when the wastewater treatment plant (WWTP) is not operating at its maximum capacity. By implementing this approach, it is possible to reduce the concentration of nitrite, as nitrite primarily originates from ammonium through nitrification.

Lastly, it is crucial to address the issue of high peak substrate concentrations, as they can have adverse environmental impacts. Even if the mean values of substrate concentrations remain below their respective limits for some substrates, the occurrence of daily peaks that significantly exceed the limits is undesirable. One potential solution to mitigate this problem is the implementation of a storage tank system. By storing the excess wastewater generated daytime peaks, it can be gradually treated during the night when the inlet flow rate is at its minimum. This approach aims to maintain a more consistent inlet flow rate to the WWTPs throughout the day, reducing the occurrence of high peaks in substrate concentrations. By leveling out the flow rate, the storage tank system can help optimize the treatment process and minimize the environmental impact associated with excessive substrate concentrations in the effluent.

These program limitations, including the computation time, the restriction on the number of flow division decisions, the challenge with nitrite concentration, and the occurrence of peaks, can have an impact on the overall performance of the program.

4.3 Modification of the objective

In this section, the solutions for rainy weather are compared using a different objective. Since NO_2^- concentration consistently exceeds the good state limit and poses a threat to the environment, more weight is given on nitrite concentration in the objective function. To achieve this, the vector η that selects the components of $S_i = [BOD_5, NH_4^+, NO_2^-, NO_3^-]$ is modified. Specifically, the second and third terms of η since nitrite originates from ammonium and ammonium is always the second substrate close to the limit. It is chosen to test this modified objective on rainy weather because it has the worst overall performance compared to the limit. By giving higher importance to nitrite concentration in the objective, the convex optimization algorithm will prioritize actions that reduce nitrite levels in the effluent. This modification aims to improve the control strategy's effectiveness in mitigating the impact of excessive nitrite concentration on the environment and respecting the WFD.

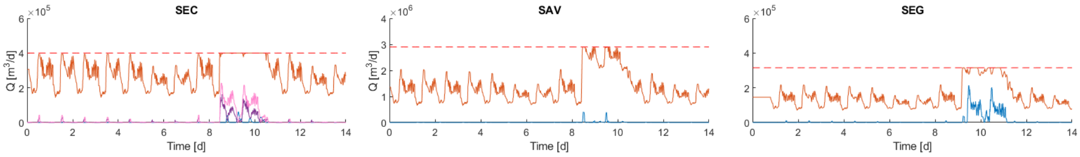

(a) $\eta = [0.1, 2, 0.3, 0.1]$

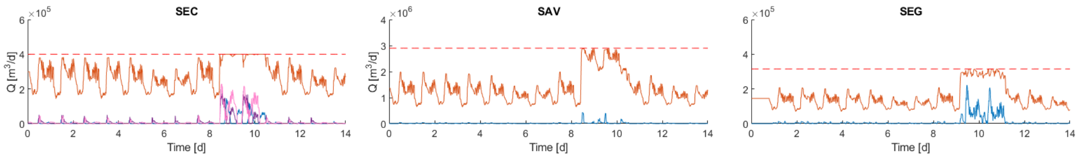

(b) $\eta = [0.1, 3, 3, 0.1]$

Figure 4.10: Comparison of the flow division during rain weather for the different η. __) Treated water, (__) By-passed water, (__) Wastewater send to SAV, (__) Wastewater send to SEG, (__) Limit.

Figure 4.10 illustrates the impact of the variation in η on the flow division at the WWTPs. The notable difference is observed in the flow division before SEC, where more water is bypassed between day 8 and day 11 when greater weight is assigned to NH_4^+ and NO_2^- in the objective function. Additionally, during the daily peaks of the influent flow rate, more wastewater is directed towards the SAV and SEG plants. These changes in the flow distribution demonstrate the influence of the objective function weighting on the allocation of wastewater among the WWTPs.

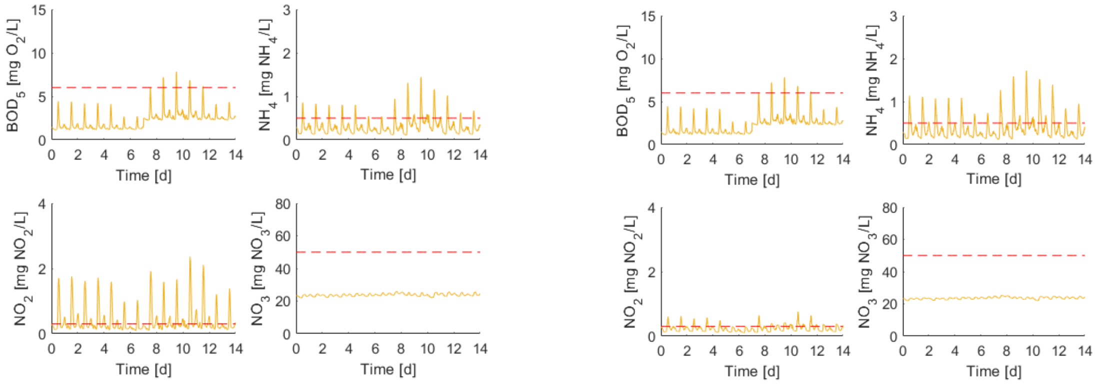

(a) $\eta = [0.1, 2, 0.3, 0.1]$ (b) $\eta = [0.1, 3, 3, 0.1]$

Figure 4.11: Results of the convex optimization program in Triel, downstream of SEG, for different η during rain weather. (—) Output of the model, (—) Limit.

Triel, being the measurement point downstream from the three WWTPs, is used to compare the state of the river under different objectives. The comprehensive results of the convex optimization for different η values during rainy weather can be found in Appendix A.1. Analyzing Figure 4.11, it is evident that the concentration of NO_2^- experiences a significant decrease when $\eta = [0.1, 3, 3, 0.1]$, even though the flow distribution remains largely unchanged. On the other hand, the concentration of NH_4^+ slightly increases, which may be attributed to the larger amount of by-passed water. Meanwhile, there is no notable change in the concentrations of BOD_5 and NO_3^- while NO_3^- comes from NO_2^- which comes from NH_4^+ through nitrification. It is worth mentioning that the nitrate concentration consistently remains close to the state of the river in Suresnes (Figure 3.3), indicating that the effluent from the WWTPs does not significantly impact the nitrate levels in the river.

Substrates	P_1 [%]	P_2 [%]
BOD_5	45.26	3.76
NH_4^+	22.56	-9.46
NO_2^-	18.35	45.97
NO_3^-	50.25	1.06

Table 4.7: Performance criteria for each substrate for a different objective during rain weather

Rainy weather			
Variable	Limit[mg/L]	$\bar{\mu}$[mg/L]	$\bar{\mu}'$[mg/L]
BOD_5	6	2.41	2.37
NH_4^+	0.5	0.27	0.31
NO_2^-	0.3	0.39	0.21
NO_3^-	50	25.11	24.90

Table 4.8: Mean value comparison for each substrate for a different objective during rain weather

To assess the impact of changing the objective value, Table 4.7 provides insights through P_1 on the performance during rainy days. It indicates that all substrate concentrations are below the limits, with improvements ranging from 18% to 50% compared to the respective limits. These findings indicate that the revised objective value enables all substrate concentrations to meet their respective good state limits. However, the performance of ammonium concentration is lower compared to the non-optimized data over the rainy days, showing a 9.48% deterioration compared to the non-optimized data. This is in contrast to the improvement of 12.32% achieved by the original objective during rainy days. On the other hand, nitrite concentration rose from 11% to 46%. The improvement in nitrate concentration has tripled, but the actual improvement value remains less than 1% of the limit. Additionally, the mean values of different datasets are compared: the optimized data with the original objective, denoted as $\bar{\mu}$, and the optimized data with $\eta = [0.1, 3, 3, 0.1]$, denoted as $\bar{\mu}'$. The results are presented in Table 4.8. Upon analysis, it is observed that the mean value of NO_2^- in the simulated data with $\eta = [0.1, 3, 3, 0.1]$ is lower than its respective good limit. This decrease in NO_2^- leads to a logical decrease in the mean value of nitrate, as it originates from nitrite. However, the mean value of NH_4^+ shows an increase compared to the data computed with the original objective. It is worth noting that despite the increase, NH_4^+ remains below the limits.

The significant reduction in the concentration of NO_2^- can be attributed to the approximation of the Monod growth rate. The model output does not align with the Monod growth rate (as illustrated in Figure 4.12) for NH_4^+. As a result, this deviation leads to a decrease in NO_2^- levels since it is formed through the conversion of ammonium via nitrification. When the concentration of NH_4^+ is high, it follows the straight line representing the lower bound (as defined by Equation (3.5)). This deviation leads to an increase in NH_4^+ concentration and a decrease in its reaction kinetics T_{NH4} for the three WWTPs. This explains the increase in ammonium concentration in the river and the decrease in nitrite concentration, as the dynamic equation for nitrite (Equation (1.15)) involves r_2, which is approximated by $T_{i,NH4}$, the reaction kinetics of NH_4^+in WWTP i. It is also noticeable that the dots representing the model output are lower on the Monod growth rate curve in Figure 4.12b compared to Figure 4.12a for nitrite and nitrate in the three WWTPs, as T_{NH4} is involved in their dynamic equations in one way or another. This observation is consistent with Figure 4.11 for nitrite, but not for nitrate, as the WWTPs' outputs do not significantly affect the river in terms of nitrate concentration.

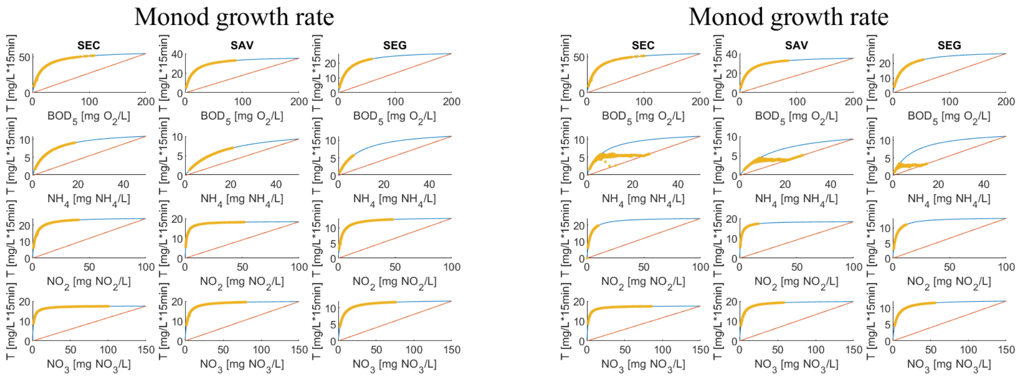

(a) $\eta = [0.1, 2, 0.3, 0.1]$

(b) $\eta = [0.1, 3, 3, 0.1]$

Figure 4.12: Results of the Monod growth rate approximation for different η during rain weather. (_) Monod growth rate, (_) Lower bound, and (_) Output model.

The adjustment of the maximum substrate concentrations vector, $S_{max,i}$, aims to improve the approximation to the Monod growth rate by approaching the maximum substrate value for each substrate and each WWTP. The modified vectors representing the maximum substrate concentrations are set as follows for each WWTP: $S_{max,SEC} = [150, 25, 50, 100]$, $S_{max,SAV} = [100, 30, 60, 100]$, and $S_{max,SEG} = [100, 25, 80, 100]$.

Figure 4.13 demonstrates that as the lower bound approaches the Monod growth rate, the model output also aligns more closely with the Monod growth rate. It is important to note that the dots representing the output model are higher on the Monod growth rate compared to those in Figure 4.12b. This occurs because T_{NH4} is higher when it is closer to the Monod growth rate.

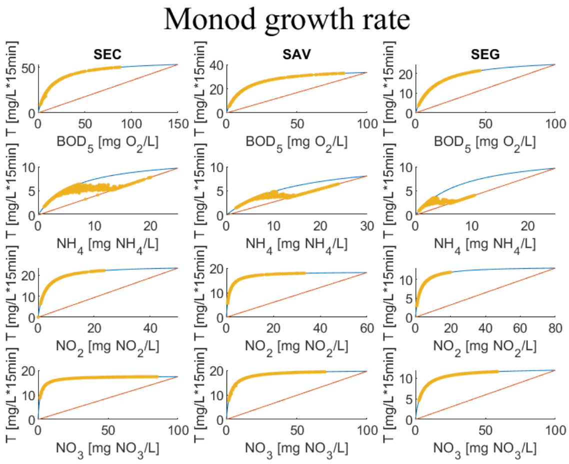

Figure 4.13: Results of the Monod growth rate approximation for $\eta = [0.1, 3, 3, 0.1]$ and $S_{max,SEC} = [150, 25, 50, 100]$, $S_{max,SAV} = [100, 30, 60, 100]$, and $S_{max,SEG} = [100, 25, 80, 100]$ during rain weather. (—) Monod growth rate, (—) Lower bound, and (—) Output model.

The full results of the convex optimization with modified maximum substrate concentration vectors can be found in Appendix A.2. However, it should be noted that the flow distribution is almost similar to Figure 4.10a, with slightly more bypassed wastewater during peak days, for SAV and SEG. Despite this small difference, it can be seen in Figure 4.14 that the nitrite concentration exhibits higher peaks above the limit compared to Figure 4.11b. However, these peaks are approximately half as high as those shown in Figure 4.11a.

Table 4.10 compares the mean values of different datasets. These datasets include the optimized data with the original objective denoted as $\bar{\mu}$, the optimized data with $\eta = [0.1, 3, 3, 0.1]$ denoted as $\bar{\mu}'$, and the optimized data with $\eta = [0.1, 3, 3, 0.1]$ along with different maximum substrate concentration vectors represented by $\bar{\mu}''$. Observations from the comparison reveal that the mean value of nitrite is higher than the original data but remains below the limit. The mean value of ammonium concentration is lower than its limit and lower than the one computed with $\eta = [0.1, 3, 3, 0.1]$ and the original S_{max}. However, it is higher than the mean value obtained from the original convex optimization. The change in the mean values of BOD_5 and NO_3^- compared to the original data and the data with $\eta = [0.1, 3, 3, 0.1]$ is less than 1% of their respective limits. P_1 is computed only from day 8 to day 12 (Table 4.10) and shows an improvement between 5% and 50% compared to the limit. The improvement for ammonium concentration rose from 22.56% to 26.53% when using the modified maximum substrate concentration vectors, while

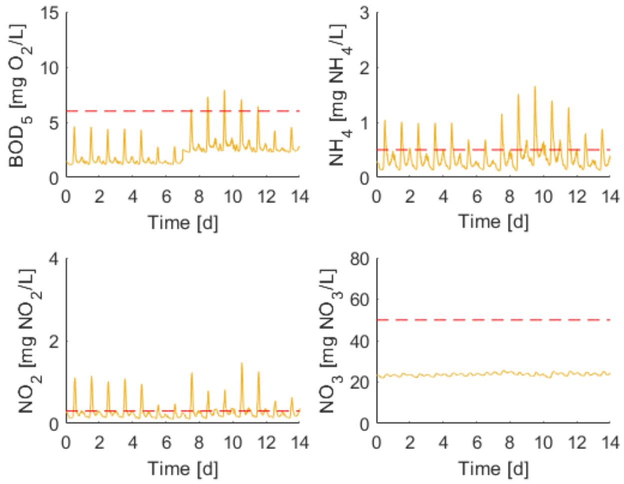

Figure 4.14: Results of the convex optimization program in Triel, downstream of SEG, for $\eta = [0.1, 3, 3, 0.1]$ and $S_{max,SEC} = [150, 25, 50, 100]$, $S_{max,SAV} = [100, 30, 60, 100]$, and $S_{max,SEG} = [100, 25, 80, 100]$ during rain weather.
(_) Output of the model, (_) Limit.

the improvement for nitrite concentration dropped from 18% to 6%. This can be explained by the fact that T_{NH4} and NH_4^+ are higher as they are closer to the Monod growth rate (Figure 4.13). For the biological demand and the nitrate, P_1 and P_2 remain almost the same. However, P_2 increases for the ammonium concentration (although it remains negative) and decreases for nitrite concentration.

Substrates	P_1 [%]	P_2 [%]
BOD_5	45.05	3.39
NH_4^+	26.53	-3.84
NO_2^-	5.97	37.78
NO_3^-	50.15	0.85

Table 4.9: Performance criteria for each substrate during rain weather

Rainy weather				
Variable	Limit[mg/L]	$\bar{\mu}$[mg/L]	$\bar{\mu}'$[mg/L]	$\bar{\mu}''$[mg/L]
BOD_5	6	2.41	2.37	2.39
NH_4^+	0.5	0.27	0.31	0.29
NO_2^-	0.3	0.39	0.21	0.24
NO_3^-	50	25.11	24.90	24.94

Table 4.10: Mean value comparison for each substrate for different objectives and different maximum substrate concentration vectors in rain weather

To conclude, although the modifications made to the objective and maximum substrate concentration vectors have led to improved river water quality, it is crucial to acknowledge that the modified control strategy does not fully align with the actual conditions. The primary difference lies in the growth rate of substrates within the WWTPs, which deviates from the reality. This discrepancy indicates that although the optimized control strategy yields better pollutant reduction in the river, it may not accurately reflect the real-world conditions and dynamics of the wastewater treatment network.

4.4 Comparison with Model Predictive Control

In order to evaluate the performance and effectiveness of the convex optimization control strategy, it is important to compare it with alternative control strategy. This comparison provides valuable insights into the relative strengths and weaknesses of each approach and helps determine the most suitable control strategy for the given wastewater treatment network. Comparing the convex optimization control strategy allows to assess their respective performance in terms of pollutant reduction, control stability, and adaptability to changing operating conditions. It provides a comprehensive understanding of the advantages and limitations of each control strategy.

4.4.1 Control strategy using model predictive control

In the study by Robles-Rodriguez et al. [17], a control strategy using Model Predictive Control (MPC) and global optimization tools, such as Particle Swarm Optimization (PSO), was implemented on the west part of the Seine wastewater treatment network. This is the same network as considered in this work. The control strategy aims to maintain the concentrations of the model output below the good quality limits by optimizing the flow management. To evaluate the performance of the control strategy, real data from two scenarios during the rainy season were used. The first scenario represents the actual rainy season, while the second scenario represents the period just after the rainy season when the remnants of rain could still have an impact on the river quality.

The studied system considers that the wastewater coming from the sewers arrives at a single point, Clichy-LaBriche, where the flow is split into three streams, each going to a different WWTP. Each WWTP has two outputs: one for treated water and the other for by-passed water. The wastewater can be by-passed even when the input flow rate is not larger than the maximum capacity of the WWTP. The idea is to use optimization-based decision-making to handle the studied system by manipulating the flow rate at Clichy-LaBriche and before each WWTP, making the control strategy twofold. The wastewater from the sewer is split by PSO at Clichy-LaBriche into three intermediate flows, which serve as the inputs of the three parallel MPCs. These MPCs decide how much water is treated or by-passed at each WWTP (Figure 4.15).

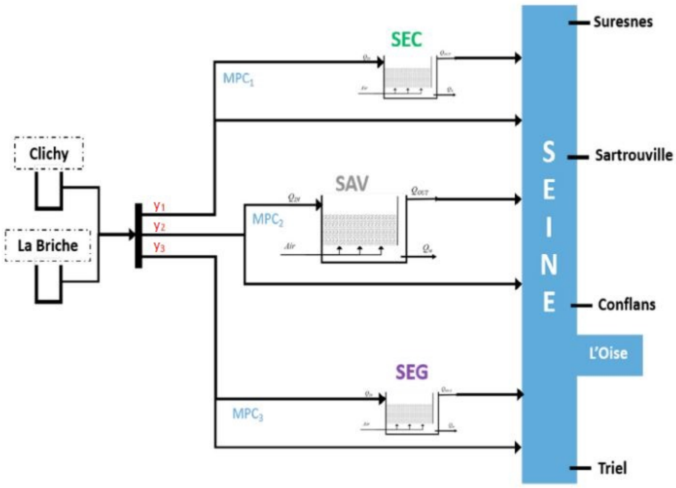

Figure 4.15: System representation of the reduced WWTP for the control strategy

MPC is a widely used control strategy that optimizes the control actions based on a predictive model of the system dynamics. The objective of MPC is to minimize a performance index over a finite prediction horizon, denoted by H, based on the predictions obtained from a system model at each time step, denoted by t. A standard MPC formulation is given by:

$$\min J = \sum_{z=t}^{t+H} \varepsilon(z)^T W \varepsilon(z) + u(z)^T P_{\Delta u} u(z)$$

where J represents the cost function, W is a weighting matrix, and $u(z)^T P_{\Delta u} u(z)$ corresponds to the input u and the weights to handle input moves, denoted $T_{\Delta u}$. For the studies conducted, the control cycle was implemented every two days with a predictive horizon of 10 days (H=10). The initial conditions were set to the values of the states at each input time t. The objective of the MPC is to minimize the error ε, which is defined as:

$$\varepsilon = \left(\hat{S}_i - R_i\right) > 0$$

where $\hat{S}_i = [\mathrm{NH_4}, \mathrm{NO_2^-}]$ represents the vector of concentrations of each WWTP i, and $R_i = [0.3, 0.5]$ mg/L represents the vector of their respective good limits values. Since the concentrations of BOD_5, $\mathrm{NO_3^-}$ are already under their respective good limit values according to experimental data, they are not included in the objective function. The problem is solved by using the model equations (1.3) - (1.6) and the flow constraint, $Q_{in,i} = Q_{i,T} + Q_{i,P}$ where T and P hold for treated and by-passed. The goal is to determine the future control sequences of the input flow rate partitions $Q_{i,T}$ and $Q_{i,P}$. Once the optimal future values of the input flow rate is determined, they are applied. At the next time step, the procedure is repeated to enable continuous optimization of the process.

PSO is a population-based stochastic optimization technique inspired by the collective behavior of bird flocking or fish schooling that is capable of finding a global optimum. In PSO, each particle $p(i)$ represents a potential solution to the optimization problem and has a velocity $v(i)$ to direct their fly. The algorithm begins by initializing a group of particles with random solutions, creating a swarm that explores the hyperdimensional search space. At each iteration, the particles are updated to determine the best solution found by each particle ($pBest$) and the best solution found by any particle in the entire swarm ($gBest$). The position of each particle is updated based on the velocity vector, which is calculated as follows:

$$\begin{aligned} v(i) = w \times v(i) + L_{f1} \times rand_1 \times (p\,\mathrm{Best}(i) - p(i)) \\ + L_{f2} \times rand_2 \times (g\,\mathrm{Best}(i) - p(i)) \end{aligned}$$

where $rand_1$ and $rand_2$ are random values. L_{f1} and L_{f2} are the best learning factors that control the attraction of a particle towards its own best solution and the global best solution, respectively. The inertia weight w determines the impact of previous velocities on the current velocity. The position of the particle $p(i)$ is then updated using the velocity:

$$p(i) = p(i) + v(i)$$

In the studied case, the cost function to be minimized is given by $\min J = \varepsilon^T \varepsilon$. The number of particles in the swarm was fixed at 50, and the number of iterations was set to 10. To simplify the optimization process, the input flow rate from the sewers Q is divided into three flow rates, one for each WWTP. To further simplify the problem, the normalized flow rates $y_i = Q_{in,i}/Q$ are used, which must satisfy the constraint $\sum_{i=1}^{3} y_i = 1$.

4.4.2 Comparison

The proposed control strategy is evaluated using real data from two scenarios representing different seasons with varying rainfall patterns. The purpose is to assess the performance of the control strategy if it had been applied during these periods. The data for the WWTPs and observation points in the Seine River were collected daily and every 7 days, respectively. The two scenarios cover a duration of 70 days each.

- **Scenario S1**: Data from March to May 2009: Spring season characterized by intermittent rain and dry periods.
- **Scenario S2**: Data from December 2009 to February 2010: Winter season characterized by heavy rain periods.

This control strategy calculates the flow rate distribution for each sample time t (1 day), and the Particle Swarm Optimization (PSO) is performed every 7 days to determine the updated flow distribution at Clichy-LaBriche. Figure 4.16a illustrates the flow rate entering Clichy-LaBriche and the distribution achieved by PSO. Both scenarios show peaks in the flow rate (Q), indicating rain events. When the flow rate exceeds 2.25×10^6, which is the maximum capacity for treated water, overflows occur.

There are some differences between the model implemented in this work and the control strategy described in the study by Robles et al. First, in this work, the decision to simulate the new flow distribution is made every 15 minutes, whereas in the study it was done every 7 days using PSO. Additionally, the decisions are not made twice at Clichy-LaBriche and before each WWTP, but only once before each WWTP in this work. Therefore, in the model implemented here, the decision made at Clichy-LaBriche remains constant over the 25-day period. The two scenarios were implemented for 25 days in the convex optimization control strategy due to computational time constraints. Implementing it for 70 days would require extensive computational resources due to the large number of variables involved. Another difference is that this work takes into account transportation time, which results in a delay in concentration and flow. However, in this work, TSS is not considered, and the biomass X is assumed to be constant throughout the process. Finally, in the study, the wastewater can be by-passed even when the input flow rate is not larger than the maximum capacity of the WWTP which cannot be the case in this work as by-passed is not allowed during dry weather. These differences highlight the variations in the control strategy implementation and model assumptions between the two works.

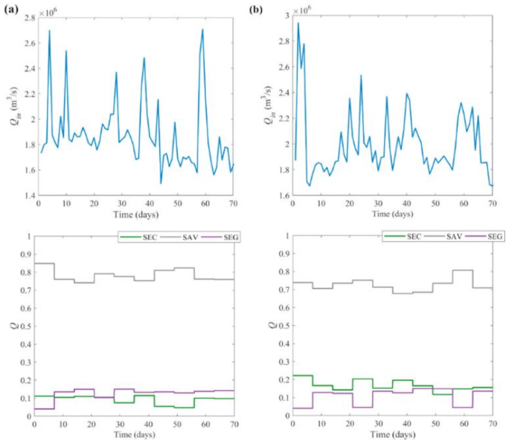

(a) MPC and PSO control strategy

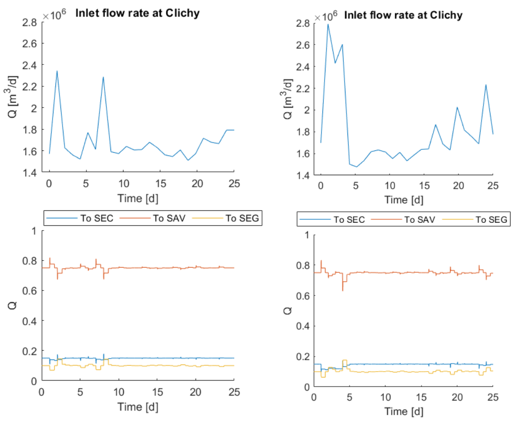

(b) Convex optimization control strategy

Figure 4.16: Inlet flow rate coming from the sewers and its distribution for the three WWTPs. Scenario S1 is on the left-hand side of each subfigure while scenario S2 is in the right-hand side.

Figure 4.16 illustrates the flow rate coming from the sewers and their distribution for the two control strategies in the two scenarios. In the lower section of the figures, it can be observed that both control strategies exhibit similar distribution patterns for both scenarios. It is noteworthy that SAV handles the majority of the wastewater since its maximum capacity is ten times greater than that of SEC and SEG. A slight difference can be observed in scenario S1, where the volume of water sent to SEC is consistently higher than that sent to SEG in the convex optimization control strategy, while this is not the case for the MPC and PSO control strategy. Furthermore, it can be observed for both control strategies that whenever a high peak occurs in the inlet flow rate at Clichy, corresponding peaks occur in the wastewater flow directed to SAV. This suggests that SAV receives a higher proportion of wastewater during peak flow periods, which is likely due to its larger maximum capacity compared to SEC and SEG.

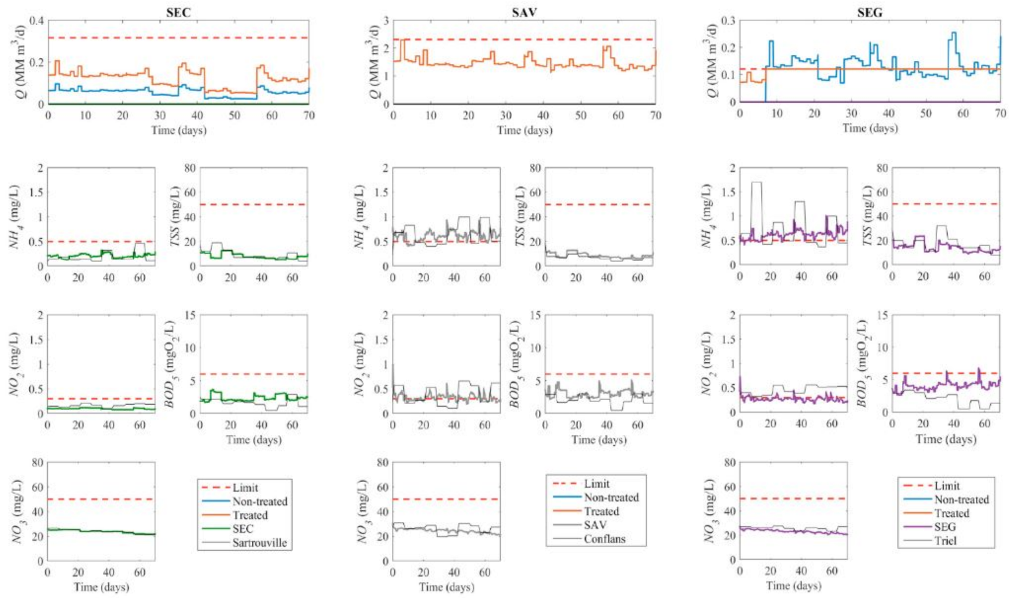

(a) MPC and PSO control strategy

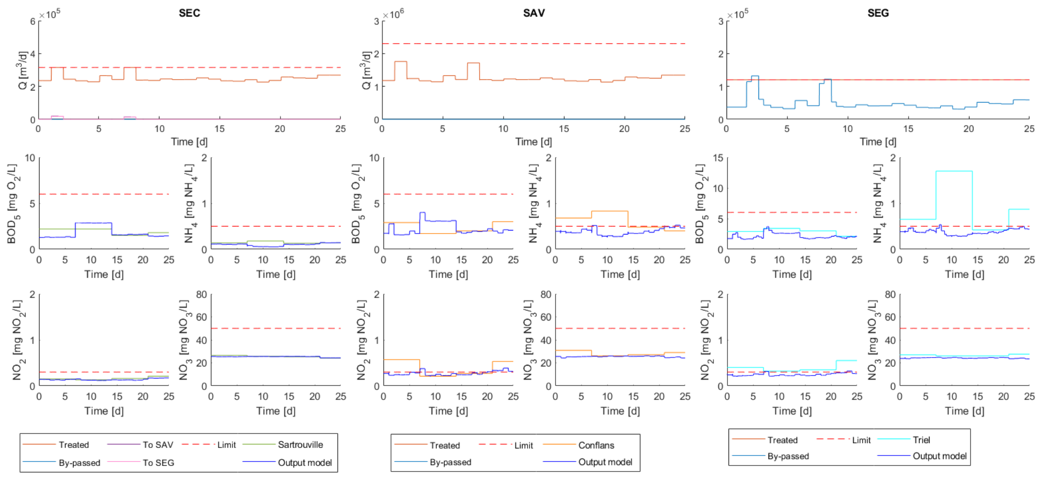

(b) Convex optimization control strategy

Figure 4.17: Comparison of the control strategies on Scenario 1. Sartrouville, Conflans and Triel correspond to the measured data. SEC, SAV and SEG are the control outputs.

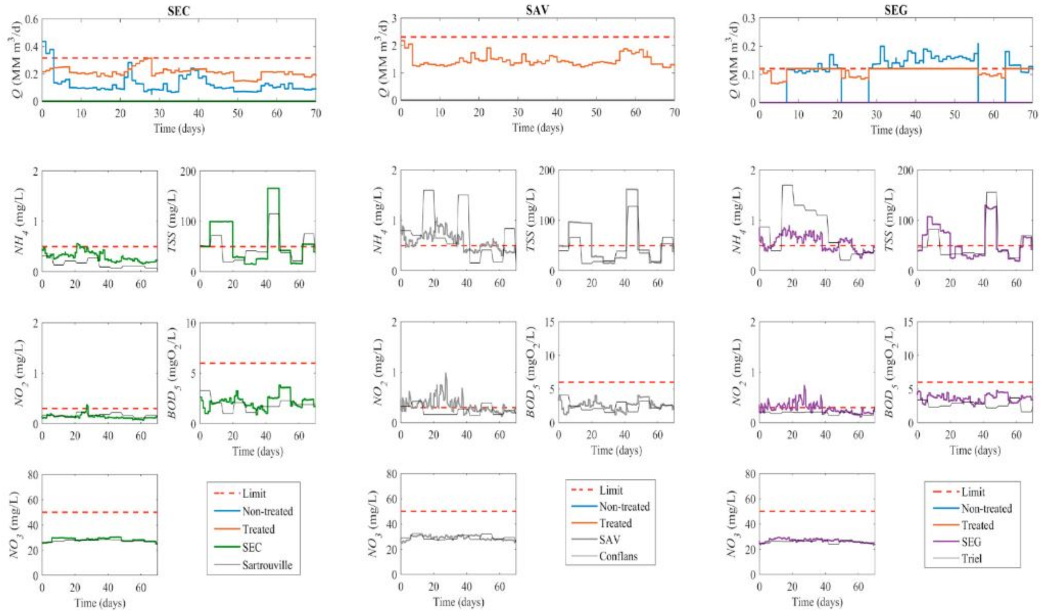

(a) MPC and PSO control strategy

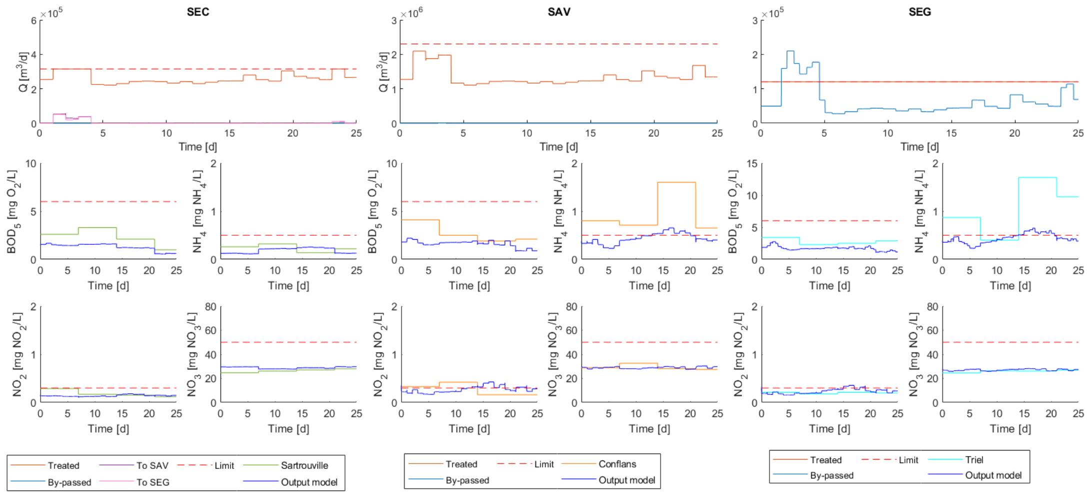

(b) Convex optimization control strategy

Figure 4.18: Comparison of the control strategies on Scenario 2. Sartrouville, Conflans and Triel correspond to the measured data. SEC, SAV and SEG are the control outputs.

Simulation results compared to real data on Scenario 1 are displayed on Figure 4.17. When analyzing the MPC and PSO control strategy, it can be observed that SEC balances its operation with a high amount of by-pass. In contrast, the convex optimization control strategy redirects the excess water to both SAV and SEG in equal proportions, where it is subsequently by-passed for SEG and treated for SAV. A similar pattern of by-passing excess wastewater is also observed for SEG in the case of the MPC and PSO strategy. In terms of concentration levels, both NH_4^+ and NO_2^- remain close to the limit in the convex optimization simulations. However, on day 7, they exceed the limit. The magnitudes of these concentrations are lower compared to both the real data and the simulated data obtained using the MPC and PSO strategy. On the other hand, for BOD_5 and NO_3^-, their concentrations consistently remain below the limits for both control strategies.

Moving on to Scenario 2 (Figure 4.18), the distribution of wastewater shows that SEG receives more wastewater until day 8 in the convex optimization control strategy compared to the MPC and PSO control strategy. In the first 8 days, it can be observed that the WWTPs are operating at full capacity to handle the high flow rate. Similarly to S1, the concentration of NH_4^+ and NO_2^- in the convex optimization control strategy remains around the limit, sometimes exceeding it in Conflans and Triel. However, the concentration of NH_4^+ is consistently below the real measurements, which is not the case for NO_2^-.

Overall, the simulation results show the performance of the control strategies in managing the flow distribution and maintaining concentration levels below the good state limits.

			S1			**S2**	
Variable	Limit	μ_{rm}	μ_{MPC}	μ_{CO}	μ_{rm}	μ_{MPC}	μ_{CO}
BOD_5	6	2.402	-	2.090	2.653	-	1.538
NH_4^+	0.5	0.561	0.498	0.288	0.750	0.611	0.352
NO_2^-	0.3	0.307	0.207	0.218	0.223	0.251	0.213
NO_3^-	50	26.778	-	25.006	27.200	-	28.257

Table 4.11: Performance of the control strategies for the two scenarios.

To evaluate the performance of the convex optimization control strategy, a comparison of the mean values of the real data μ_{rm}, simulated data obtained using the MPC control strategy μ_{MPC}, and simulated data obtained using the convex optimization control strategy μ_{CO} is conducted. The μ_{MPC} values are scaled to a 25-day period using the ratio between the measured data for a 25-day period and a 70-day period. The results are presented in Table 4.11. It can be observed that the convex optimization control strategy keeps the values below the limit for both scenarios S1 and S2. This is also true for the MPC and PSO control strategy, except for the ammonium concentration in S2. However, even in that case, it remains below the real measurement. Both control strategies aim to guarantee a global solution, and the substrate concentrations are below the real measurements for S1. For S2, the concentrations are below the real measurements for the biological demand, ammonium, and nitrite, and slightly above for nitrate, but still within the limit. Additionally, it can be observed that the convex optimization control strategy consistently performs better than the MPC and PSO control strategy, keeping the concentrations lower.

However, it is important to consider the difference in the time scales used. Convex optimization is performed every 15 minutes, MPC and PSO control strategy are performed on a daily basis, and real measurements are taken once a week at each measurement point and daily at WWTPs. As a result, the comparison is primarily based on mean values. It should be noted that convex optimization captures fluctuations at an hourly level, while MPC captures daily fluctuations, and real measurements have limitations in capturing daily or hourly variations. This is why the convex optimization control strategy was initially tested on three weather conditions using the BSM1 model, which provides 15-minute fluctuations.

Overall, the results demonstrate that the convex optimization control strategy performs well in maintaining concentrations below the limits.

Conclusion

This master thesis aimed to develop a control strategy for optimizing the distribution of wastewater among wastewater treatment plants in Paris and its suburbs, with the objective of improving the quality of water discharged into the Seine.

To achieve this objective, a comprehensive review of the state-of-the-art related to wastewater treatment networks was conducted. This included a detailed analysis of wastewater composition and a description of the network infrastructure on which the control strategy will be conducted. The sewer model was then described, followed by a brief explanation of the main steps involved in wastewater treatment. The general dynamical model of bioreactors was discussed to lead to the model of the WWTPs and a model of the river was provided.

In the next step, the theoretical foundations for formulating a convex optimization problem and second-order cone programming were presented. Second-order cone programming was necessary to compute the convex approximation required due to the nonlinearity of the reaction rates. The formulation of the general optimization problem for the wastewater treatment network with a second-order cone constraint was presented, and the biconvexity in its objective was addressed using the alternating direction method of multipliers (ADMM) algorithm. The review of existing literature, theoretical aspects, and the general problem formulation using ADMM were covered.

The thesis then described the implementation of the model, which involved formulating the convex optimization problem by defining the objective of minimizing the substrates concentration entering the river, discretizing in time, and setting the parameters. The ADMM formulation, the chosen approach for solving the WWTP network, was explained. Details regarding initial conditions and the stopping criterion were provided, and a brief description of the code implementation was given.

The results of the study were presented, evaluating the performance of the control strategy using performance criteria. The convex optimization control strategy was assessed under different weather conditions: dry, rain, and storm weather. A comparison was made with non-optimized data to demonstrate its effectiveness. The results showed good performance across all weather periods especially on rainy and stormy days, with a notable 12% and 11% improvement in ammonia nitrogen and nitrite, respectively, during rainy weather. Additionally, modifications were made to the objective to further enhance efficiency, resulting in all substrate concentrations being below their respective limits but with the dynamic within the WWTP not accurately reflect the real-world. Furthermore, a comparison with Model Predictive Control (MPC) using real data demonstrated promising solutions and improvements in Seine River quality.

In conclusion, the study showed that the convex optimization control strategy yielded positive results within a reasonable amount of time. It is worth noting that several assumptions were made to simplify the model, such as assuming constant biomass and delay. Complexifying the model to better reflect reality would likely improve the accuracy of the control strategy. Additionally, including phosphorus in the optimization process would enhance fidelity to reality, as phosphorus is a pollutant that must adhere to specific limits. Implementing a two-stage optimization approach to allow variable decision-making on the flow distribution at Clichy-LaBriche would further enhance the control strategy.

Bibliography

[1] Meenakshi Choudhary, C. N. Peter, Sudheesh K. Shukla, Penny Poomani Govender, Girish P. Joshi, and Rong Wang. *Environmental Issues: A Challenge for Wastewater Treatment*. Springer International Publishing, 1 2020.

[2] Tauseef Ahmad Rangreez, Inamuddin, Mu. Naushad, and Hamid E. Ali. Synthesis and characterisation of poly(3,4-ethylenedioxythiophene)-poly(styrenesulfonate) (PEDOT:PSS) Zr(IV) monothiophosphate composite cation exchanger: analytical application in the selective separation of lead metal ions. *International Journal of Environmental Analytical Chemistry*, 95(6):556–568, 5 2015.

[3] Shanna Freeman. How Water Works. *HowStuffWorks*, 2023. Available online at: http://science.howstuffworks.com/environmental/earth/geophysics/h2o1.htm, last accessed on 20.05.2023.

[4] EU. Council directive establishing a framework for community action in the field of water policy. 2000/60/ec of october 23. *Official Journal of the European Communities*, L 327, December 2000.

[5] EU. Council directive concerning urban wastewater treatment. 91/271/ec of may 21. *Official Journal of the European Communities*, L 135/40, May 1991.

[6] Directorate-General for Environment. Urban wastewater, 2022. Available online at: https://environment.ec.europa.eu/topics/water/urban-wastewater_en, last accessed on 28.03.2023.

[7] Directorate-General for Environment. Proposal for a revised urban wastewater treatment directive, 2022. Available online at: https://environment.ec.europa.eu/publications/proposal-revised-urban-wastewater-treatment-directive_en, last accessed on 28.03.2023.

[8] Mocopee, 2018. Available online at: http://mocopee.com/, last accessed on 28.03.2023.

[9] SIAAP. Presentation. Available online at: https://www.siaap.fr/le-siaap/missions/presentation/, last accessed on 28.03.2023.

[10] Agreste Île-de France-SSP-Enquête. Eau et assainissement. 2008.

[11] Gouvernement Français. Article l 1331-10-code de la santé publique, 2000. Available online at: https://www.legifrance.gouv.fr/codes/article_lc/LEGIARTI000006686518/2000-06-22, last accessed on 24.05.2023.

[12] SIAAP. Fiches usines : Unsine d'épuration Seine Centre. Technical report, 2013.

[13] SIAAP. Fiches usines : Usine d'épuration Seine Aval. Technical report, 2013.

[14] SIAAP. Fiches usines : Unsine d'épuration Seine Grésillons. Technical report, 2013.

[15] G. Bastin and D. Dochain. On-line estimation and adaptive control of bioreactors. *Elsevier Science*, 1990.

[16] C.E. Robles-Rodriguez, J. Bernier, V. Rocher, and D. Dochain. A simple model of wastewater treatment plants for managing the quality of the seine river. *IFAC-PapersOnLine*, 51(18):880–885, 2018. 10th IFAC Symposium on Advanced Control of Chemical Processes ADCHEM 2018.

[17] C.E. Robles-Rodriguez, A. Ben-Ayed, J. Bernier, V. Rocher, and D. Dochain. Management of an integrated network of wastewater treatment plants for improving water quality in a river basin. *IFAC-PapersOnLine*, 52(1):358–363, 2019. 12th IFAC Symposium on Dynamics and Control of Process Systems, including Biosystems DYCOPS 2019.

[18] Josh A. Taylor, Alain Rapaport, and Denis Dochain. Convex Optimization of Bioprocesses. *IEEE Transactions on Automatic Control*, 67(9):4932–4938, 1 2022.

[19] Jacques Monod. THE GROWTH OF BACTERIAL CULTURES. *Annual Review of Microbiology*, 3(1):371–394, 10 1949.

[20] D. E. Contois. Kinetics of Bacterial Growth: Relationship between Population Density and Specific Growth Rate of Continuous Cultures. *Journal of General Microbiology*, 21(1):40–50, 8 1959.

[21] LLC Gurobi Optimization. Gurobi Optimizer Reference Manual, 2022. Available online at: https://www.gurobi.com, last accessed on 28.03.2023.

[22] MOSEK ApS. MOSEK Modeling Cookbook, 2018. Available online at: https://www.mosek.com/documentation/, last accessed on 28.03.2023.

[23] Stephen P. Boyd and Lieven Vandenberghe. Convex optimization. *IEEE Transactions on Automatic Control*, 51:1859–1859, 2004.

[24] François Glineur. Topics in Convex Optimization: Interior-Point Methods, Conic Duality and Approximations. *Polytechnic College of Mons*, January 2001.

[25] Farid Alizadeh and Donald Goldfarb. Second-order cone programming. *Mathematical Programming*, 95(1):3–51, 1 2003.

[26] Stephen Boyd, Neal S. Parikh, Eric Chu, Borja Peleato, and Jonathan Eckstein. Distributed Optimization and Statistical Learning via the Alternating Direction Method of Multipliers. *Foundations and trends in machine learning*, January 2010.

[27] Hugh Everett. Generalized Lagrange Multiplier Method for Solving Problems of Optimum Allocation of Resources. *Operations Research*, 11(3):399–417, 6 1963.

[28] Magnus R. Hestenes. Multiplier and gradient methods. *Journal of Optimization Theory and Applications*, 4(5):303–320, 11 1969.

[29] Richard L. Dykstra. An Algorithm for Restricted Least Squares Regression. *Journal of the American Statistical Association*, 78(384):837–842, 12 1983.

[30] MATLAB. version 9.13.0 (R2022b). Natick, Massachussetts : The MathWorks Inc., 2022.

[31] A. n°0046, 24 février 2010, Arrêté du 25 janvier 2010 relatif aux méthodes et critères d'évaluation de l'état écologique, de l'état chimique et du potentiel écologique des eaux de surface pris en application des articles R. 212-10, R. 212-11 et R. 212-18 du code de l'environnement, NOR : DEVO1001032A.

[32] Jens Alex, Lorenzo Benedetti, Jb Copp, Krist Gernaey, Ulf Jeppsson, Ingmar Nopens, Marie-Noelle Pons, Leiv Rieger, Christian Rosen, and J-P Steyer. Benchmark simulation model no. 1 (bsm1). *Report by the IWA Taskgroup on Benchmarking of Control Strategies for WWTPs*, 01 2008.

[33] Vector and matrix norms - MATLAB norm. Available online at: https://www.mathworks.com/help/matlab/ref/norm.html, last accessed on 24.05.2023.

Appendices

Appendix A

Results

A.1 Convex optimization results for different η during rain weather

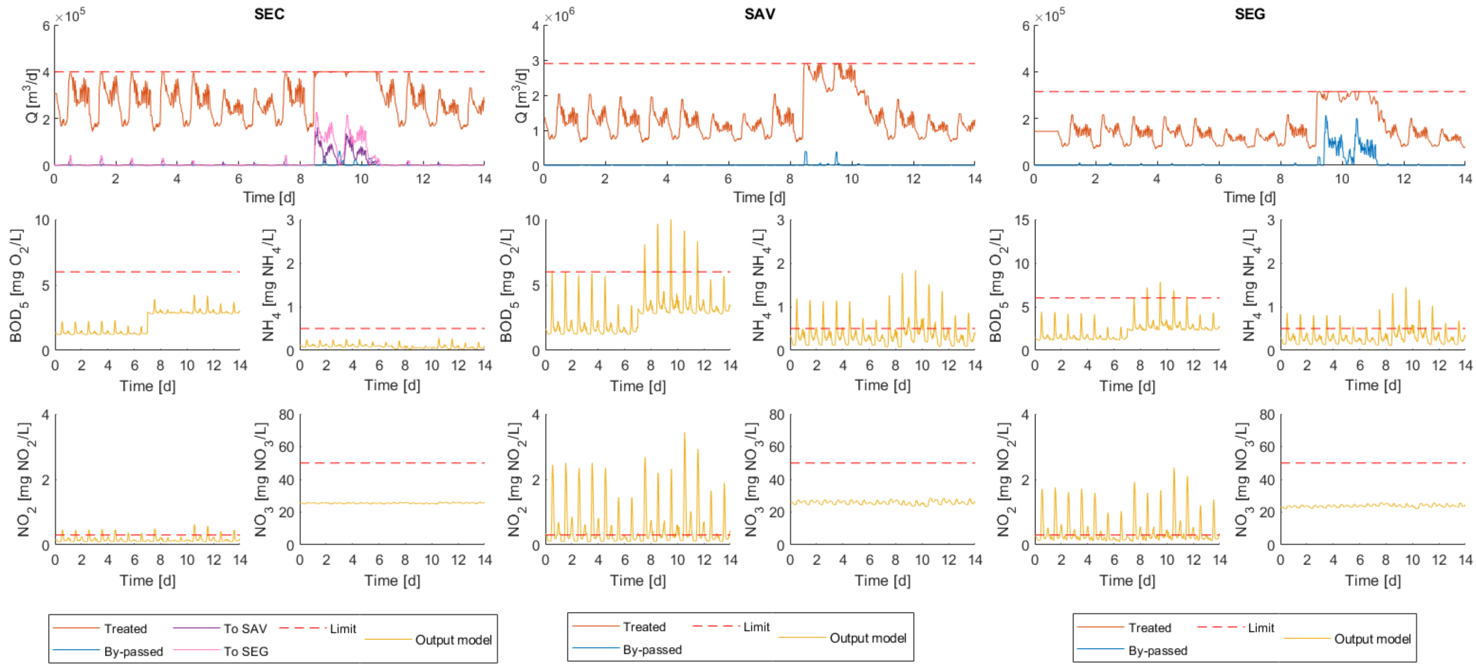

Figure A.1: Results of the convex optimization on rain weather for $\eta = [0.1, 2, 0.3, 0.1]$. The output of the model is obtained at the measurement points after each WWTP: Sartrouville for SEC, Conflans for SAV, and Triel for SEG.

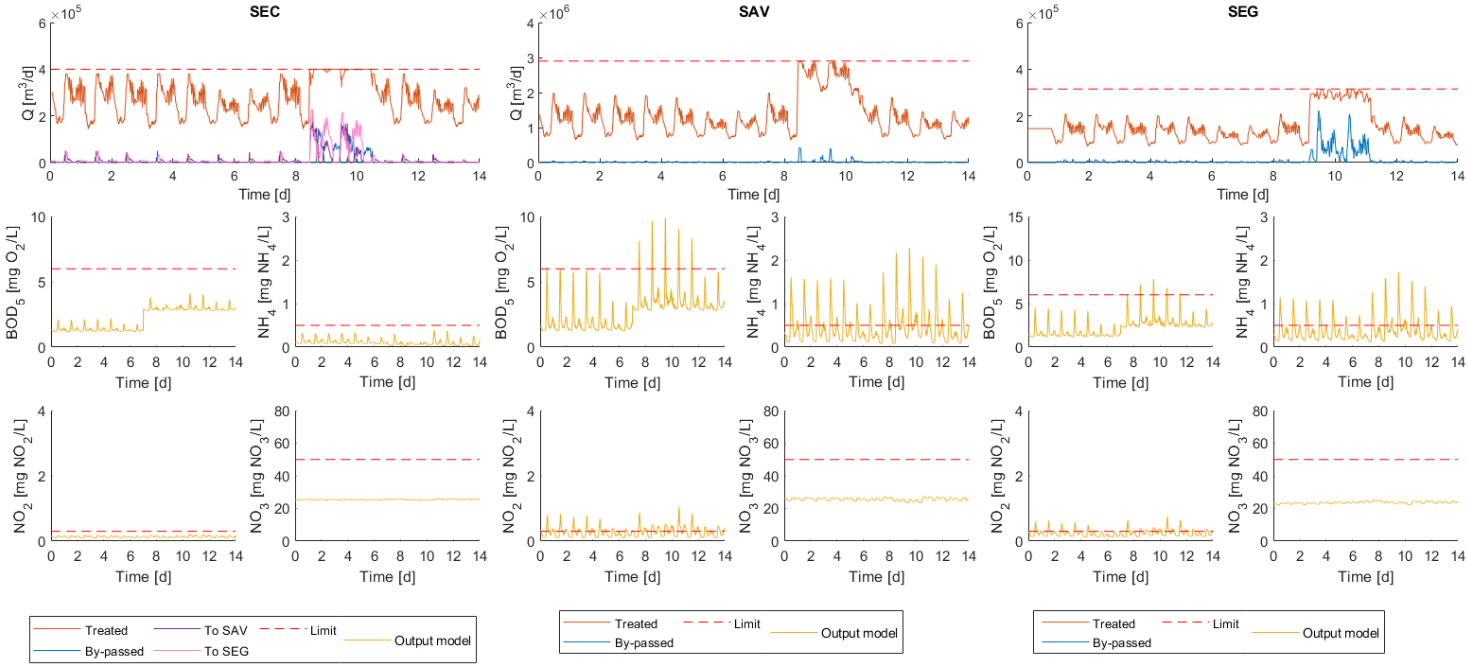

Figure A.2: Results of the convex optimization on rain weather for $\eta = [0.1, 3, 3, 0.1]$. The output of the model is obtained at the measurement points after each WWTP: Sartrouville for SEC, Conflans for SAV, and Triel for SEG.

A.2 Convex optimization results for $\eta = [0.1, 3, 3, 0.1]$ and other values for S_{max} during rain weather

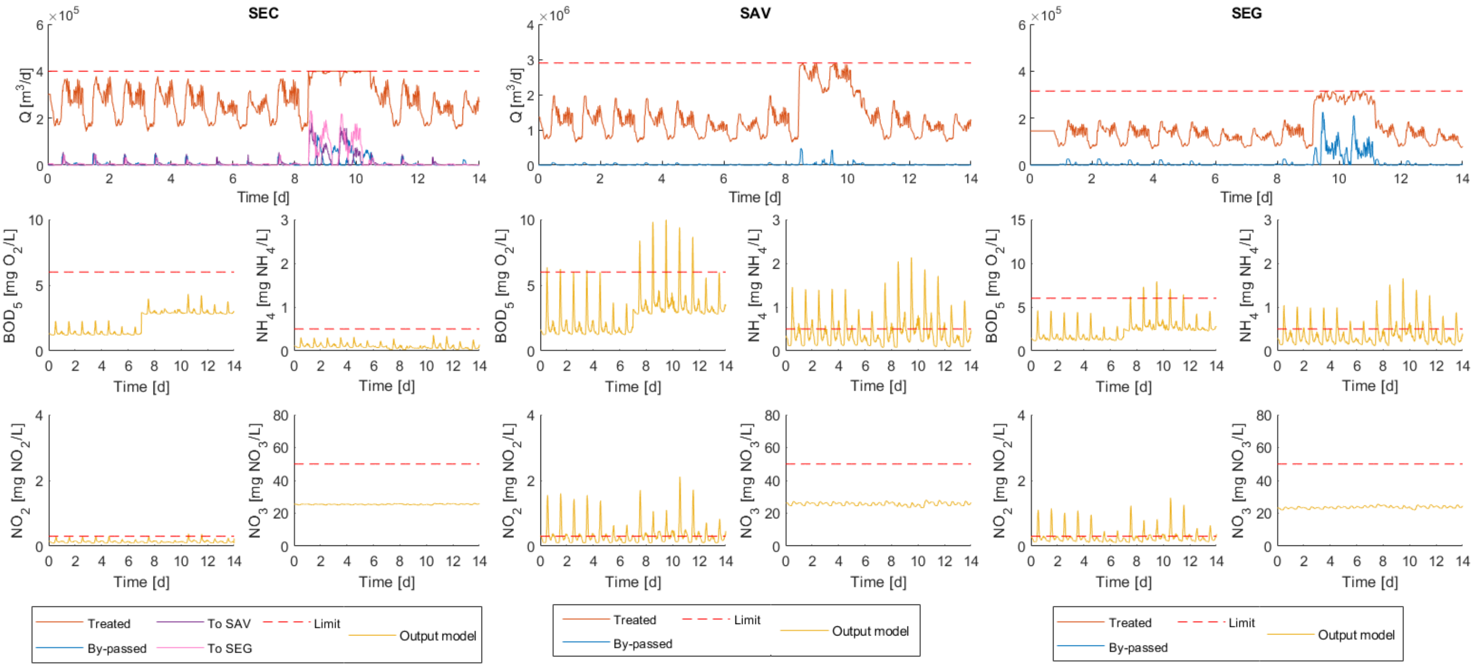

Figure A.3: Results of the convex optimization on rain weather for $\eta = [0.1, 3, 3, 0.1]$ and $S_{max,SEC} = [150, 25, 50, 100]$, $S_{max,SAV} = [100, 30, 60, 100]$, and $S_{max,SEG} = [100, 25, 80, 100]$. The output of the model is obtained at the measurement points after each WWTP: Sartrouville for SEC, Conflans for SAV, and Triel for SEG.

Appendix B

Programming

```
%% ALGORITHM ADMM
while (abs(obj_log(counter-2)-obj_log(counter-1)) >= (0.001*obj_log(counter-1)))
    if counter >= max_counter
        break;
    else

    cvx_begin
    cvx_solver mosek

        %alpha update
        variable alpha_var(4,nb_day*tau + delay_max)
        variable Qin_SEG(nb_day*tau + delay_max,1)
        variable Qin_SAV(nb_day*tau + delay_max,1)
        variable C(nm ,nb_day*tau + delay_max)


        minimize(alpha_var(1,:).*Qin_SEC0'*S0(1:4,1:(nb_day*tau + delay_max))'*eta + alpha_var(2,:).*Qin_SEC0'*S_in(1:4,1:(nb_day*tau + delay_max))'*eta + ...
            beta0(1,:).*Qin_SAV'*S0(5:8,1:(nb_day*tau + delay_max))'*eta + beta0(2,:).*Qin_SAV'*S_in(5:8,1:(nb_day*tau + delay_max))'*eta +...
            gamma0(1,:).*Qin_SEG'*S0(9:12,1:(nb_day*tau + delay_max))'*eta + gamma0(2,:).*Qin_SEG'*S_in(9:12,1:(nb_day*tau + delay_max))'*eta +...
            penalty/2 * sum_square_abs(C + U)*ones((nb_day*tau + delay_max),1))

        subject to

            C(1:4,:) >= V(1).*(-S0(1:4,2:(nb_day*tau + delay_max)+1) + S0(1:4,1:(nb_day*tau + delay_max)) + kappa{1}(1:4,:)*T0(1:4,:) - ...
            diag([1/V(1);1/V(1);1/V(1);1/V(1)])*S0(1:4,1:(nb_day*tau + delay_max))*diag(alpha_var(1,:)'.*Qin_SEC0)+...
            diag([1/V(1);1/V(1);1/V(1);1/V(1)])*S_in(1:4,:)*diag(alpha_var(1,:)'.*Qin_SEC0));

            C(5:8,:) >= V(2).*(-S0(5:8,2:(nb_day*tau + delay_max)+1) + S0(5:8,1:(nb_day*tau + delay_max)) + kappa{2}(1:4,:)*T0(5:8,:) - ...
            diag([1/V(2);1/V(2);1/V(2);1/V(2)])*S0(5:8,1:(nb_day*tau + delay_max))*diag(beta0(1,:)'.*Qin_SAV)+...
            diag([1/V(2);1/V(2);1/V(2);1/V(2)])*S_in(5:8,:)*diag(beta0(1,:)'.*Qin_SAV));

            C(9:12,:) >= V(3).*(-S0(9:12,2:(nb_day*tau + delay_max)+1) + S0(9:12,1:(nb_day*tau + delay_max)) + kappa{3}(1:4,:)*T0(9:12,:) - ...
            diag([1/V(3);1/V(3);1/V(3);1/V(3)])*S0(9:12,1:(nb_day*tau + delay_max))*diag(gamma0(1,:)'.*Qin_SEG)+...
            diag([1/V(3);1/V(3);1/V(3);1/V(3)])*S_in(9:12,:)*diag(gamma0(1,:)'.*Qin_SEG));

            alpha_var >= 0 ;

            Qin_SEG == [Qin_SEG_wo_al(1:delay_5_flow); Qin_SEG_wo_al(delay_5_flow+1:nb_day*tau + delay_5_flow)+alpha_var(4,1:nb_day*tau)'.*Qin_SEC0(1:nb_day*tau)];
            Qin_SAV == [Qin_SAV_wo_al(1:delay_3_flow); Qin_SAV_wo_al(delay_3_flow+1:nb_day*tau + delay_3_flow)+alpha_var(3,1:nb_day*tau)'.*Qin_SEC0(1:nb_day*tau)];

            for t = 1:(nb_day*tau + delay_max)
                alpha_var(1,t)*Qin_SEC0(t) <= Qin_max(1);
                alpha_var(1,t)*Qin_SEC0(t) >= Qin_min(1);
                1 == alpha_var(:,t)'*ones([4,1]);
            end
    cvx_end

    alpha0 = alpha_var;
    Qin_SEG0 = Qin_SEG;
```

```
    S_in(9:12,:) = S_in3_wo_al;
    for t=1:nb_day*tau
        S_in(9:12,t + delay_5_conc) = (S_in3_wo_al(:,t + delay_5_conc)*Qin_SEG_wo_al(t + delay_5_conc) + S_in(1:4,t)*alpha0(4,t)*Qin_SEC0(t))./(Qin_SEG_wo_al(t + delay_5_conc) + alpha0(4,t)*Qin_SEC0(t));
    end
    Qin_SAV0 = Qin_SAV;
    S_in(5:8,:) = S_in2_wo_al;
    for t=1:nb_day*tau
        S_in(5:8,t + delay_3_conc) = (S_in2_wo_al(:,t + delay_3_conc)*Qin_SAV_wo_al(t + delay_3_conc) + S_in(1:4,t)*alpha0(3,t)*Qin_SEC0(t))./(Qin_SAV_wo_al(t + delay_3_conc) + alpha0(3,t)*Qin_SEC0(t));
    end

    %beta update
    cvx_begin
    cvx_solver mosek

        variable beta_var(2,nb_day*tau + delay_max)
        variable C(nm ,nb_day*tau + delay_max)


        minimize(alpha0(1,:).*Qin_SEC0'*S0(1:4,1:(nb_day*tau + delay_max))'*eta + alpha0(2,:).*Qin_SEC0'*S_in(1:4,1:(nb_day*tau + delay_max))'*eta + ...
            beta_var(1,:).*Qin_SAV0'*S0(5:8,1:(nb_day*tau + delay_max))'*eta + beta_var(2,:).*Qin_SAV0'*S_in(5:8,1:(nb_day*tau + delay_max))'*eta +...
            gamma0(1,:).*Qin_SEG0'*S0(9:12,1:(nb_day*tau + delay_max))'*eta + gamma0(2,:).*Qin_SEG0'*S_in(9:12,1:(nb_day*tau + delay_max))'*eta +...
            penalty/2 * sum_square_abs(C + U)*ones((nb_day*tau + delay_max),1))

        subject to

            C(5:8,:) >= V(2).*(-S0(5:8,2:(nb_day*tau + delay_max)+1) + S0(5:8,1:(nb_day*tau + delay_max)) + kappa{2}(1:4,:)*T0(5:8,:) - ...
            diag([1/V(2);1/V(2);1/V(2);1/V(2)])*S0(5:8,1:(nb_day*tau + delay_max))*diag(beta_var(1,:)'.*Qin_SAV0)+...
            diag([1/V(2);1/V(2);1/V(2);1/V(2)])*S_in(5:8,:)*diag(beta_var(1,:)'.*Qin_SAV0));

            beta_var >= 0 ;

            for t = 1:(nb_day*tau + delay_max)
                beta_var(1,t)*Qin_SAV0(t)<= Qin_max(2);
                beta_var(1,t)*Qin_SAV0(t)>= Qin_min(2);
                1 == beta_var(:,t)'*ones([2,1]);
            end
    cvx_end

    beta0 = beta_var;

    %gamma update
    cvx_begin
    cvx_solver mosek

        variable gamma_var(2,nb_day*tau + delay_max)
        variable C(nm ,nb_day*tau + delay_max)


        minimize(alpha0(1,:).*Qin_SEC0'*S0(1:4,1:(nb_day*tau + delay_max))'*eta + alpha0(2,:).*Qin_SEC0'*S_in(1:4,1:(nb_day*tau + delay_max))'*eta + ...
            beta0(1,:).*Qin_SAV0'*S0(5:8,1:(nb_day*tau + delay_max))'*eta + beta0(2,:).*Qin_SAV0'*S_in(5:8,1:(nb_day*tau + delay_max))'*eta + ...
            gamma_var(1,:).*Qin_SEG0'*S0(9:12,1:(nb_day*tau + delay_max))'*eta + gamma_var(2,:).*Qin_SEG0'*S_in(9:12,1:(nb_day*tau + delay_max))'*eta +...
            penalty/2 * sum_square_abs(C + U)*ones((nb_day*tau + delay_max),1))

        subject to

            C(9:12,:) >= V(3).*(-S0(9:12,2:(nb_day*tau + delay_max)+1) + S0(9:12,1:(nb_day*tau + delay_max)) + kappa{3}(1:4,:)*T0(9:12,:) - ...
            diag([1/V(3);1/V(3);1/V(3);1/V(3)])*S0(9:12,1:(nb_day*tau + delay_max))*diag(gamma_var(1,:)'.*Qin_SEG0)+...
            diag([1/V(3);1/V(3);1/V(3);1/V(3)])*S_in(9:12,:)*diag(gamma_var(1,:)'.*Qin_SEG0));

            gamma_var >= 0 ;

            for t = 1:(nb_day*tau + delay_max)
                gamma_var(1,t)*Qin_SEG0(t)<= Qin_max(3);
                gamma_var(1,t)*Qin_SEG0(t)>= Qin_min(3);
                1 == gamma_var(:,t)'*ones([2,1]);
```

```
            end
    cvx_end

    gamma0 = gamma_var;

    % update S, T
    cvx_begin
    cvx_solver mosek

    variable S(nm, (nb_day*tau + delay_max)+1)
    variable T(nr, (nb_day*tau + delay_max))
    variable C(nm ,(nb_day*tau + delay_max))

    minimize(alpha0(1,:).*Qin_SEC0'*S(1:4,1:(nb_day*tau + delay_max))'*eta + alpha0(2,:).*Qin_SEC0'*S_in(1:4,1:(nb_day*tau + delay_max))'*eta + ...
        beta0(1,:).*Qin_SAV0'*S(5:8,1:(nb_day*tau + delay_max))'*eta + beta0(2,:).*Qin_SAV0'*S_in(5:8,1:(nb_day*tau + delay_max))'*eta +...
        gamma0(1,:).*Qin_SEG0'*S(9:12,1:(nb_day*tau + delay_max))'*eta + gamma0(2,:).*Qin_SEG0'*S_in(9:12,1:(nb_day*tau + delay_max))'*eta +...
        penalty/2 * sum_square_abs(C + U)*ones((nb_day*tau + delay_max),1))

    subject to

        S(:,1) == S00;

        C(1:4,:) >= V(1).*(-S(1:4,2:(nb_day*tau + delay_max)+1) + S(1:4,1:(nb_day*tau + delay_max)) + kappa{1}(1:4,:)*T(1:4,:) - ...
        diag([1/V(1);1/V(1);1/V(1);1/V(1)])*S(1:4,1:(nb_day*tau + delay_max))*diag(alpha0(1,:)'.*Qin_SEC0)+...
        diag([1/V(1);1/V(1);1/V(1);1/V(1)])*S_in(1:4,:)*diag(alpha0(1,:)'.*Qin_SEC0));

        C(5:8,:) >= V(2).*(-S(5:8,2:(nb_day*tau + delay_max)+1) + S(5:8,1:(nb_day*tau + delay_max)) + kappa{2}(1:4,:)*T(5:8,:) - ...
        diag([1/V(2);1/V(2);1/V(2);1/V(2)])*S(5:8,1:(nb_day*tau + delay_max))*diag(beta0(1,:)'.*Qin_SAV0)+...
        diag([1/V(2);1/V(2);1/V(2);1/V(2)])*S_in(5:8,:)*diag(beta0(1,:)'.*Qin_SAV0));

        C(9:12,:) >= V(3).*(-S(9:12,2:(nb_day*tau + delay_max)+1) + S(9:12,1:(nb_day*tau + delay_max)) + kappa{3}(1:4,:)*T(9:12,:) - ...
        diag([1/V(3);1/V(3);1/V(3);1/V(3)])*S(9:12,1:(nb_day*tau + delay_max))*diag(gamma0(1,:)'.*Qin_SEG0)+...
        diag([1/V(3);1/V(3);1/V(3);1/V(3)])*S_in(9:12,:)*diag(gamma0(1,:)'.*Qin_SEG0));


        for t = 1:(nb_day*tau + delay_max)
        for i = 1:n
            for j = 1:r
                Sind = (i-1)*(m)+j;
                Tind = (i-1)*r+j;

                hS = mumax(i,j)*S(Sind,t)*Xin(i,t);
                hT = K(i,j)*T(Tind,t);
                hX = mumax(i,j)*K(i,j)*Xin(i,t);

                norm([hS;hT;hX],2) <= hX + hS - hT;

                TL = mumax(i,j)*smin(Sind)*Xin(i,t)/(K(i,j) + smin(Sind));
                TU = mumax(i,j)*smax(Sind)*Xin(i,t)/(K(i,j) + smax(Sind));

                T(Tind,t) >= TL + (TU-TL).*(S(Sind,t)-smin(Sind))./(smax(Sind)-smin(Sind));

            end
        end
        end

    S >= 0;
    T >= 0;

    cvx_end

    S_old = S0;
    T_old = T0;

    S0 = S;
    T0 = T;

    U_new = zeros(nm, (nb_day*tau + delay_max));
    for t = 1:(nb_day*tau + delay_max)
        Qhh = [alpha0(1,t).*Qin_SEC0(t) beta0(1,t).*Qin_SAV0(t) gamma0(1,t).*Qin_SEG0(t)];
```

```
        Qh = kron(diag(Qhh),Im);
        U_new(:,t) = (Vh*(-S0(:,t+1))+ Vh*S0(:,t) + Vh*Kap*T0(:,t)-Qh*S0(:,t)+Qh*S_in(:,t));
    end

    U = U + U_new;

    obj_log(counter) = cvx_optval;

    U_log(:,counter-1) = sum(U,2);

    counter = counter + 1;
    end

end

sol.y = y0;
sol.alpha = alpha0;
sol.beta = beta0;
sol.gamma = gamma0;
sol.S = S0;
sol.T = T0;
sol.counter = counter-3;
sol.U = U;
sol.Ulog = U_log;
sol.obj_log = obj_log;
```

Listing B.1: 'Algorithm.m'

UNIVERSITÉ CATHOLIQUE DE LOUVAIN
École polytechnique de Louvain
Rue Archimède, 1 bte L6.11.01, 1348 Louvain-la-Neuve, Belgique | **www.uclouvain.be/epl**